Theses and Dissertations   1. Thesis and Dissertation Collection, all items

1987-09

An acoustic bubble density measurement technique for surface ship waters

Hampton, Stephen Wallace

https://hdl.handle.net/10945/22590

NAVAL POSTGRADUATE SCHOOL
Monterey, California

THESIS

AN ACOUSTIC BUBBLE DENSITY MEASUREMENT TECHNIQUE FOR SURFACE SHIP WAKES

by

Stephen Wallace Hampton

September 1987

Thesis Advisor: Anthony A. Atchley

Approved for public release; distribution is unlimited.

REPORT DOCUMENTATION PAGE

REPORT SECURITY CLASSIFICATION UNCLASSIFIED		1b RESTRICTIVE MARKINGS		
SECURITY CLASSIFICATION AUTHORITY		3 DISTRIBUTION/AVAILABILITY OF REPORT Approved for public release; distribution is unlimited.		
DECLASSIFICATION/DOWNGRADING SCHEDULE				
PERFORMING ORGANIZATION REPORT NUMBER(S)		S MONITORING ORGANIZATION REPORT NUMBER(S)		
NAME OF PERFORMING ORGANIZATION aval Postgraduate School	6b OFFICE SYMBOL (If applicable) 3A	7a NAME OF MONITORING ORGANIZATION Naval Postgraduate School		
ADDRESS (City, State, and ZIP Code) onterey, California 93943-5000		7b ADDRESS (City, State, and ZIP Code) Monterey, California 93943-5000		
NAME OF FUNDING/SPONSORING ORGANIZATION	8b OFFICE SYMBOL (If applicable)	9 PROCUREMENT INSTRUMENT IDENTIFICATION NUMBER		
ADDRESS (City, State, and ZIP Code)		10 SOURCE OF FUNDING NUMBERS		
		PROGRAM ELEMENT NO	PROJECT NO	TASK NO	WORK UNIT ACCESSION NO

TITLE (Include Security Classification)

n Acoustic Bubble Density Measurement Technique for Surface Ship Wakes

PERSONAL AUTHOR(S)
HAMPTON, Stephen W.

TYPE OF REPORT aster's Thesis	13b TIME COVERED FROM _____ TO _____	14 DATE OF REPORT (Year Month Day) 1987 September 30	15 PAGE COUNT 187

SUPPLEMENTARY NOTATION

COSATI CODES			18 SUBJECT TERMS (Continue on reverse if necessary and identify by block number)
FIELD	GROUP	SUB-GROUP	Acoustic Bubble Density Measurements, Surface
			Ship Wakes, Bubble Resonance, Duel Frequency
			Bubble Detection, Ultrasonic Bubble Detection

ABSTRACT (Continue on reverse if necessary and identify by block number)

ABSTRACT (Continue on reverse if necessary and identify by block number)

The Dual Frequency Pump Method of acoustically determining point
by point bubble cloud densities was studied to determine the practi-
cality of using this acoustic technique to determine bubble densities
in surface ship wakes. The dual-frequency technique of acoustically
detecting bubbles utilizes a high- and low-frequency sound field to
insonify the target bubbles. The bubbles themselves then radiate
sound at the sidebands of the higher frequency. The frequency of
the return sound is proportional to the bubble sizes present. The
Dual Frequency Pump Method of bubble detection can differentiate
and count many different-sized bubbles and is, therefore, well
suited for determining ship wake bubble density distributions. The

DSTRIBUTION/AVAILABILITY OF ABSTRACT ☑ UNCLASSIFIED/UNLIMITED ☐ SAME AS RPT ☐ DTIC USERS	21 ABSTRACT SECURITY CLASSIFICATION UNCLASSIFIED	
NAME OF RESPONSIBLE INDIVIDUAL of Anthony Atchley	22b TELEPHONE (Include Area Code) (408) 646-2848	22c OFFICE SYMBOL 61 Ay

FORM 1473, 84 MAR   83 APR edition may be used until exhausted   SECURITY CLASSIFICATION OF THIS PAGE
All other editions are obsolete

19. theory, considerations, experimental results, and recommendations of this thesis support the application of the dual-frequency acoustic technique to the ship wake problem.

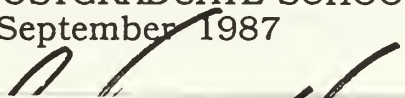# An Acoustic Bubble Density Measurement Technique for Surface Ship Wakes

by

Stephen Wallace Hampton
Lieutenant, United States Navy
B.S.M.E., United States Naval Academy, 1981

Submitted in partial fulfillment of the
requirements for the degree of

MASTER OF SCIENCE IN SYSTEMS TECHNOLOGY
(Antisubmarine Warfare)

from the

NAVAL POSTGRADUATE SCHOOL
September 1987

ABSTRACT

The Dual Frequency Pump Method of acoustically determining point by point bubble cloud densities was studied to determine the practicality of using this acoustic technique to determine bubble densities in surface ship wakes. The dual-frequency technique of acoustically detecting bubbles utilizes a high- and low-frequency sound field to insonify the target bubbles. The bubbles themselves then radiate sound at the sidebands of the higher frequency. The frequency of the return sound is proportional to the bubble sizes present. The Dual Frequency Pump Method of bubble detection can differentiate and count many different-sized bubbles and is, therefore, well suited for determining ship wake bubble density distributions. The theory, considerations, experimental results, and recommendations of this thesis support the application of the dual-frequency acoustic technique to the ship wake problem.

THESIS DISCLAIMER

The computer programs provided in the appendices of this thesis are solely to provide insight into the possible applications of the equations presented within these pages. The programs are not verified or documented and use of these programs is at the user's own risk.

TABLE OF CONTENTS

7

LIST OF TABLES

LIST OF FIGURES

13

ACKNOWLEDGMENTS

14

I. INTRODUCTION

New torpedo technology utilizes the surface ship wake and the near-surface region of the ocean to give their torpedos advanced capabilities. To better understand and counter these capabilities, the Naval Sea Systems Command Surface Ship Torpedo Defense (SSTD) program has identified the need to study surface ship wake characteristics (CNO project 0779) in support of U.S. weapon system development [Ref. 1]. In addition, both the Pacific and Atlantic Fleet Anti-Submarine Warfare Improvement Programs have listed surface ship wake data collection as a high priority action item [Ref. 2].

The purpose of this thesis is to investigate a new and more accurate acoustic technique of detecting small bubbles in bubble clouds which could be used to determine the bubble density distributions in surface ship wakes. This new method of acoustic bubble detection uses a dual frequency resonance technique originally investigated by P. M. Shankar and V. L. Newhouse of Drexel University [Ref. 3]. Acoustic bubble cloud density measurements are useful as they could serve as a practical verification for new optical measurement techniques being developed by the Naval Coastal Systems Center (NCSC) Panama City, Florida, in support of the SSTD program. Accurate bubble cloud density measurements would also aid in the development of ship wake computer models and provide insights into acoustic weapon performance in the wake region.

A. BACKGROUND

The need to determine surface ship wake characteristics is not a new problem in the areas of Anti-Submarine Warfare (ASW) and Surface Ship Torpedo Defense (SSTD). Ever since the development of the torpedo, studies have been conducted on how wake characteristics could be used to enhance defensive or offensive opportunities for both targets and weapons. During World War II, acoustic means of detecting bubbles in surface ship wakes were developed specifically for submarines and their torpedos. These techniques were crude and actual instances of attempting bubble density measurements were rare [Ref. 4]. However, advances during the past ten years in acoustic-type torpedo technology have drastically increased the need to understand surface ship wake mechanisms and bubble density distributions.

In this thesis, the specific area of interest with regard to the surface ship wake study is the bubble density distributions in the near-surface region, both inside and outside the wake. Acoustically, the bubble density distribution is extremely important because of the direct relation to sound propagation and absorption in sea water. The number of bubbles within a specified volume of water, that is, the bubble density, will determine how much sound is scattered and how much sound passes through that volume. If bubbles present within the specified volume of water have the same resonance frequency as that of the passing sound wave, the bubbles resonate and the effects of attenuation are very pronounced. If point-by-point bubble density distributions can be determined, then the performance of the new

16

acoustic weapons can be predicted and modified for operations in the near–surface regions. Measuring the bubble density distribution as a function of bubble size (bubble size and resonance frequency are directly related) and knowing the bubble density for different points in the wake are also critical to validating computer wake models.

Several methods of acoustic bubble density distribution measurement have been tried in the past or are currently underway. The Naval Research Laboratory (NRL) in Washington, D.C., the Naval Postgraduate School (NPS) in Monterey, the David Taylor Research and Development center (DTRDC) in Carter Rock, and the Naval Coastal Systems Center (NCSC) in Panama City are just a few activities which have experimented with, or considered, the bubble density measurement problem for the Navy.

The Naval Research Laboratory conducted a program of ship wake research in the late 1960s. The most noteworthy study was done with reverberation chambers which were used to probe ship wakes and determine sound absorption profiles. This research included ship wake geometry, wake dissolution, bubble rise, and sound absorption measurements. [Ref. 5]

The microbubble measurement effort at the Naval Postgraduate School has been led by Dr. Herman Medwin. He is well published on the methods of Resonant Scattering and Second Harmonic Generation for bubble detection. Both methods are practical when counting bubbles of approximately the same size but are somewhat inaccurate when

measuring bubble clouds which contain many bubbles of different sizes. [Refs. 6, 7, 8]

The David Taylor Research and Development Center was recently contacted by NCSC Panama City to develop an acoustic bubble detector to measure actual distributions in ship wakes and ship wake models. DTRDC proposed developing the detector in fiscal year 1988, but due to the lack of funds current plans for this project are now on hold. [Ref. 9]

Finally, the Naval Coastal Systems Center has the most extensive ship wake research effort to date. The NCSC effort is based around a wake map vehicle which can make actual sound pressure level measurements looking upward through the wake to the surface. This map vehicle provides a profile of the wake and data that can be used to calculate the vertical transmission loss from the vehicle to the surface. However, the map vehicle does not provide horizontal wake data or the point–by–point bubble density distribution measurements needed for computer models of sound propagation. For this reason, NCSC is developing an optical measurement device which should be able to provide the point–by–point bubble density wake measurements. Still, this exact method of measurement has never been tried. Therefore, an accurate acoustic measurement device which will count all bubble sizes is highly desirable for verification of the optical technique. [Refs. 10, 11]

Acoustic bubble density measurements have been made in association with cavitation, diver decompression sickness, contrast

echocardiology, and pressure flow gradients [Ref. 3]. These methods have been successful when measuring small numbers of bubbles of a single particular size. However, success has been limited when the bubble cloud contains many bubbles of different sizes such as those bubbles found in surface ship wakes. Previously attempted methods, which included Resonant Scattering, Doppler, and Second Harmonic Generation, are at a disadvantage when used for measuring a bubble cloud. In Resonant Scattering, a particular bubble provides peak echos at its resonance frequency. However, a larger bubble may reflect an even greater amount of energy at that particular frequency due to its large cross-section, resulting in a false bubble count. The Doppler technique by itself provides no way of separating the returns from different size bubbles. Second Harmonic Generation is inaccurate in a bubble cloud because the second harmonic radiation from large bubbles suffers resonant absorption by the smaller bubbles. None of these methods seems to provide the accurate acoustic bubble cloud measurements required for the surface ship wake problem. [Ref. 12]

B. SCOPE

A method to acoustically measure bubble cloud densities using a "Double Frequency Pump" sum and difference technique shows considerable potential in obtaining a high degree of accuracy when counting bubbles of various radii. This method involves insonifing the bubble cloud with two different sound fields— an "imaging" field of frequency ω_i and a "pump" field of frequency ω_p. The imaging field employs high-frequency sound to image the bubbles in the cloud.

19

Because of its short wavelength, the high frequency (ω_i) sound field provides good spatial resolution. The pump sound field sweeps through a range of lower frequencies (ω_p) to excite resonant oscillations in the bubbles. The pump frequency range is selected to encompass the expected range of bubble resonance frequencies. A bubble which is excited near resonance by the pump field in the presence of the imaging field will undergo large amplitude, nonlinear oscillations. These oscillations cause the bubble to radiate energy at several different frequencies, specifically at ω_p and $\omega_i \pm \omega_p$. The radiated energy can be displayed on a spectrum analyzer and the bubble size distribution inferred from the sideband frequencies $(\omega_i \pm \omega_p)$ and their peak pressure amplitudes. [Ref. 12]

The Double Frequency Pump method appears to solve the previous problems related to the inability to count bubbles of different sizes in a bubble cloud. It is this method that we will investigate for use in a simple acoustic bubble density measurement device.

C. GOALS

This thesis will concentrate on determining the practicality of the Double Frequency Pump technique for near-surface, open-ocean bubble density measurements. Specifically, the feasibility of using this technique to measure bubble densities in surface ship wakes will be considered. To obtain that goal, it will be necessary to complete several tasks. First, re-create the Double Frequency Pump experiment in sea water utilizing a rigorous bubble generator to generate bubbles with radii similar to those found in ship wakes. Part of this task will

require calculating the resonance frequencies of these bubbles so that the pump sound field can resonate all bubbles present. Second, a partial validation of the experimental accuracy of bubble size and bubble cloud density will be attempted using photographic methods. Third, the effects of the bubbles screening each other from the receiving transducer so that the energy radiated from the bubbles is never received need to be studied. These topics include the consideration of transducer types, transducer frequencies, near and far field beam patterns, and transducer placement for obtaining the best bubble count. Lastly, it will be necessary to briefly examine the transducer inputs required for complete isonification of the bubble cloud and the ideal volume in which to measure, or sample, the bubble density. These goals are only a few of those necessary to begin designing an acoustic bubble density measurement device, but they are enough to help show the concept practical for conducting bubble density measurements in the ship wake environment.

II. THEORY

In order to appreciate and understand the Dual Frequency Pump technique for the measurement of bubble cloud densities, it is important to examine the theories behind bubble resonance, dual frequency bubble excitation, and transducer beam patterns. These are the three major concepts needed for this acoustic bubble detection method.

A. BUBBLE RESONANCE

When a sound wave strikes a bubble, the bubble undergoes radial oscillations. The response of the bubble depends on its size as well as the frequency and the pressure amplitude of the incident sound wave. These radial oscillations, in the form of compressions and expansions, are analogous to the motion of a simple, damped harmonic oscillator and, in fact, can be described by similar differential equations. Just as the damped harmonic oscillator has a resonance frequency where the displacement becomes maximum, the bubble also has a resonance frequency where amplitude of the radial oscillation becomes maximum. When a bubble oscillates at resonance, the maximum amount of energy is extracted from the incident sound wave. A large portion of this energy is then re-radiated by the bubble in all directions with the rest converted to heat. It is this scattering and absorption of the sound energy that causes large amounts of attenuation as sound passes through a bubbly medium. [Ref. 13]

22

As previously mentioned, a gaseous bubble in seawater behaves similarly to a damped harmonic oscillator, a schematic of which is shown in Figure 1. The differential equation for this model can be written by setting the sum of the forces exerted on the mass equal to the mass times its acceleration and then rearranging the terms. This well-known equation, shown below, will be used to derive an expression for the angular resonance frequency ω_d of the damped oscillator. For the damped harmonic oscillator

$$m \frac{d^2x}{dt^2} + Rm \frac{dx}{dt} + sx = 0,$$

where:

    m   = mass
    Rm = mechanical resistance
    s   = stiffness of spring
    x   = displacement
    t   = time.

Dividing through by the mass m, and letting

$$\omega_o = \sqrt{s/m} = \text{undamped angular resonance frequency}$$

yields

$$\frac{d^2x}{dt^2} + \frac{Rm}{m} \frac{dx}{dt} + \omega_o^2 x = 0. \tag{1}$$

This equation can now be solved using the standard complex exponential method [Ref. 14]. The solution yields the equation for the natural (resonance) angular frequency of the damped oscillator,
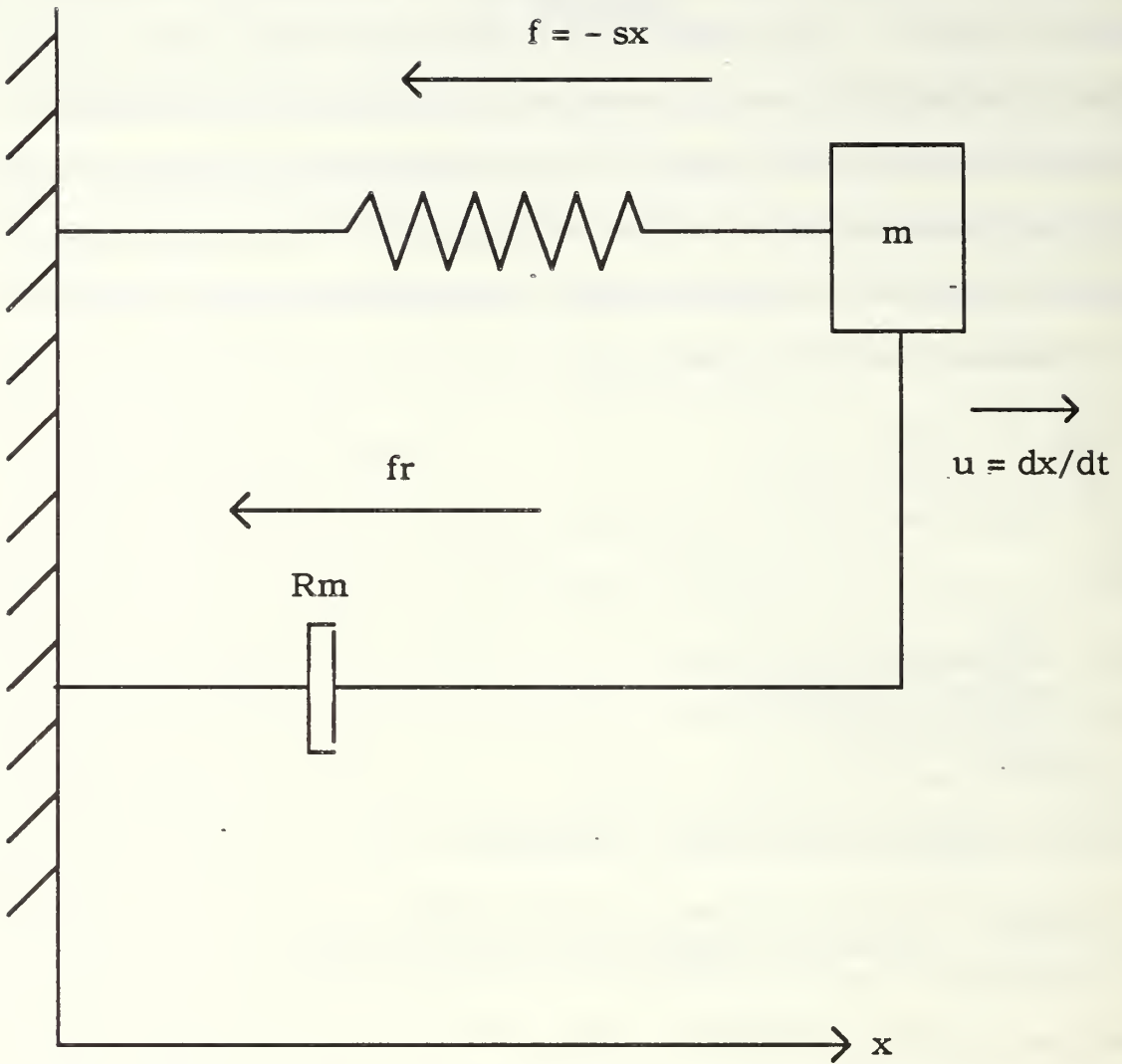
Figure 1

Simple Harmonic Oscillator with Damping

Source: Ref. 14:7

24

$$\omega_d = \sqrt{\omega_0^2 - \beta^2} \equiv \text{damped angular resonance frequency,}$$

where

$$\beta = \frac{1}{2}\frac{Rm}{m} \equiv \text{dissipation or damping coefficient.}$$

Several assumptions which apply to both the damped harmonic oscillator and the pulsating bubble now become important. First, the amplitude of the oscillation for both systems is considered to be small. Secondly, when considering a system at its resonance frequency, the effects of damping are small and can, therefore, be ignored. In other words, the dissipation coefficient is much smaller than that of the natural frequency. In this case,

$$\beta = \frac{1}{2}\frac{Rm}{m} \rightarrow 0$$

and

$$\omega_d \approx \omega_0 = \sqrt{s/m}. \tag{2}$$

The damped resonance frequency is approximately the same as the undamped resonance frequency. [Ref. 14]

The bubble may now be considered in terms of volume pulsations, v. A volume pulsation is an expansion and contraction of the bubble which results in a constantly changing volume. This volume pulsation, or so-called radial mode, is the simplest mode of bubble oscillation, and the one that causes the most energy radiation. Because of this, it

is the only mode of interest for acoustic bubble detection. Other modes involve shape, not volume, changes in the bubble and, therefore, do not radiate sufficient energy for easy detection. [Ref. 15]

Volume pulsations of the bubble are analogous to the displacement of the mass in the damped harmonic oscillator. Consider the bubble in Figure 2, where

v   = volume pulsation
V_o = equilibrium volume
V(t) = instantaneous volume
s   = bubble stiffness
m   = inertial constant
β   = dissipation (damping)
R   = instantaenous bubble radius
R_o = average bubble radius.

Using the same assumptions as were used for the damped harmonic oscillator, the equation for the bubble volume pulsations shown in Figure 2 can be written as

$$v = V(t) - V_o.$$

The second–order differential equation for the oscillating bubble is then written as

$$m \frac{d^2v}{dt^2} + \beta \frac{dv}{dt} + sv = 0. \tag{3}$$

The solution of equation (3) is the same as that of equation (1) and, therefore, the angular resonance frequency is still defined by equation (2),

$$\omega_d \approx \omega_o = \sqrt{s/m}.$$
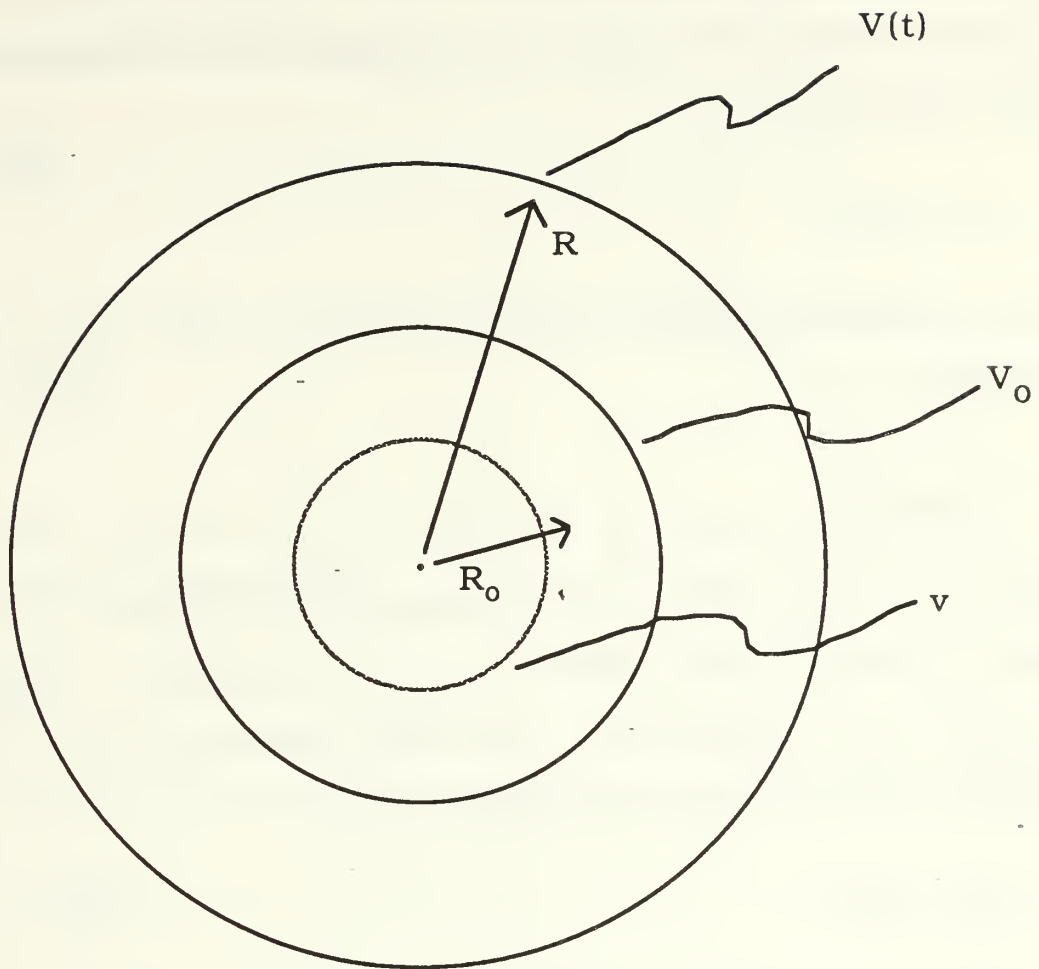
$v \equiv$ volume pulsation

$V_o \equiv$ equilibrium volume

$V(t) \equiv$ instantaneous volume

Figure 2

Pulsating Bubble

Source: Ref. 5:20

Bubble stiffness is defined by the change in pressure within the bubble versus the change in bubble volume as the bubble undergoes oscillation [Ref. 16], that is:

$$s = -dp/dv.$$

For a bubble containing gas at pressure p_o, the bubble stiffness becomes

$$s = \gamma p_o / V_o, \tag{4}$$

where $\gamma = c_p/c_v$ is the specific heat ratio and is equal to 1.4 for air. The unit for the total pressure p_o is the atmosphere, which equals 1.0133×10^6 dynes/cm^2. The inertial constant m for a spherical bubble of mean radius R_o is defined as

$$m = \rho / 4\pi R_o \tag{5}$$

where ρ is the density of seawater (1.026 g/cm^3). Substituting equations (4) and (5) into equation (2) gives [Ref. 16],

$$\omega_o = \sqrt{s/m} = \sqrt{\frac{\gamma p_o / V_o}{\rho / 4\pi R_o}}.$$

Using

$$V_o = \frac{4}{3} \pi R_o^3,$$

the final result for the angular resonance frequency of a gas bubble in a liquid as a function of bubble radius is

$$\omega_0 = \sqrt{\frac{3\gamma p_0}{\rho R_0^2}},$$

or

$$\omega_0 = \frac{1}{R_0}\sqrt{\frac{3\gamma p_0}{\rho}}. \qquad (6)$$

The resonance frequency f_0 is related to the angular resonance frequency ω_0 by the relationship

$$f_0 = \omega_0/2\pi.$$

Therefore, the final result (in hertz) is

$$f_0 = \frac{1}{2\pi R_0}\sqrt{\frac{3\gamma p_0}{\rho}}. \qquad (7)$$

Equation (7), alone, can be used to calculate the range of resonance frequencies for bubbles in seawater. More accurate equations which account for surface tension, viscosity, and thermal effects have been derived, but the effects of these factors on the resonance frequency of bubbles typical of those found in ship wakes is very small. As an example, the equation for the resonance frequency containing a surface tension term σ is [Ref. 3],

$$f_0 = \frac{1}{2\pi R_0}\sqrt{\frac{3\gamma(p_0 + 2\sigma/R_0) - 2\sigma/R_0}{\rho}}. \qquad (8)$$

By examining equation (8), it can be seen that, as bubbles of increasing size are considered, the surface tension term becomes negligible (the value for surface tension in seawater is approximately 70.0 dynes/cm). However, surface tension and viscosity terms will become important in the next section when calculating the pressure amplitudes of the sound energy re-radiated from bubbles under the influence of dual-frequency excitation.

Equations (7) and (8) show the relationship between bubble resonance frequency and radius. The most abundant bubbles in the surface ship wake environment are assumed to have approximate radii varying from 10 to 170 micrometers (µm) and extend downward from the surface to a depth corresponding to approximately three atmospheres of pressure [Ref. 17]. Appendix A is a listing of a Fortran program for calculating resonance frequencies using both equations (7) and (8). For the purpose of comparison, the results of these two equations are tabulated in Tables Ia, Ib, and Ic using radii from 10 to 170 mm and pressures from one to three atmospheres. These assumed values of bubble radii and their corresponding resonance frequencies are of primary interest for the Dual Frequency Pump method of bubble density measurement in ship wakes.

B. DUAL FREQUENCY BUBBLE RESPONSE

The theory of dual frequency bubble response is more complex than that previously used to find the resonance frequency of a bubble of a given radius. Part of this complexity is due to the inclusion of shear viscosity and surface tension terms, which become necessary for

TABLE Ia

RESONANCE FREQUENCY VS. RADIUS FOR
BUBBLES IN SEAWATER AT 1.0 ATMOSPHERE

RADIUS (cm)	RESONANCE FREQUENCY (KHz)	FREQUENCY WITH SURFACE TENSION (KHz)
0.0010	324.1	340.8
0.0020	162.1	166.3
0.0040	81.0	82.1
0.0060	54.0	54.5
0.0080	40.5	40.8
0.0090	36.0	36.2
0.0100	32.4	32.6
0.0120	27.0	27.1
0.0150	21.6	21.7
0.0170	19.1	19.1

TABLE Ib

RESONANCE FREQUENCY VS. RADIUS FOR
BUBBLES IN SEAWATER AT 2.0 ATMOSPHERES

RADIUS (cm)	RESONANCE FREQUENCY (KHz)	FREQUENCY WITH SURFACE TENSION (KHz)
0.0010	458.4	470.3
0.0020	229.2	232.2
0.0040	114.6	115.4
0.0060	76.4	76.7
0.0080	57.3	57.5
0.0090	50.9	51.1
0.0100	45.8	46.0
0.0120	38.2	38.3
0.0150	30.6	30.6
0.0170	27.0	27.0

TABLE Ic

RESONANCE FREQUENCY VS. RADIUS FOR
BUBBLES IN SEAWATER AT 3.0 ATMOSPHERES

RADIUS (cm)	RESONANCE FREQUENCY (KHz)	FREQUENCY WITH SURFACE TENSION (KHz)
0.0010	561.4	571.2
0.0020	280.7	283.2
0.0040	140.4	141.0
0.0060	93.6	93.8
0.0080	70.2	70.3
0.0090	62.4	62.5
0.0100	56.1	56.2
0.0120	46.6	46.9
0.0150	37.4	37.5
0.0170	33.0	33.1

extremely small bubbles. Another reason for the complexity is that the bubble must now be viewed as a system of forced volume pulsations in the steady state.

Once again, a bubble model must be utilized and certain assumptions made. The bubble shown in Figure 3 is being radiated by two sound fields (note that the bubble size is not scaled to compare to sound field wavelength). The bubble will remain approximately spherical throughout its volume pulsation and is considered to be surrounded by an infinitely extended incompressible fluid. Thermal effects and gas diffusion through the bubble wall are considered negligible. Also, damping of the bubble oscillation is considered through the inclusion of surface tension and shear viscosity in the bubble model with shear viscosity being taken as a constant for Newtonian fluids such as seawater. [Ref. 18]

The mathematical form of the bubble model is a non–linear differential equation for volume pulsations [Ref. 3],

$$\rho R \ddot{R} + \tfrac{3}{2} \rho \dot{R}^2 = (p_0 + 2\sigma/R_0)(R_0/R)^{3\gamma} - (p_0 + 2\sigma/R) - 4\mu \dot{R}/R + p_i(t) + p_p(t), \tag{9}$$

where

p_0	= ambient pressure
μ	= shear viscosity of the liquid
σ	= surface tension
$p_i(t)$	= instantaneous pressure of imaging sound wave
ω_i	= frequency of imaging sound
$p_p(t)$	= instantaneous pressure of pump sound wave
ω_p	= frequency of pump sound

Liquid Properties $\left\{\begin{array}{l} \rho \\ \mu \\ p_o \end{array}\right.$

R

R_o

γ

σ

$p_i(t)$
ω_i

Imaging Sound Waves

$p_p(t)$
ω_p
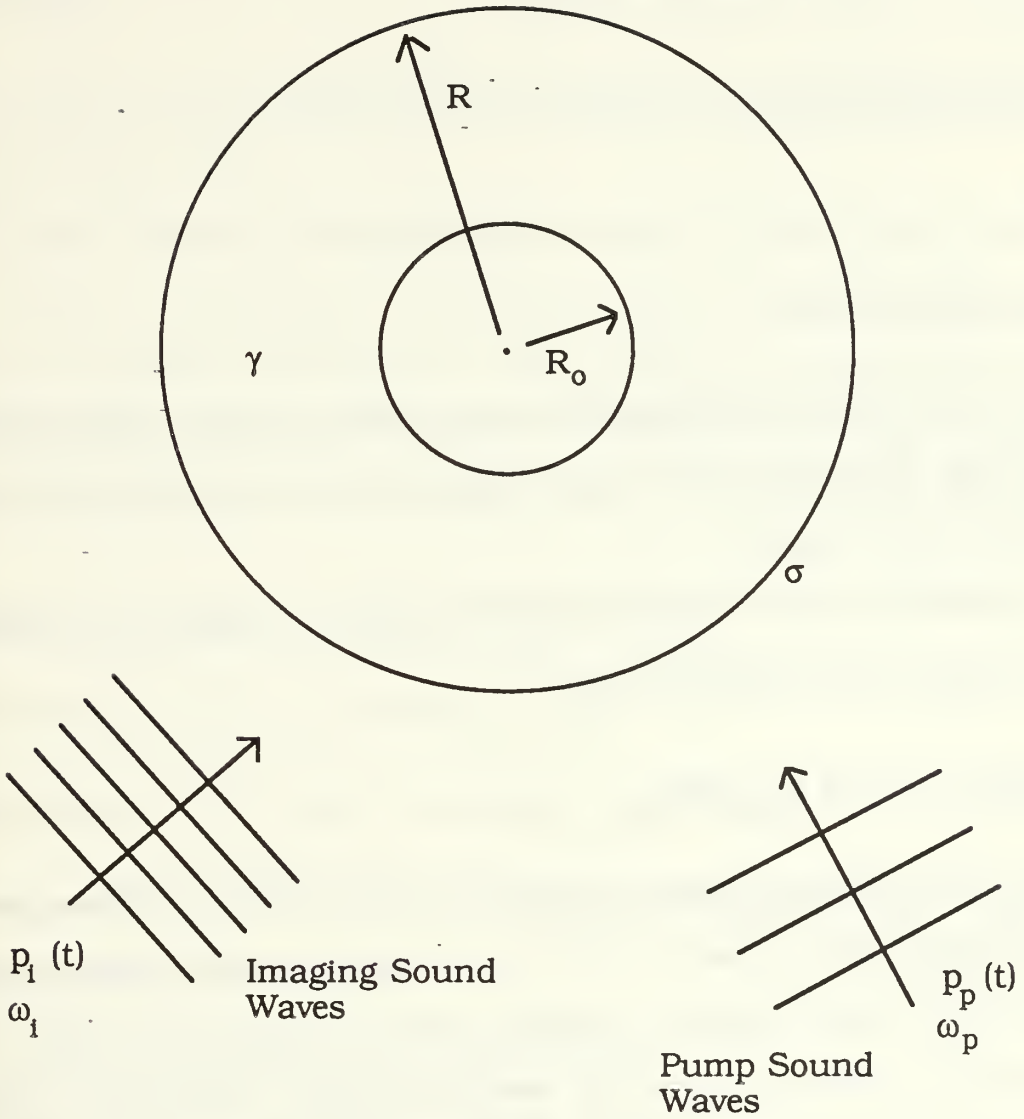
Pump Sound Waves

Figure 3

Pulsating Bubble Undergoing Radiation by Two Sound Waves

Source: Ref. 18:283

35

γ = ratio of specific heats
R   = instantaneous bubble radius
R_0 = average bubble radius

and the dots represent time derivatives. The incident sound waves are assumed to be sinusoidal, that is,

$$p_i(t) = p_i \cos \omega_i t$$

and

$$p_p(t) = p_p \cos \omega_p t,$$

where p_i and p_p are simplified expressions for the peak pressure amplitudes (imaging and pump, respectively) at a particular distance from the sound source.

In order to solve equation (9), it is useful to expand the instantaneous radius R in a Taylor series,

$$R = R_0 (1 + x) = R_0 + xR_0, \tag{10}$$

where R_0 is the mean bubble radius and $|x|$ is much less than one. It is emphasized that equation (10) is valid only for small volume pulsations in the linear region. Because the pulsations are small, and because the solution for the dual-frequency excitation method requires only first and second harmonics, cubic and higher order terms of the expansion are ignored [Ref. 19]. Substitution of equation (10) into equation (9) yields,

$$\rho R_0^2 (1 + x)\ddot{x} + \tfrac{3}{2}\rho R_0^2 \dot{x}^2 = (p_0 + 2\sigma/R_0)\left[1 - 3\gamma x + \tfrac{3}{2}\gamma(3\gamma + 1)x^2\right]$$

$$- [p_0 + (2\sigma/R_0)(1 - x + x^2)] - 4\mu(\dot{x} - x\dot{x}) + p_i \cos \omega_i t$$

$$+ p_p \cos \omega_p t. \tag{11}$$

Equation (11) is now a second-order differential equation for volume pulsation in terms of x.

The Dual Frequency Pump Method involves incident sound waves at two different frequencies. Therefore, a solution for x using dual frequency excitation includes the first harmonics (ω_i and ω_p), the second harmonics ($2\omega_i$ and $2\omega_p$), and the two sidebands ($\omega_i + \omega_p$ and $\omega_i - \omega_p$). With all frequencies included, the solution may be written as,

$$x = A_0 + A_1 \cos (\omega_i t + \varnothing_1) + A_2 \cos (\omega_p t + \varnothing_2)$$

$$+ A_3 \cos (2\omega_i t + \varnothing_3) + A_4 \cos (2\omega_p t + \varnothing_4)$$

$$+ A_5 \cos [(\omega_i + \omega_p)t + \varnothing_5] + A_6 \cos [(\omega_i - \omega_p)t + \varnothing_6]. \tag{12}$$

The solution for x contains the amplitudes A_j for the changes in radius during pulsations. For example:

A_0 = amplitude change of the average radius,
A_1 = first harmonic amplitude change for ω_i,
A_2 = first harmonic amplitude change for ω_p,
A_3 = second harmonic amplitude change for ω_i,

and so on. The phase angles $\varnothing_j$ are the relative phase differences between the incident wave and the particular harmonic pulsations. [Ref. 3, 19]

The goal of this development is to derive a set of equations giving the pressure amplitude in seawater as a function of the distance r from the bubbles insonified by the Dual Frequency Pump Method. These pressure amplitudes, when measured at discrete frequencies, can be used to determine the number of bubbles at each radius. The tools to do this have now been supplied. The amplitudes of the radius excursion, A_j, may be solved for by substituting equation (12) into equation (11). Algebra for this step is quite lengthy, so only the results are shown below. The problem–solving technique is simpler for a single sound wave (Miller's single sound wave reduces the assumed solution from seven terms to three) [Ref. 19]. Numerical values for the amplitudes of the radial pulsations in equation (12) are best solved with a computer using the following:

$$A_1 = p_i X_1 / \rho \omega_o^2 R_o^2 \tag{13}$$

$$A_2 = p_p X_2 / \rho \omega_o^2 R_o^2 \tag{14}$$

$$A_5 = A_1 A_2 X_{12} X_5 \tag{15}$$

$$A_6 = A_1 A_2 X'_{12} X_6 \tag{16}$$

where,

$$X_1 = \left[(1 - \Omega_1^2)^2 + \delta^2 \Omega_1^2 \right]^{-1/2} \tag{17}$$

$$X_2 = \left[(1 - \Omega_2^2)^2 + \delta^2 \Omega_2^2 \right]^{-1/2} \tag{18}$$

$$X_{12} = \left[\left(\frac{\Omega_1^2 + \Omega_2^2}{2} + \frac{3}{2}\Omega_1\Omega_2 + \frac{3\gamma(3\gamma+1)(p_o + 2\sigma/R_o) - 4\sigma/R_o}{2\rho R_o^2 \omega_o^2}\right)^2\right.$$

$$\left. + \left(\frac{\delta^2}{4}\right)(\Omega_5)^2\right]^{1/2} \tag{19}$$

$$X'_{12} = \left[\left(\frac{\Omega_1^2 + \Omega_2^2}{2} - \frac{3}{2}\Omega_1\Omega_2 + \frac{3\gamma(3\gamma+1)(p_o + 2\sigma/R_o) - 4\sigma/R_o}{2\rho R_o^2 \omega_o^2}\right)^2\right.$$

$$\left. + \left(\frac{\delta^2}{4}\right)(\Omega_6)^2\right]^{1/2} \tag{20}$$

$$X_5 = \left[(1 - \Omega_5^2)^2 + \delta^2\Omega_5^2\right]^{-1/2} \tag{21}$$

$$X_6 = \left[(1 - \Omega_6^2)^2 + \delta^2\Omega_6^2\right]^{-1/2}. \tag{22}$$

The parameter Ω is a dimensionless ratio relating the pump, image, and sideband frequencies to the resonance frequency ω_o of the bubble. That is,

$$\Omega_1 = \omega_i/\omega_o \qquad\qquad \Omega_2 = \omega_p/\omega_o$$
$$\Omega_5 = (\omega_i + \omega_p)/\omega_o \qquad\qquad \Omega_6 = (\omega_i - \omega_p)/\omega_o \tag{23}$$

The expression δ is the viscous damping coefficient without thermal and radiation considerations. It is written as

$$\delta = 4\mu/\rho\omega_o R_o^2.$$

The radiated pressures (fundamental and sideband) from the bubble excited by two frequencies may now be determined in terms of A_j using equations (13) through (23) [Ref. 3].

In order to derive the equation for pressures as a function of the distance from the bubble, it is necessary to model the bubble as a monopole radiator [Ref. 14]. A monopole radiator is really nothing more than a simple source. The equation for pressure at a distance r from a simple source is [Ref. 14]

$$\underline{p}_j\,(r,t) = j\rho_0 c\,\frac{Qk_1}{4\pi r}\,e^{j(\omega t - kr)}$$

Since the Dual Frequency Pump Method requires that only amplitude be considered, and not phase, the above equation can be rewritten as

$$\underline{p}_j\,(r,t) = \underline{P}_j\,e^{j(\omega t - kr)} \tag{24}$$

where the pressure amplitude is

$$P_j = \rho_0 c\,\frac{Qk_1}{4\pi r}\,. \tag{25}$$

Equation (24) represents the pressure amplitude for the jth frequency. Recall that

$$k_j = \omega_j / c \tag{26}$$

and for the pulsating sphere [Ref. 14]

$$Q = 4\pi R_o^2 U_o \tag{27}$$

40

where U_o is the speed amplitude. In order to solve equation (25) using amplitude changes, equation (27) must be in terms of the mean radius R_o and the amplitude changes A_j. It is shown in Appendix B that

$$U_o = R_o A_j \omega_j.$$

Therefore,

$$P_j = \rho_o \frac{Q\omega_j}{4\pi r}$$

$$= \rho_o \frac{4\pi R_o^2 U_o \omega_j}{4\pi r}$$

which yields

$$P_j = \rho_o R_o^3 A_j \omega_j^2 / r. \tag{28}$$

Equation (28) is the pressure amplitude at a distance r from a bubble under the influence of a sound wave at frequency ω_j. For the Dual Frequency Pump, the frequencies are $\omega_j = \omega_i$, ω_p, and $\omega_i \pm \omega_p$. The amplitudes are $A_j = A_1$, A_2, A_5, and A_6. Equations (13) through (22) are substituted into equation (28) to give the desired equation for pressure amplitude that results from the imaging, pump, and sideband energy reradiated by the bubble. These pressure amplitudes are P_1, P_2, P_5, and P_6, respectively, where P_5 and P_6 will be referred to as the upper and lower sideband pressure amplitudes P_+ and P_-, respectively.

The key equations are summarized below for P_1, P_2, P_+, and P_-:

$$P_1 = p_i \, X_1 \, \Omega_1^2 \, R_o/r$$

$$P_2 = p_p \, \acute{X}_2 \, \Omega_2^2 \, R_o/r$$

$$P_+ = \frac{p_i p_p \rho X_1 X_2}{\left(\rho \omega_o^2 R_o^2\right)} X_{12} \, X_5 \, (\omega_i + \omega_p)^2 \, R_o^3/r$$

$$P_- = \frac{p_i p_p \rho X_1 X_2}{\left(\rho \omega_o^2 R_o^2\right)} X'_{12} \, X_6 \, (\omega_i - \omega_p)^2 \, R_o^3/r.$$

V. L. Newhouse and P. M. Shankar simplified these equations because the imaging frequency is much greater than the pump frequency. It is possible to say

$$X_5 \approx X_1$$

$$X_6 \approx X_1$$

and

$$X_{12} \approx \omega_1^2/\omega_o^2. \text{ [Ref. 3]}$$

The advantage of dual frequency bubble detection can be demonstrated by examining the sum sideband pressure amplitude P_+. Consider a single bubble of resonance frequency ω_o. When the pump frequency sweeps past the bubble's resonance frequency ($\omega_p = \omega_o$), the bubble undergoes maximum oscillations. At this point, the sum frequency sideband pressure is at its peak and can be written as

$$P_+ = \frac{\rho p_i p_p}{(\rho \omega_o R_o)^2} \cdot \frac{R_o}{\delta} \cdot \frac{1}{r} . \tag{28a}$$

At all other frequencies, that is $\omega_p \neq \omega_o$, the expression for P_+ becomes

$$P_+ = \frac{\rho p_i p_p}{(\rho \omega_o R_o)^2} \cdot X_2 \cdot \frac{R_o}{r} . \tag{28b}$$

It should be noted that the X_2 term of equation (28b) contains the δ term of equation (28a) and the dimensionless frequency term Ω_2. When $\omega_p = \omega_o$, the Ω_2 term is equal to one and equation (28b) becomes equation (28a). In equation (28a), with the pump frequency equaling the bubble resonance frequency, the pressure amplitude of the sideband is proportional to the mean bubble radius R_o. At all other frequencies, the upper sideband pressure amplitude is proportional to both X_2 and R_o as shown in equation (28b). This is significant because the sideband pressure P_+ radiated by the bubble provides a maximum pressure amplitude for a particular bubble radius, even though that sideband pressure amplitude is much smaller than that of the pump pressure amplitude P_2. For a single bubble, Figure 4 shows the correlation between the sideband pressure amplitude P_+ of curve "a" and the pump pressure amplitude P_2 of curve "b" when plotted as a function of the pump frequency f_p in kHz. Figure 4 demonstrates that, for a single bubble, the maxima, or spikes, of both pressure amplitudes coincide with the resonance frequency of the bubble. [Ref. 3]

If the sideband pressure amplitude P_+ and the pump pressure amplitude P_2 are plotted as a function of the mean bubble radius, the difference between single-frequency resonance excitation and the

difference between single-frequency resonance excitation and the dual-frequency pump method becomes clear. Figure 5 shows the pump pressure amplitude on curve "b" and the sideband pressure amplitude on curve "a" plotted against the mean bubble radius. This means Figure 5 considers bubbles of many radii with the frequency of the pump sound field fixed. While the pump pressure amplitude has a local maximum pressure at the point where bubbles of corresponding resonance frequency $(\omega_p = \omega_0)$ are emitting maximum energy, the pump pressure amplitude rises above that local maximum as energy is reflected from the larger, nonresonating bubbles. The sideband pressure amplitude P_+ of curve "a," however, still maintains a single sharp peak for the one bubble radius undergoing resonance and does not show any sound energy reflected from larger bubbles. Sound pressure from the nonresonant bubbles is not present in the sideband pressure peak. The reason for this difference lies in the fact that sideband production is a nonlinear process which occurs only when the pulsation amplitude is large. In general, only resonant bubbles undergo large enough pulsations to produce the sidebands. Larger, nonresonant bubbles scatter significant amounts of the pump and imaging fields, but their pulsation amplitude is too small to produce the sidebands. Thus, the Dual Frequency Pump method can distinguish bubbles of different sizes much better than single-frequency excitation. [Ref. 3]

44
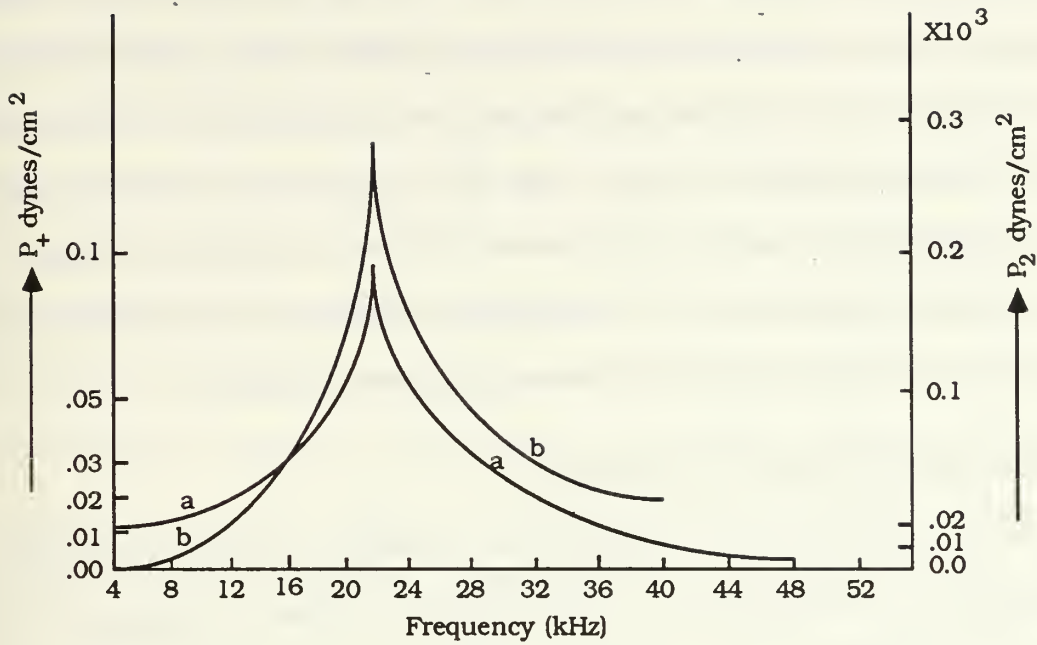
Figure 4

Pressure Amplitude (P_2 and P_+) vs. Frequency (f_p)

Source: Ref. 3:1475
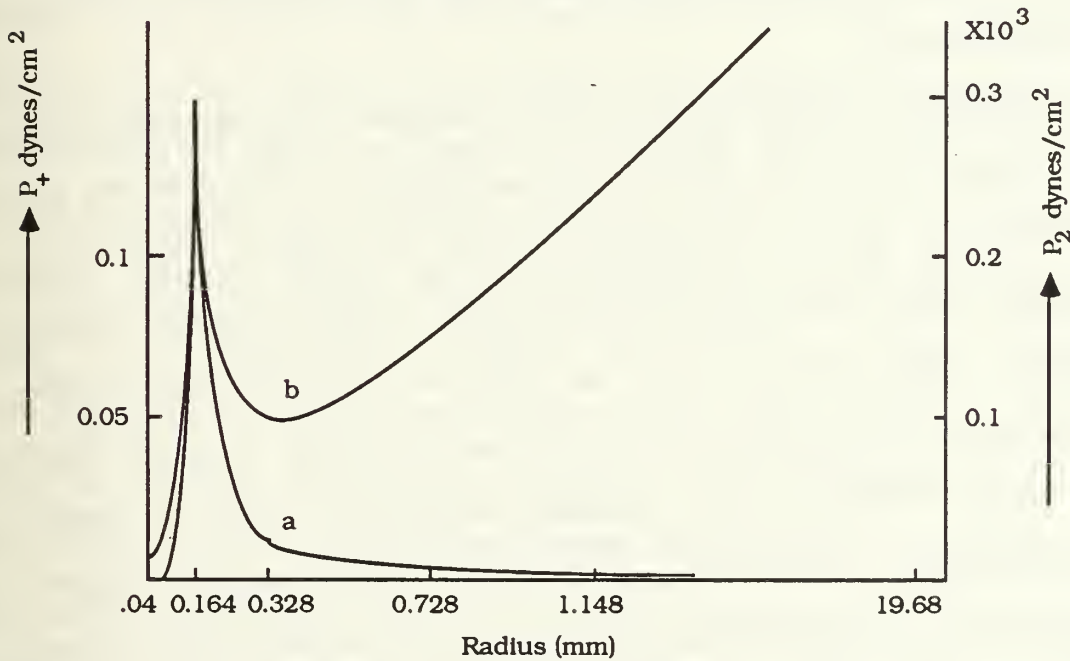
Figure 5

Pressure Amplitude (P_2 and P_+) vs. Radius (R_o)

Source: Ref. 3:1475

45

When bubbles of different radii are irradiated with both the pump and imaging fields, several "sum–difference" sideband pressure peaks corresponding to those various bubble radii will be present. The magnitudes of these pressure peaks give an indication of how many bubbles of a particular radius are present. The methods of determining the number of bubbles of a particular radius will be discussed further in the "Considerations" section of the next chapter.

C. TRANSDUCER BEAM PATTERNS

It is now necessary to consider the volume of water insonified while sampling the bubble cloud. This sample volume is important in determining the bubble cloud density. Because the sample volume is specifically determined by the beam patterns of the imaging and pump transducers, the final theory section will study far field beam patterns and their importance.

The first step in defining the sample volume is to examine the near and far field of the transducer's beam pattern. Sound waves in the near field have pressure amplitude "nulls" and phase shifts as a function of the range which are undesirable when using sound to make measurements. Sound waves in the far field are expanding spherically and the pressure amplitudes decrease only as a function of range from the sound source. There are no pressure amplitude "nulls" or phase shifts in the far field. Therefore, it is best to have the target of interest in the far field, where calculation of the sound pressure amplitudes is easiest. Several methods of calculating the start of the far field are available. Here, a conservative estimate of the far field range will be

derived. Also, the angular beam widths are needed to define the sample volume. These angular beam widths and far field points for both pump and imaging sound field transducers will be calculated for representative frequencies used by the Dual Frequency Pump method.

The Dual Frequency Method of bubble detection is based on sensing the radiated pressure amplitudes of the bubbles at the side-band frequencies of the imaging sound field ($\omega_l \pm \omega_p$). In calculating the transmitted pressure amplitudes at the point where the bubbles are located, both the pump and imaging sound waves are considered to be planar at that location. Insonifying the target bubbles with sound waves independent of phase and without nulls requires that the bubbles be in the far field of the transducer beam. To find expressions for the start of the far field for both the pump and the imaging trans-ducers, it is easiest to take a linear systems approach. The physical situation can be described as a volume–type aperture serving as one of the transducers shown in Figure 6. A volume aperture is a description which can apply to any shape of sound source which is transmitting acoustic signals. Figure 6 shows the vector $\underline{r}$ from the coordinate origin to the target point in space. The vector $\underline{r}_0$ is from the coordi-nate origin to a point on the surface of the volume aperture and iden-tifies the location of each sound source. The volume aperture can be either the pump or imaging transducer which transmits sound energy or, due to reciprocity, can be the receive transducer which senses the radiated sound energy from the bubbles. The velocity potential solution to the wave equation can be written in terms of the free space

47

Green's function. It is from Green's Function that the near and far fields of the transducer beam pattern are defined. [Ref. 20]

The free space Green's Function can be written as

$$g(\underline{r}/\underline{r}_0) = \frac{\exp\left[-jk\left|\underline{r} - \underline{r}_0\right|\right]}{\left|\underline{r} - \underline{r}_0\right|},$$

where

$$k = 2\pi/\lambda.$$

Here, the $\left|\underline{r} - \underline{r}_0\right|$ range term appears as both an amplitude (denominator) and a phase (exponential). To determine the point where phase is no longer a factor, it is necessary to define the maximum extent of the near field. Green's Function is used for this purpose, and after undergoing a binomial expansion can be written as

$$g(\underline{r}/\underline{r}_0) \approx \frac{\exp(-jkr)}{r} \exp\left[jk(\hat{a}_r \cdot \underline{r}_0)\right] \exp\left[-jk(r_0^2 - (\hat{a}_r \cdot \underline{r}_0)^2/2r)\right] \quad (29)$$

where $\hat{a}_r$ is a unit vector in the direction of $\underline{r}$. The last complex term of equation (29) is the critical expression in determining the near field. It is written as

$$\exp\left[-jk(r_0^2 - (\hat{a}_r \cdot \underline{r}_0)^2/2r)\right]. \quad (30)$$

The magnitude of the exponential argument in equation (30) is written as

$$\pi\left[r_0^2 - (\hat{a}_r \cdot \underline{r}_0)^2\right]/\lambda r$$

48
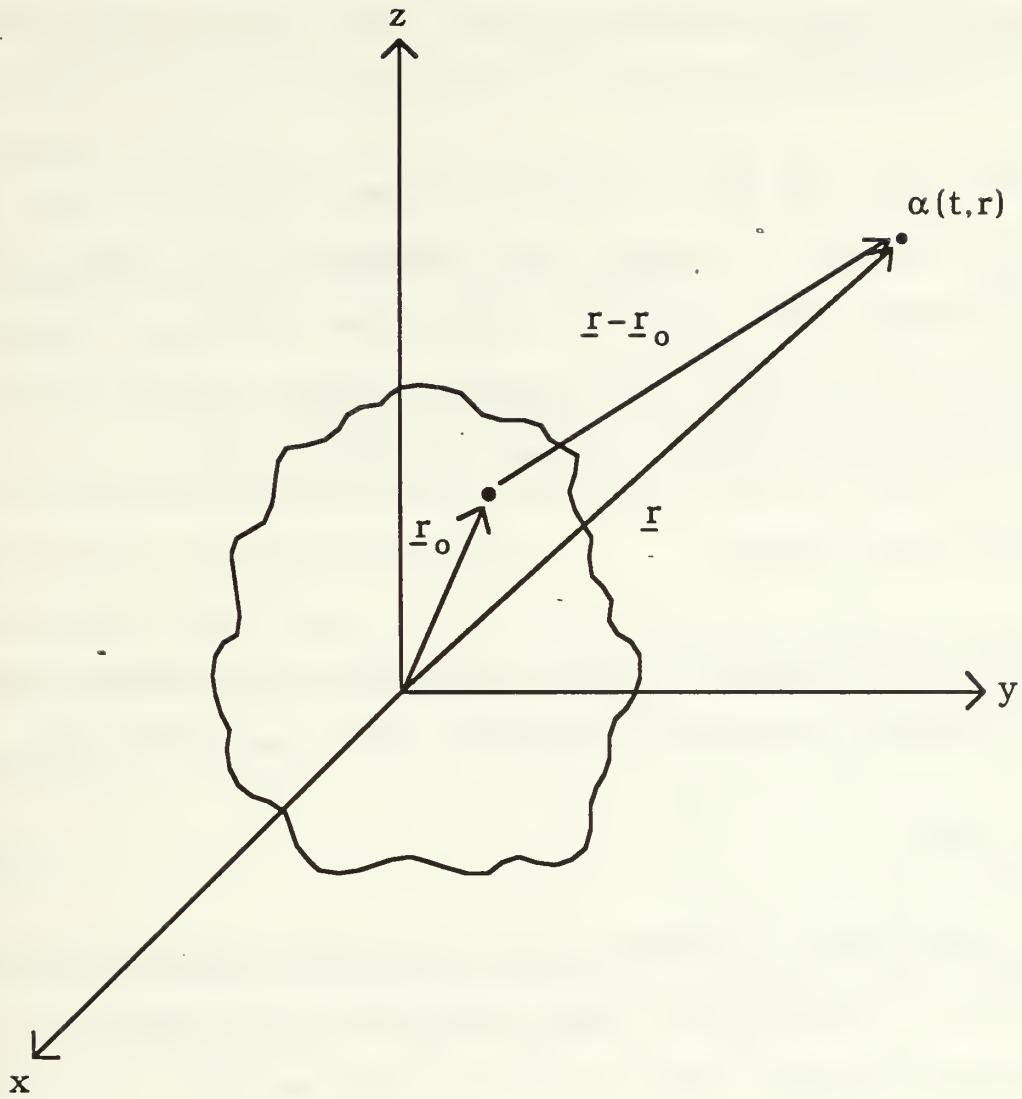
Figure 6

Volume Aperture Transducer

Source: Ref. 20:2

49

and can be rearranged to yield

$$\frac{\pi\left[r_o^2 - (\hat{a}_r \cdot \underline{r}_o)^2\right]/\lambda}{r}.$$ (31)

Equation (30) will be a significant phase term of the free space Green's Function if equation (31) becomes large. Equation (31) becomes large if the numerator is larger than the range r. Because it is defined as the region having significant phase, equation (31) can be used to define the near field. Phase is significant when

$$r < \pi\left[r_o^2 - (\hat{a}_r \cdot \underline{r}_o)^2\right]/\lambda.$$ (32)

A Fresnel approximation is now used, which is equivalent to setting the dot product in equation (32) equal to zero, that is [Ref. 20]

$$(\hat{a}_r \cdot \underline{r}_o)^2 \to 0.$$

If the worst case is considered, the radial aperture distance r_o can be replaced by the maximum radial dimension of the aperture R. The final form of equation (32), the extent of the near field, is now written as

$$r < \pi R^2/\lambda,$$ (33)

where

r = range from the transducer
R = maximum radial dimension of the transducer
λ = wavelength of transmit signal.

Further manipulation of the transmitted acoustic signal with Fourier Transforms yields the Near Field Directivity Function D(f,r, α) in terms of the complex aperture function (A_T), spatial frequencies (α), and range (r) [Ref. 20]. It is

$$D_T\ (f,r,\alpha) = \int_{r_o} A_T\ (f,\underline{r}_o)\ e^{-jkr_o^2/2r}\ e^{j2\pi(\underline{\alpha}\cdot\ \underline{r}_o)}\ dV_o \qquad (34)$$

The Near Field Directivity Function describes a beam pattern which does not assume plane waves over a small space since the directivity is a function of the range and phase terms.

As previously mentioned, it is desirable to be in the far field, where the directivity is not a function of range. The far field point is now defined as

$$r > \pi R^2/\lambda. \qquad (35)$$

The Far Field Directivity Function is obtained by using Green's Function and a Fraunhofer approximation [Ref. 20]. The result is

$$D_T\ (f,\alpha) = \int_{V_o} A_T\ (f,\underline{r}_o)\ e^{j2\pi(\underline{\alpha}\cdot\ \underline{r}_o)}\ dV_o\ . \qquad (36)$$

Equation (36) is not a function of range and therefore will be used with equation (35) to develop transducer placement for the Dual Frequency Method of bubble detection. While it is not important to understand all the terms of equations (34) and (36), it is important to see that the acoustic frequency, the physical size of the transducer,

and the range to the target point from the transducer are key factors in determining beam patterns.

Previously, the general physical situation was that of a transducer considered to be a volume aperture (Figure 6) from which the general form of the Far Field Directivity Function (equation (36)) was obtained. It is now possible to be more specific. The transducers to be used in the Dual Frequency Pump method of bubble detection are closely approximated by planar, circular piston apertures. The circular piston aperture is shown in Figure 7. The general expression for complex aperture function is written in polar coordinates as

$$A(f,r,\varnothing) = a(f,r,\varnothing) \; e^{j\varnothing(f,r,\varnothing)} .$$

Circular symmetry is assumed for both the above aperture function and the Far Field Directivity [Ref. 20]. Therefore, they can be written as

$$A(f,r,\varnothing) = A_r(f,r) = \begin{cases} 1, & r \leq a \\ 0, & r > a \end{cases}$$

and

$$D(f,\theta,\psi) = H_0 \{A_r (f,r)\},$$

where H_0 is the zero order Hankel Transform [Ref. 20]. The Directivity Function is independent of the angle due to circular symmetry. Because the Hankel Transform can be written as

$$H_0 \{A_r (f,r)\} = 2\pi \int_0^a rA_r(f,r)J_0 \left(\frac{2\pi r}{\lambda} \sin \theta \right) dr,$$

52
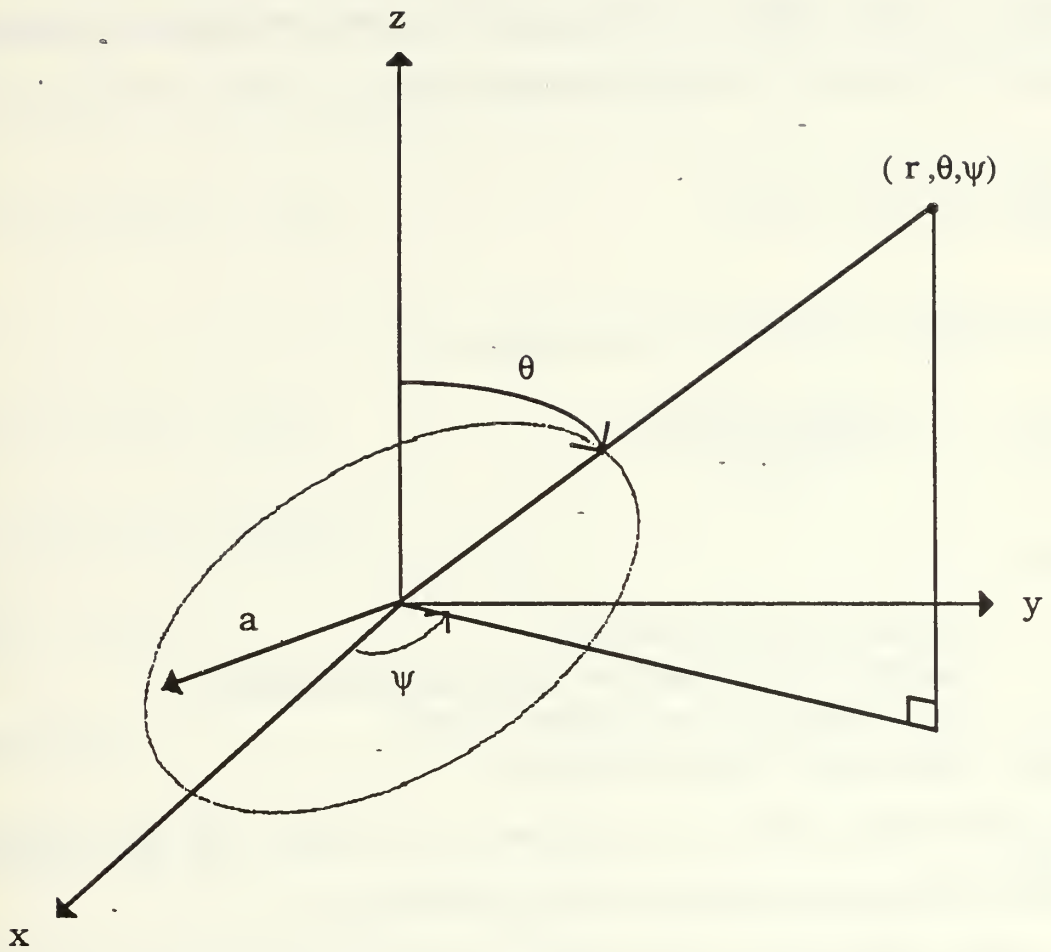
Figure 7

Circular Piston Aperture

Source: Ref. 20:80

53

the Far Field Directivity Function of the circular piston is

$$D(f,\theta) = 2\pi \int_{0}^{a} rJ_0\left(\frac{2\pi r}{\lambda}\sin\theta\right) dr$$

where "a" is the radius of the transducer face as shown in Figure 7. Using the identity for Bessel Functions

$$\int_{0}^{x} \alpha J_0(\alpha)\, d\alpha = xJ_1[x],$$

the Directivity Function is now written as

$$D(f,\theta) = a\,\frac{J_1\,[(2\pi a/\lambda)\sin\theta]}{\sin\theta/\lambda}, \tag{37}$$

where

a   = radius of the transducer
θ = angle off of transducer axis (half beamwidth)
λ = wavelength of transmitted sound
$J_1(x)$ = first–order Bessel function.

The normalizing factor for equation (37) is given by the directivity along the transducer axis, and can be written as

$$D(f,\theta)\,|_{\theta=0} = \pi a^2.$$

Therefore, the Normalized Far Field Directivity Function is

$$D_N(f,\theta) = \frac{2J_1[(2\pi a/\lambda)\sin\theta]}{(2\pi a/\lambda)\sin\theta}. \tag{38}$$

In order to define the volume of seawater that will be insonified by the transducers, equation (38) must be used to determine the beamwidths of the main lobes at their 3 decibel down points. No standard value for the ratio of intensities has ever been established for determining the beamwidth, but 3 decibels has been used by many authors and will be used here [Ref. 14]. Letting

$$20 \ Log_{10} \ D_N \ (f,\theta) = -3 \ dB \qquad\qquad (39)$$

so that

$$D_N \ (f,\theta) = \sqrt{2}/2 = .7079$$

then equation (38) becomes

$$\frac{2 \ J_1 \ [x]}{x} = .7079$$

by substituting

$$x = [(2\pi a/\lambda) \ \sin \theta]. \qquad\qquad (40)$$

A solution can be found for x by referring to a standard table of first–order Bessel Functions for a circular piston [Ref. 14]. The result is x = 1.614. The half angle θ of the beams can now be calculated for each transducer using equation (40). The results of the far field determinations (equation (35)) and the beamwidths are given in Table II. The sound speed in seawater was assumed to be 1,500 meters/second. This information provided a basis for determining

transducer placement and calculating the volume of seawater which contained the target bubbles. A total of three transducers were used during the experiment. Two high–frequency transducers provided the imaging sound field and the receiver, and the third transducer provided the pump sound field. Table II results are for pump frequencies of 100 and 500 kHz, and an imaging frequency of 2.25 MHz to reflect samples of the frequencies used.

TABLE II

TRANSDUCER BEAM PATTERN DATA

	Pump Transducer 100 KHZ	Pump Transducer 500 KHZ	Imaging Transducer 2.25 MHz
Wavelength λ	.015 m = 1.50 cm	0.003 m = 0.3 cm	0.00067 m = 0.067 cm
Radius a	0.5 inches = 1.27 cm	0.5 inches = 1.27 cm	.125 inches = .318 cm
Far Field r>	1.3 inches = 3.38 cm	6.65 inches = 16.89 cm	4.74 cm
1/2 Beamwidth θ	17.66°	3.48°	3.10°
Total Beamwidth 2θ	35.32°	6.96°	6.20°

III. PROBLEM APPROACH

A. OVERVIEW

As discussed in the introduction, the goal of this thesis experiment is to show that the Double Frequency Pump technique is practical for ship wake bubble density measurements. Chapter II provided the basic theoretical background for calculating the resonance frequency of different size bubbles, the pressure amplitudes at the sum-difference sidebands, and the far-field beam patterns of the transducers.

Other factors to be considered in the practicality of this bubble detection technique include the frequency range of the swept pump sound field, the sideband pressure amplitudes, sample volume placement and sizes, distructive interference, bubble screening, transducer orientation, and transducer response. The statistical sample time that a point in the bubble cloud is measured and the imaging frequency are also important.

B. CONSIDERATIONS

1. Pump Frequencies

Knowing the range of resonance frequencies for the different bubble sizes present is essential so that the correct pump frequencies can be used. In order for the bubbles to radiate the maximum amount of sound energy at the dual-frequency sidebands $(\omega_i \pm \omega_p)$, the bubbles

58

must be driven at resonance. The bubble sizes chosen here are those ranging in radius from approximately 10 to 170 micrometers (μm). Bubbles much smaller than 5 μm in radius resonate at very high frequencies and do not affect sound of particular interest to the surface ship wake problem at the ocean surface. Due to the effects of diffusion, small bubbles diffuse and disappear into the water. Larger bubbles (above the 170–200 μm radius range) tend to rise quickly or split up into smaller bubbles, and therefore do not persist very long in the wake.

In order to drive the bubbles present in the bubble cloud at resonance, the selection of the pump frequency range and the pressure amplitude (p_p) is important. However, these characteristics also control the harmonics produced as the bubbles react to the pump sound field. Harmonics of the pump sound field and the resonating bubbles are critical because they can create background noise at higher frequencies. If the pump field frequencies (ω_p) are of a very wide range, the harmonics (each of wide frequency) extend farther up the frequency spectrum. If the pump field amplitude is too high, the harmonics created by bubble resonance will be multiple, and again the result is the same. Harmonics can defeat the detection of the dual-frequency sidebands about the imaging frequency if the resonance harmonics extend to high enough frequencies. If the pump frequency range is small, the harmonics induced will have a short frequency range and, therefore, will not extend to higher spectrum frequencies. If the pump pressure amplitudes (p_p) at the bubble location are kept low (yet large enough to resonate bubbles), the number harmonics will

be less and the result the same; the harmonics will not extend to higher frequencies on the spectrum.

2.   Sideband Pressure Amplitude

The pressure amplitude of the sum sideband (P_+) that is calculated using equations (28a) and (28b) makes it possible to determine the exact number of bubbles of a specific radius present within a given sample, or measurement, volume. This is done by calculating the radiated pressure amplitude (P_+) for each bubble radius present and then comparing the results with the actual received pressure amplitudes. Table III contains sample results from equations (28a) and (28b). Appendix C contains a listing of a simple Fortran program which will calculate the P_+ amplitudes for bubbles using equations (28a) and (28b). The Fortran program uses input values for pump pressure amplitude (p_p) and imaging pressure amplitudes (p_i) that are calculated in Appendices D and E. The bubbles were assumed to be at a distance (r) of 6.7 cm from the transducer. An example of the output at one atmosphere of pressure is plotted in Figure 8 for a single bubble. The curve that has been plotted is not actual data, but only represents the pressure amplitude as it rises from the noise. The data points are the computer results. Figure 9 is plotted for bubbles of the same radii as that shown in Tables I and III (same curve estimates as Figure 8). For the sideband pressure calculation to be accurate, the location of the target bubbles relative to the transducers must be known. Also, the size of the volume in which the bubbles are located is important. This volume of water where the bubbles are detected

TABLE III

THEORETICAL CALCULATION RESULTS FOR
UPPER SIDEBAND PRESSURE AMPLITUDES

BUBBLE RADIUS (cm)	RESONANCE FREQUENCY (kHz)	SUM SIDEBAND PRESSURE PEAK (dynes/cm^2)	SUM SIDEBAND PRESSURE NOISE (dynes/cm^2)
0.0010	324.1	0.0010	0.000429
0.0020	162.1	0.0040	0.000925
0.0040	81.0	0.0161	0.001890
0.0060	54.0	0.0362	0.002846
0.0080	40.5	0.0643	0.003801
0.0090	36.0	0.0814	0.004277
0.0100	32.4	0.1004	0.004754
0.0120	27.0	0.1446	0.005707
0.0150	21.6	0.2260	0.007135
0.0170	19.0	0.2903	0.008088
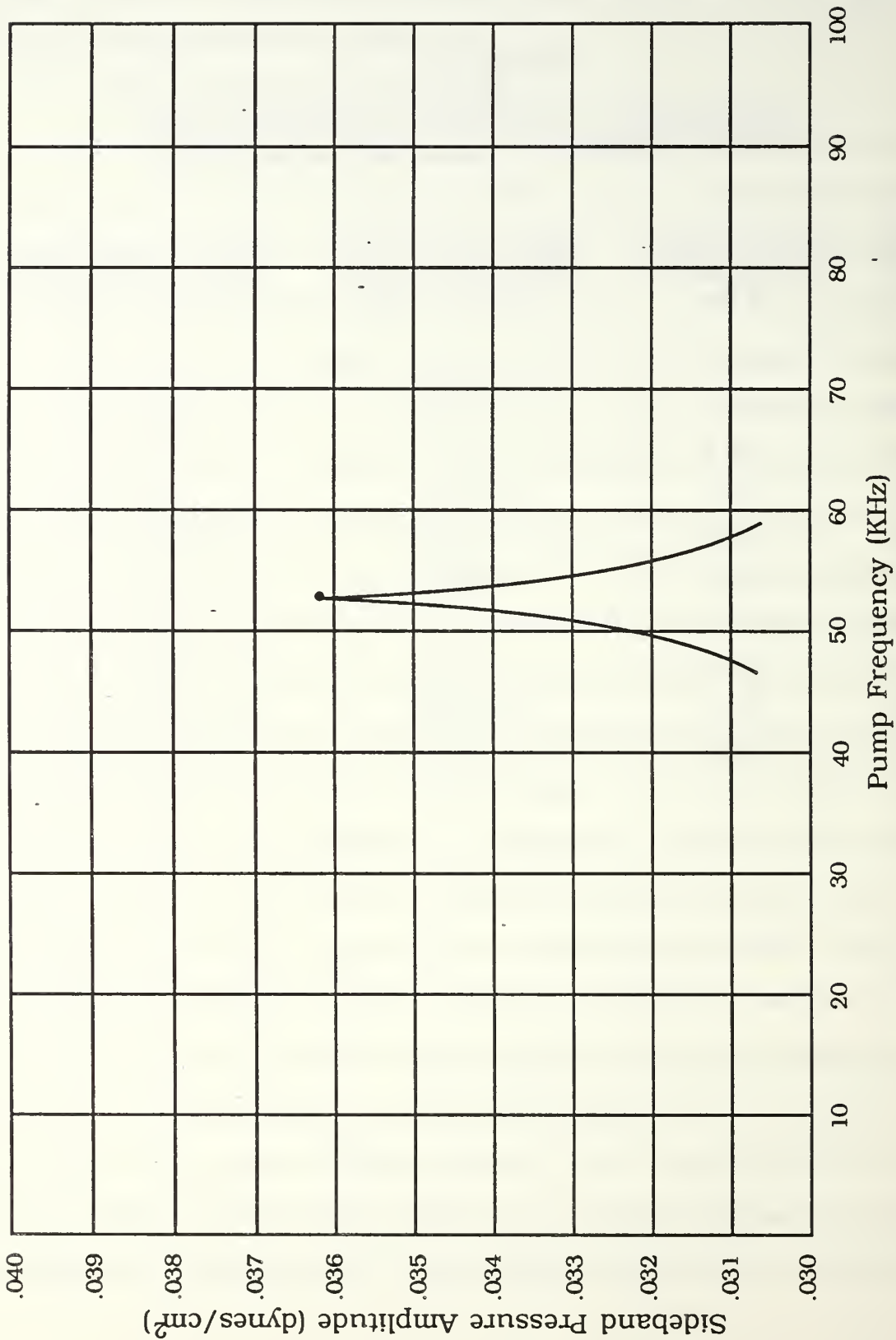
Figure 8. Plot of Computed Sideband Sound Pressure Amplitude
For a Single Bubble of Sixty Micron Radius

62
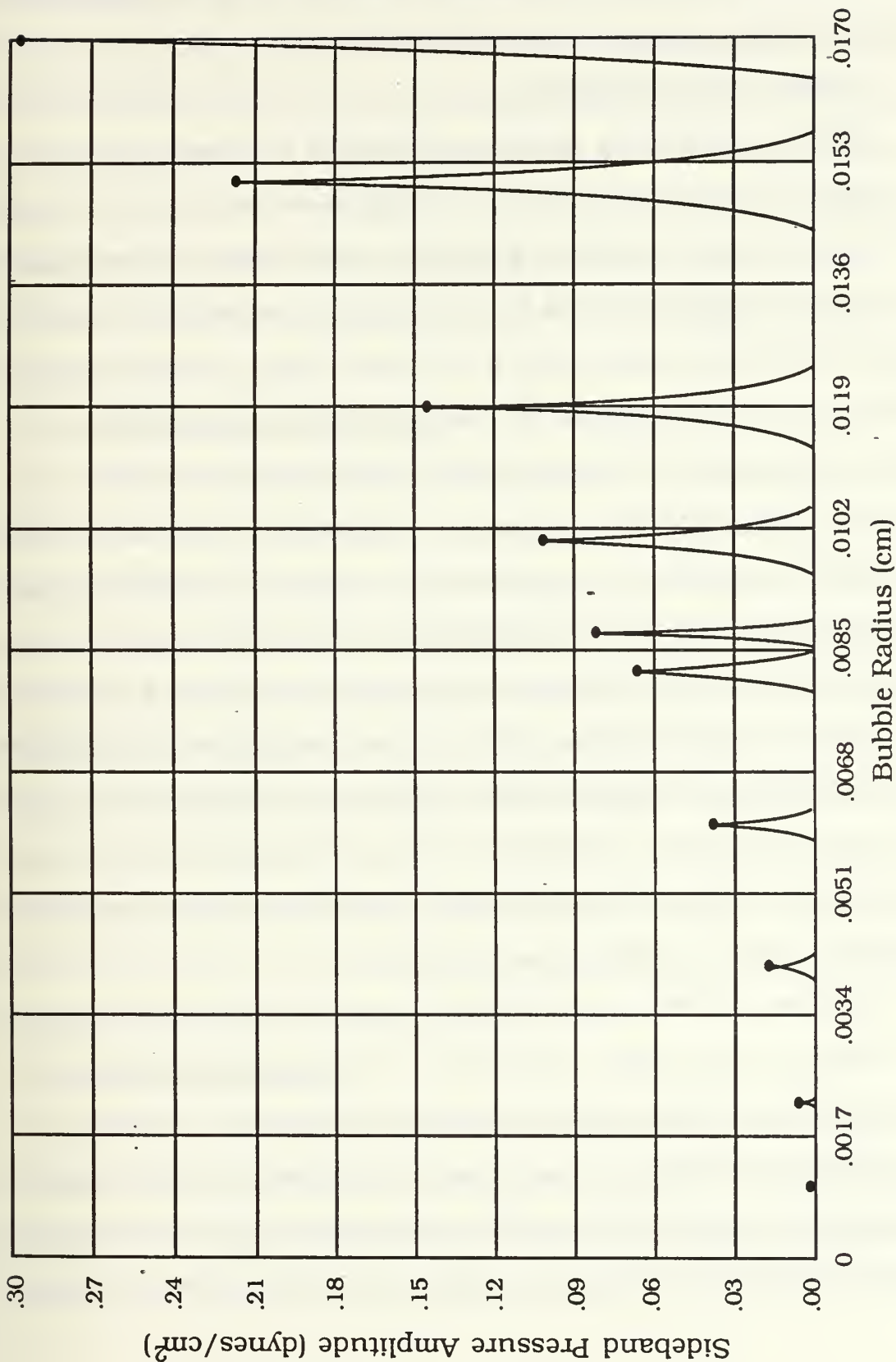
Figure 9. Computed Sideband Sound Pressure Amplitudes
For Bubbles of Many Different Radii

63

and measured will be called the sample volume. Sample volume considerations are discussed in the next three sections.

3.   Sample Volume Placement

The first parameter which could define a sample volume is the Far Field of the beam pattern. As mentioned in the section of Chapter II on Transducer Beam Patterns, it is considered desirable that the target bubbles lie in the far field of the beam pattern to avoid the "nulls' and phase shifts found in the near field. In the far field, the radiated pressure amplitude of a sound source drops steadily proportional to the inverse of the range [Ref. 14]. The equations for calculating the sum–difference pressure amplitudes (28a and 28b) require that the pump and image sound pressure amplitudes be known at the point where the target bubble is located. It is easiest to calculate the pump and imaging sound energy present at the location of the bubbles in the far field. Due to the principle of reciprocity, which now considers the target bubble as the sound source, it is also desirable that the target bubble be in the far field of the receive transducer so that the sideband pressure amplitude P_+ may be accurately calculated at the receive transducer face.

Placement of the target bubbles in the far field of the beam pattern appears to be ideal. However, it is important to provide enough imaging and pump sound pressure to the bubbles to create the sideband pressure amplitudes and raise them above the noise level. Dr. P. M. Shankar noted that it may be necessary to locate the imaging and pump transducers close to the bubble cloud, that is in the near

64

field, to provide the bubbles with these pressures [Ref. 21]. The receiver may also need to be close to the bubble cloud to detect the sound pressures reflected and radiated by the bubbles. It is possible to make this argument in favor of a near field sample volume placement, despite the fact that it complicates the calculations of the imaging and pump pressure amplitudes (p_1 and p_2) presented to the bubbles. The effects of transducer placement closer to the target bubbles will, therefore, be examined.

4. Destructive Interference

Consider the example of two bubbles of exactly the same radius within a sample volume where all transducer beams (Pump, Image, and Receive) meet. It is possible for destructive interference to occur due to differences in the range from the receive transducer while the bubbles are emitting sound energy at the sideband frequency, $\omega_i + \omega_p$. This results in the possibility of not recording the full P_+ amplitude for two bubbles in the sample volume at the same time. The likelihood of destructive interference can be reduced by designing a small or a thin sample volume in order to reduce the probability of two or more bubbles of the exact size being present in the sample volume at the same moment.

5. Bubble Screening

Bubble screening could also cause a false recording of the sideband pressure amplitude for a particular bubble. Bubble screening occurs when a large bubble blocks the radiated energy from a smaller, resonating bubble [Ref. 12]. Again, a possible solution would be the

design of a small or thin sample volume so that the receive transducer has a clear view of all bubbles passing through the sample volume. Fewer bubbles in the smaller volume cause less screening. Having bubbles present outside the sample volume would also screen the bubbles as they radiated sideband sound pressures.

6.   Sample Volume Size

The factors of far field, destructive interference, and bubble screening all favor the use of a small sample volume to measure bubble density at points within a bubble cloud. These factors also favor isolating the sample volume from the bubble cloud. The bubble cloud could screen the sound from the sample volume. The placement of the imaging and receiving transducers can be used to determine-the sample volume size. Table II provided values for the far field points and beam widths for the 2.25 MHz imaging and receive transducers. Using the Table II values produces a calculated sample volume of approximately .107 cm^3. The calculations and assumptions are shown in Appendix F. This sample volume may to be small enough to eliminate substantial bubble screening or destructive interference.

7.   Transducer Orientation

Another important consideration which determines transducer placement is the direction that the transducers are pointed. It is undesirable to directly radiate the face of the receive transducer with either pump or imaging sound fields. Direct irradiation increases the probability of raising the noise level and obscuring the desired dual–frequency sidebands. In addition, direct irradiation can result in

the generation of sum–difference sidebands. In the Shankar and Newhouse experiment, the image and receive transducer beams intersected at right angles. The pump transducer was set slightly off the vertical in a downward–looking configuration. The pump transducer orientation used by Shankar and Newhouse was compared to an upward–looking transducer in our experiment.

8.   Transducer Frequency Response and Side Lobe Effects

Another factor in considering the sound pressures provided to the bubble by the imaging and pump transducers is the frequency response of each transducer. The section on transducer beam patterns in Chapter II pointed out that the output of the transducer is dependent on the input signal. If the frequency of the input signal is varied, the acoustic output at a fixed distance from the transducer face will also vary depending on the frequency response of that particular transducer. This is not a problem for the imaging transducer as the image frequency ω_i is fixed. The acoustic output is, therefore, also fixed. However, it is a problem for the pump transducer as the pump frequency ω_p is swept. The pump transducer will not provide flat sound pressure amplitude values at a fixed point in space when the pump frequency is swept and, therefore, does not provide a fixed value of p_p to be used in equations (28a) and (28b). Some examples of the different sound pressure levels for the pump transducer frequency response and calculations of the pump pressure amplitude (p_p) from those levels are provided in Appendix D. Shankar and Newhouse also encountered this frequency response problem in their original Dual

Frequency bubble detection work [Ref. 12]. They solved the problem by slowly stepping through the pump frequencies and adjusting the power of the input electrical signal to the pump transducer. Adjusting the input electrical power at the different frequencies gave a fairly flat frequency response of the pump sound field and allowed the calculations of equation (28a) and (28b) to be carried out [Ref. 21]. This method of obtaining flat frequency response is fine in the laboratory, but would prove difficult due to the bubble detection problem in surface ship wakes. Surface ship wakes generate bubble clouds of unknown size distribution; therefore a constant acoustic pressure level at all frequencies is necessary. One of four methods might be available to obtain the correct output. The first might be to control the input level to the pump transducer with a computer so that as the frequency range of interest is swept the power is adjusted. A graphic equalizer performs the same function. The second might be to find a high-quality transducer that has a flat frequency response over the range of pump frequencies used. The use of several pump transducers of different center frequencies to cover the pump frequency range may also work. Third, a high-quality, calibrated broadband noise source may provide equal levels of acoustic energy to the sample volume at all the pump frequencies. Lastly, a computer could solve the problem by calculating the sideband pressure amplitudes for every different input pump pressure amplitude.

Yet another source of inaccurate bubble measurement using acoustic means could be the energy transmitted or received by the

side lobes of the transducers. It is not likely that side lobes are a problem because the first side lobe of a circular planar transducer is approximately 17 decibels down from the main lobe [Ref. 20]. Due to the relatively small amounts of energy available from the resonating bubbles, side lobes are probably not a factor in the accuracy of bubble detection or the transducer placement.

9. Statistical Sample Times

Assuming that the Dual Frequency Pump Method detects and counts the bubbles passing through the sample volume, it should also be considered as to how many sample volumes must be "looked at" by the receiver to consider the bubble density measurement accurate. The number of sample volumes "looked at" can be converted to the time duration of the "look," if the speed of either the measurement device or the bubbles passing through the device is known.

The number of sample volumes necessary to make the bubble density measurement statistically accurate for a given bubble stream is given by a general sample size equation [Ref. 22]. This equation is written

$$n = \frac{1}{4} \left[\frac{z_{\alpha/2}}{E} \right]^2 \tag{41}$$

where,

n $\equiv$ number of samples

$z_{\alpha/2}$ $\equiv$ confidence factor from the normal standard distribution tables

E $\equiv$ maximum allowed error

69

Once the number of sample volumes necessary is determined by using equation (41), the duration of the sample is calculated using the speed of the bubbles and the dimensions of the sample volume, specifically the sample volume length. Appendix G provides an example of this calculation technique using a bubble rise speed of 1.50 cm/s [Ref. 23]. The statistical sample duration, for example, needed to provide a 95-percent confidence factor and only 5-percent error is approximately 132 seconds.

C. EXPERIMENTAL PROCEDURE

This study of dual frequency bubble detection was carried out in three phases. The first phase was conducted in a small ten-gallon aquarium. It used fresh water for the purpose of making initial measurements, adjustments, and calibration. The second phase was also conducted in the ten-gallon aquarium, but this time using seawater. This phase was used to test the seawater medium and to test or refine different transducer arrangements. The third and final phase was carried out in a large, acoustically insulated fresh-water tank to investigate the effects of an acoustically quiet environment on bubble detection. The large insulated tank measured approximately four by two by three (4 x 2 x 3) meters.

As mentioned previously, the first two phases of the experiment for the Dual Frequency Pump Method were done in a ten-gallon aquarium. This experimental setup is shown in Figure 10. The aquarium was first filled with purified deionized water produced in the laboratory, and later with seawater drawn from the Hopkins Marine Station in
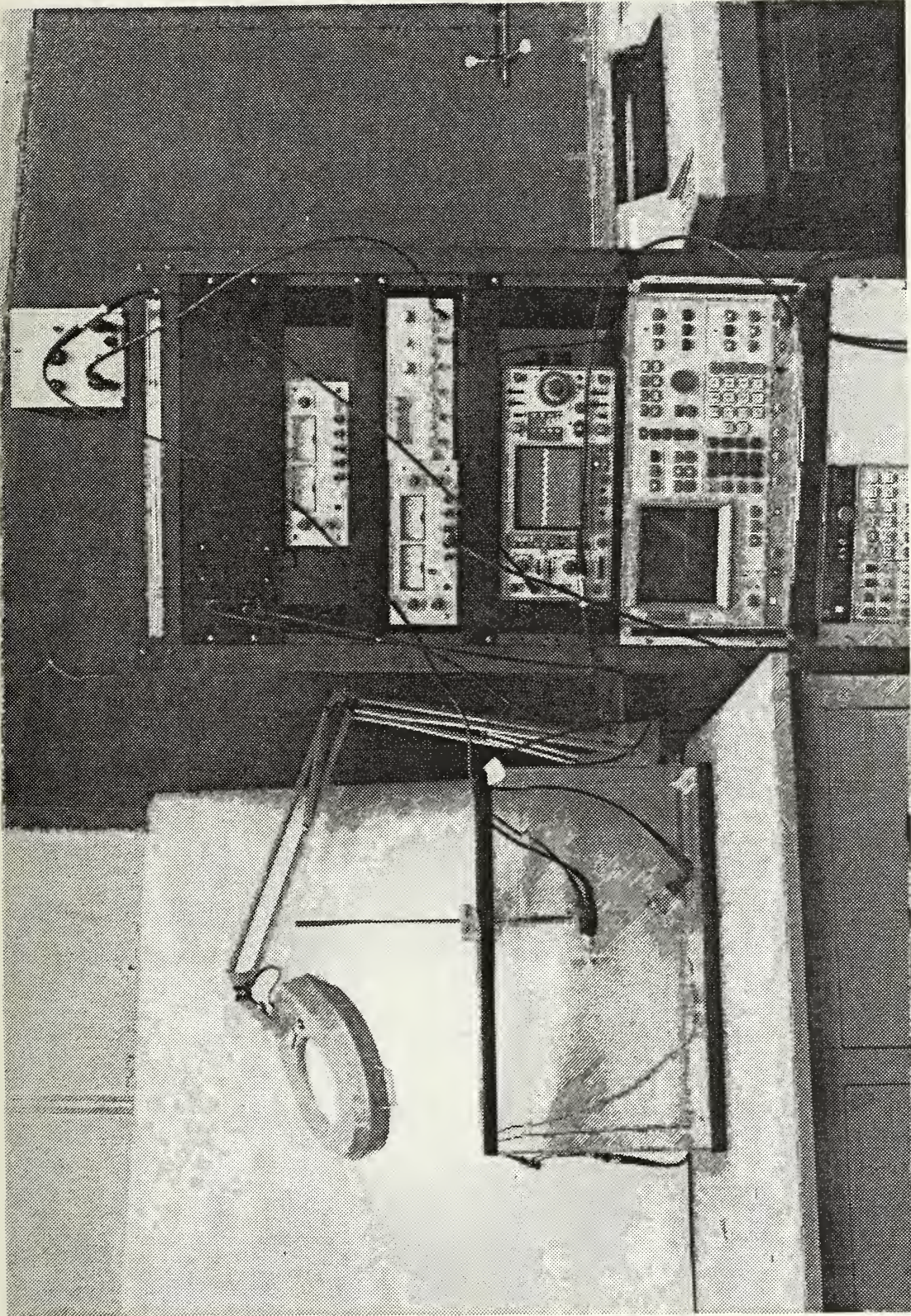
Figure 10. Experimental Aquarium Setup and Equipment Rack

Monterey. The seawater was relatively clean and closely approximated the salinity of open ocean seawater.

Bubble generation techniques were briefly investigated with electrolysis being selected as the best method. Electrolysis provided for easy and controllable bubble clouds and generated bubbles of the size closest to those found in surface ship wakes. Insulated brass wire with the ends exposed was found to produce the fewest by-products and the best bubbles. The brass wire was laid on the bottom of the aquarium and the bubbles were allowed to rise through the sample volume of the transducer beam patterns under their own buoyancy. Power for bubble generation was supplied by an HP 6237B Power Supply and varied between .5 and 10 volts. Both large bubble clouds and small bubble streams were generated by varying the voltage to test the effects of bubble screening.

The transducers were fixed within the aquarium (AQ), and later in the large acoustic tank (LT), using plexiglass mounts. Three transducers were used during the entire experiment. For testing in the aquarium, both the imaging (center frequency 2.25 MHz) and receive (center frequency 2.25 MHz) transducers were mounted in the same plane at a 90-degree angle to each other as shown in Figures 10 and 11. This transducer mount had two sets of holes available for mounting the image and receive transducers such that the sample volume (defined by the beam intersection) could lie in either the near (image near field or INF) or the far fields (image far field or IFF) of the beam patterns. The pump transducer (500 kHz center frequency), which was physically the largest of the
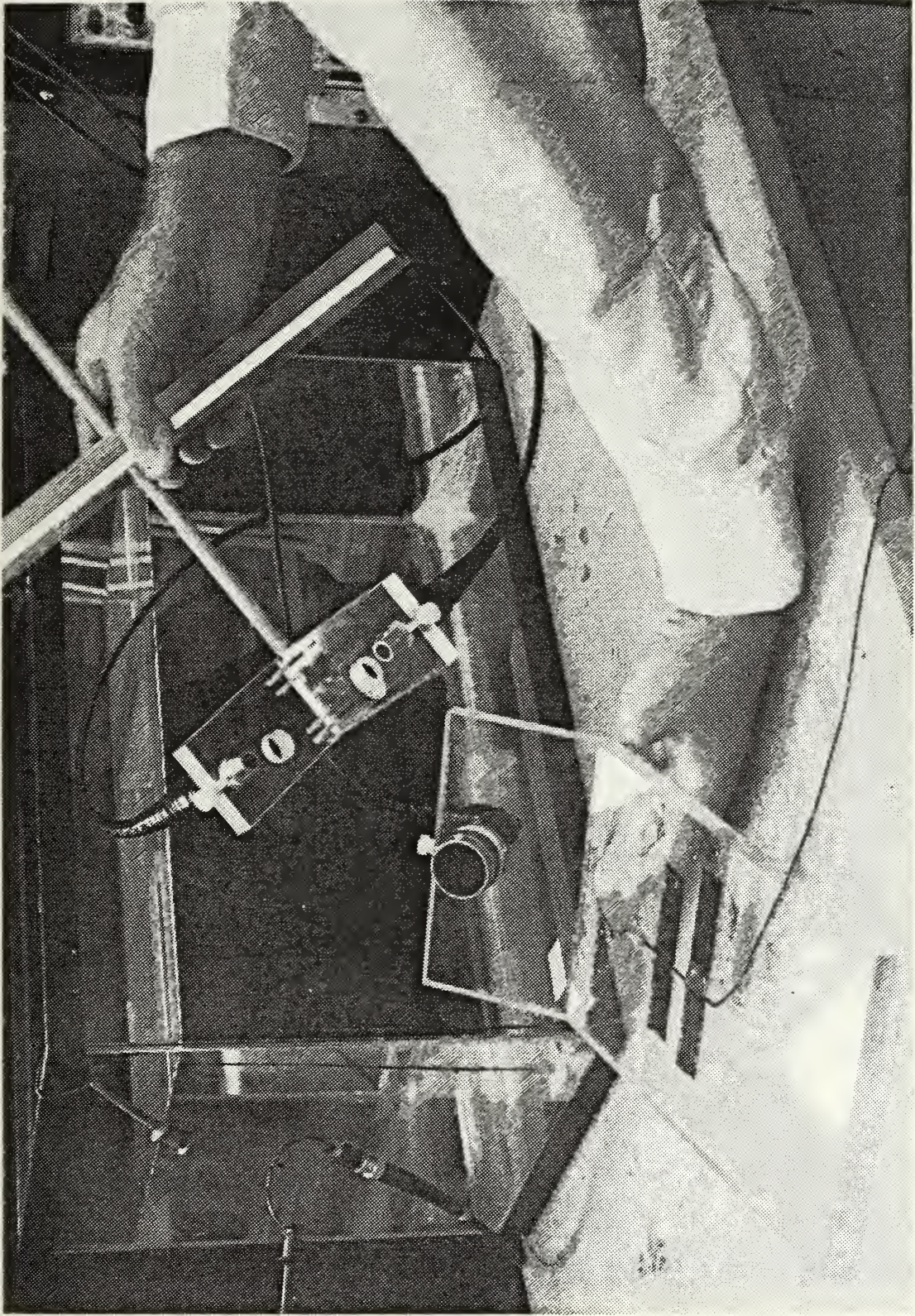
Figure 11. Image, Receive, and Upward Looking Pump Transducer Mounts

three, was mounted with two different placements so as to study the effects of radiating the rising bubble cloud at an upward or downward angle. The upward-facing pump transducer mount (designated "UP" for Upward Pump) for use in the aquarium is also shown in Figures 11, 12a, and 12b. The downward-facing pump transducer arrangement (designated "DP" for Downward Pump) can be seen in Figures 13, 14, and 15. For testing within the aquarium, the pump transducer mounts were kept separate to allow flexibility in movement of the mounts while investigating the best transducer alignment relative to the bubble stream. Testing during phase three (in the large tank) required that the transducer mounts be a single apparatus as shown in Figure 15.

All the transducers used in our experiments were manufactured by Panametrics Inc. The high-frequency imaging and receive transducers had a center frequency of 2.25 MHz. The low-frequency pump transducer had a center frequency of 500 kHz. The output of all three transducers was checked using a calibrated hydrophone.

The receive transducer was used to pick up signals reflected or radiated from the bubbles, or to receive noise from the other transducers. The signal received by the receive transducer was amplified by a 27 dB pre-amplifier. The signal was then passed on to an HP3585A spectrum analyzer and a Kikusui C056100A oscilloscope. The oscilloscope was used for several applications, including the measurement of reflected signals, calibration checks of the signal generators, and as an indicator of the generated bubble stream placement. The HP3585A spectrum analyzer was used for picking out
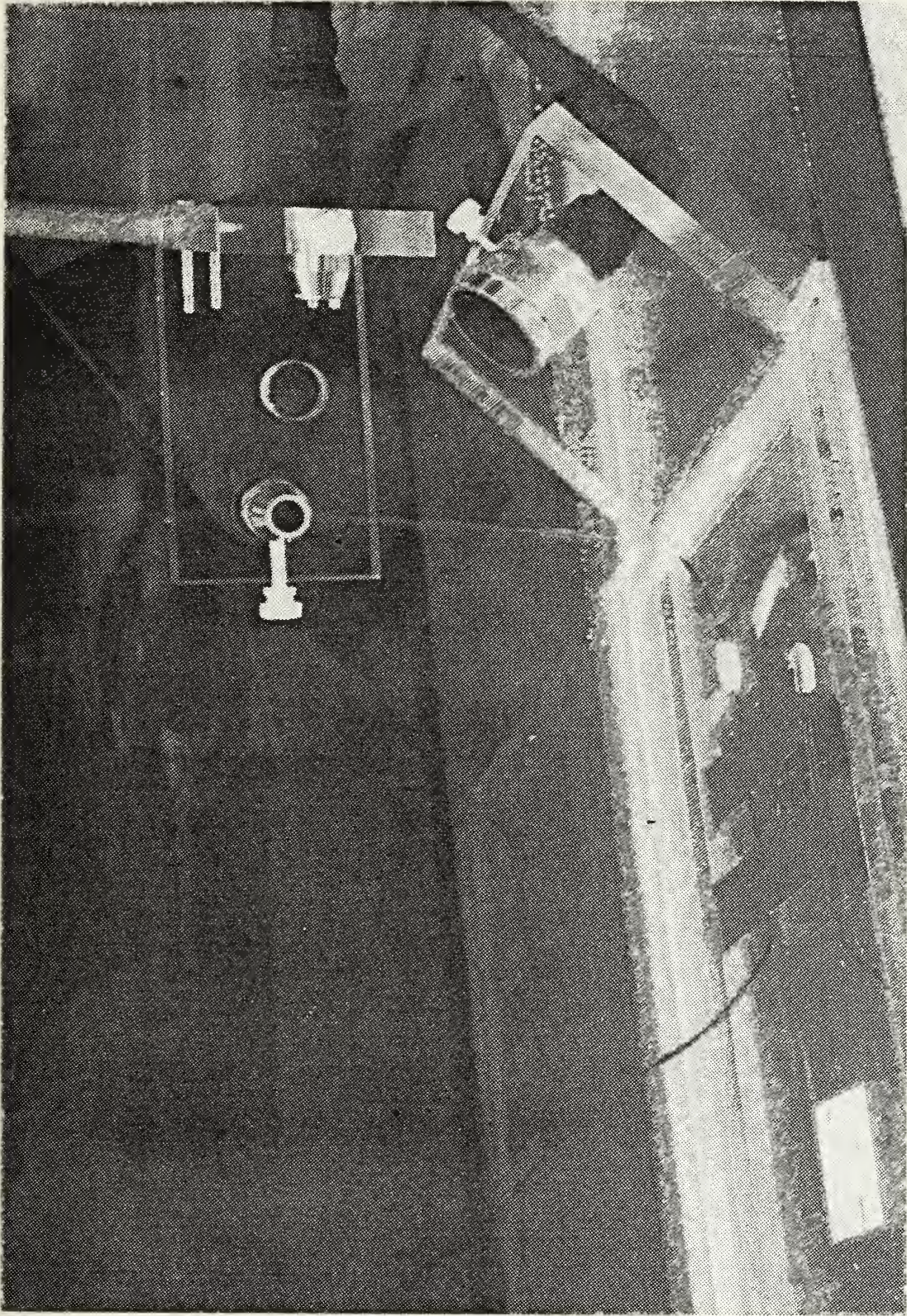
Figure 12a. Imaging (Far Field), Receive, and Upward Looking Pump (AGUPIFF) in Aquarium
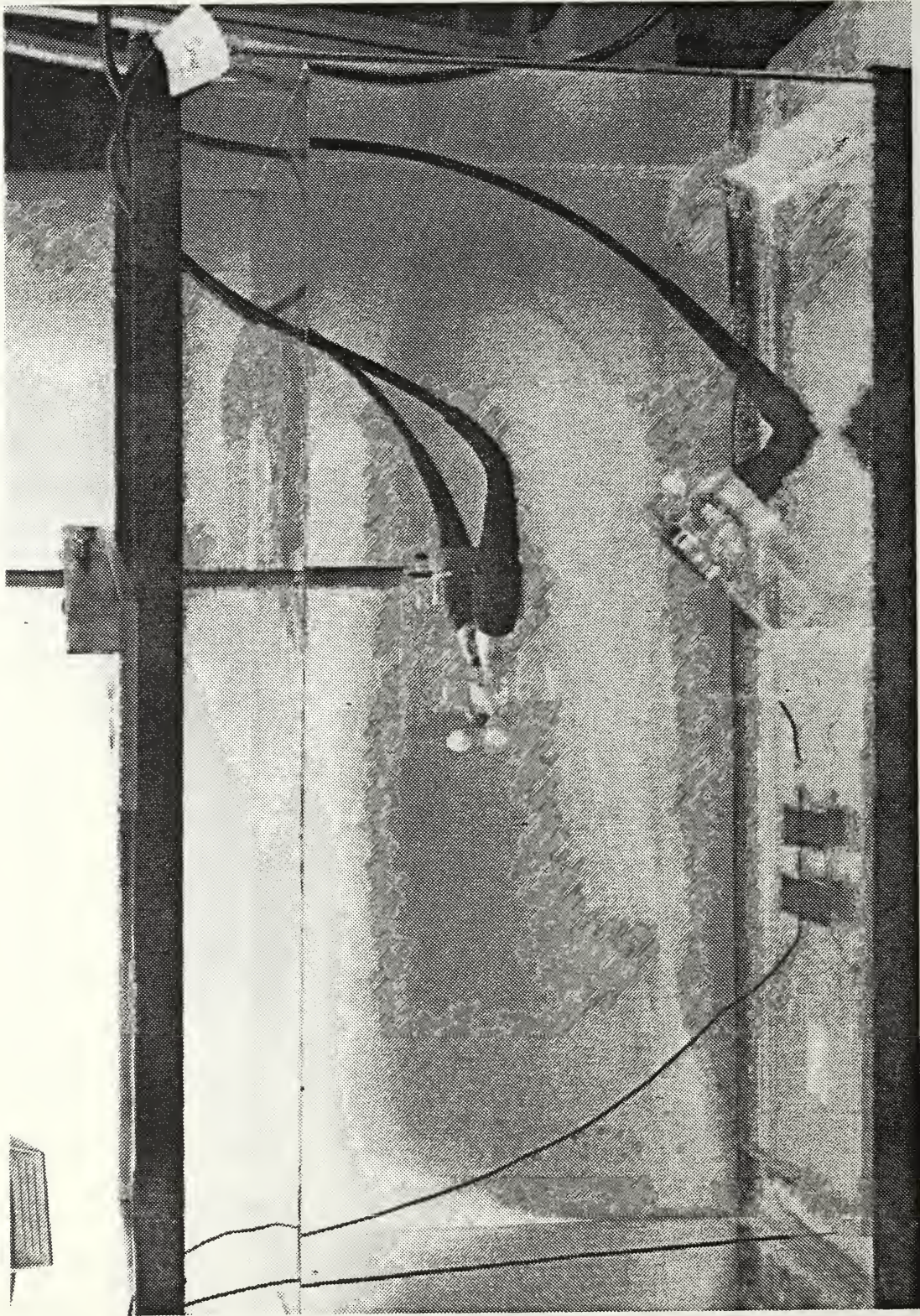
Figure 12b. Imaging (Near Field), Receive, and Upward Looking Pump (AQUPINF) in Aquarium
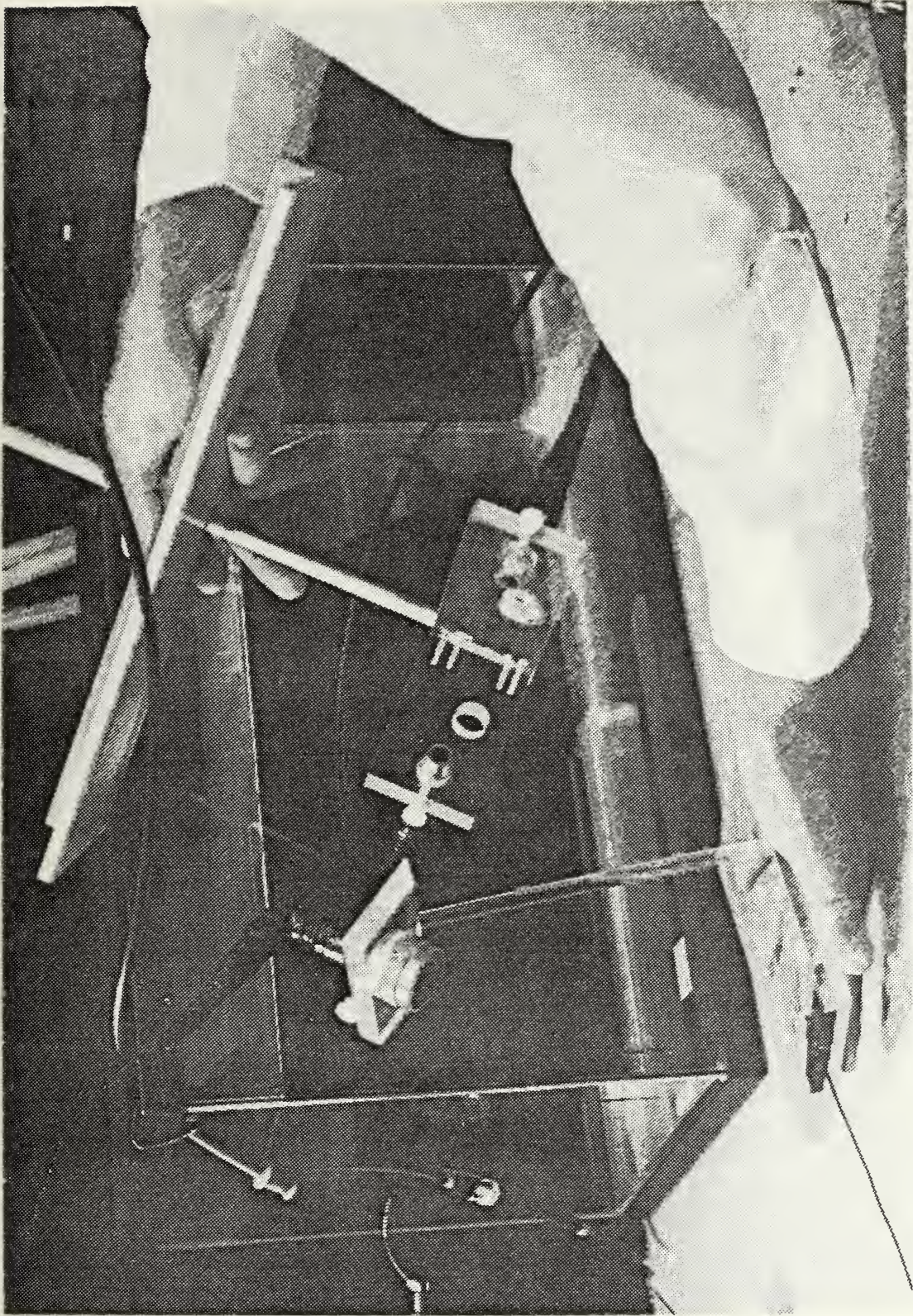
Figure 13. Imaging (Far Field), Receive, and Downward Looking
Pump Transducer Mounts
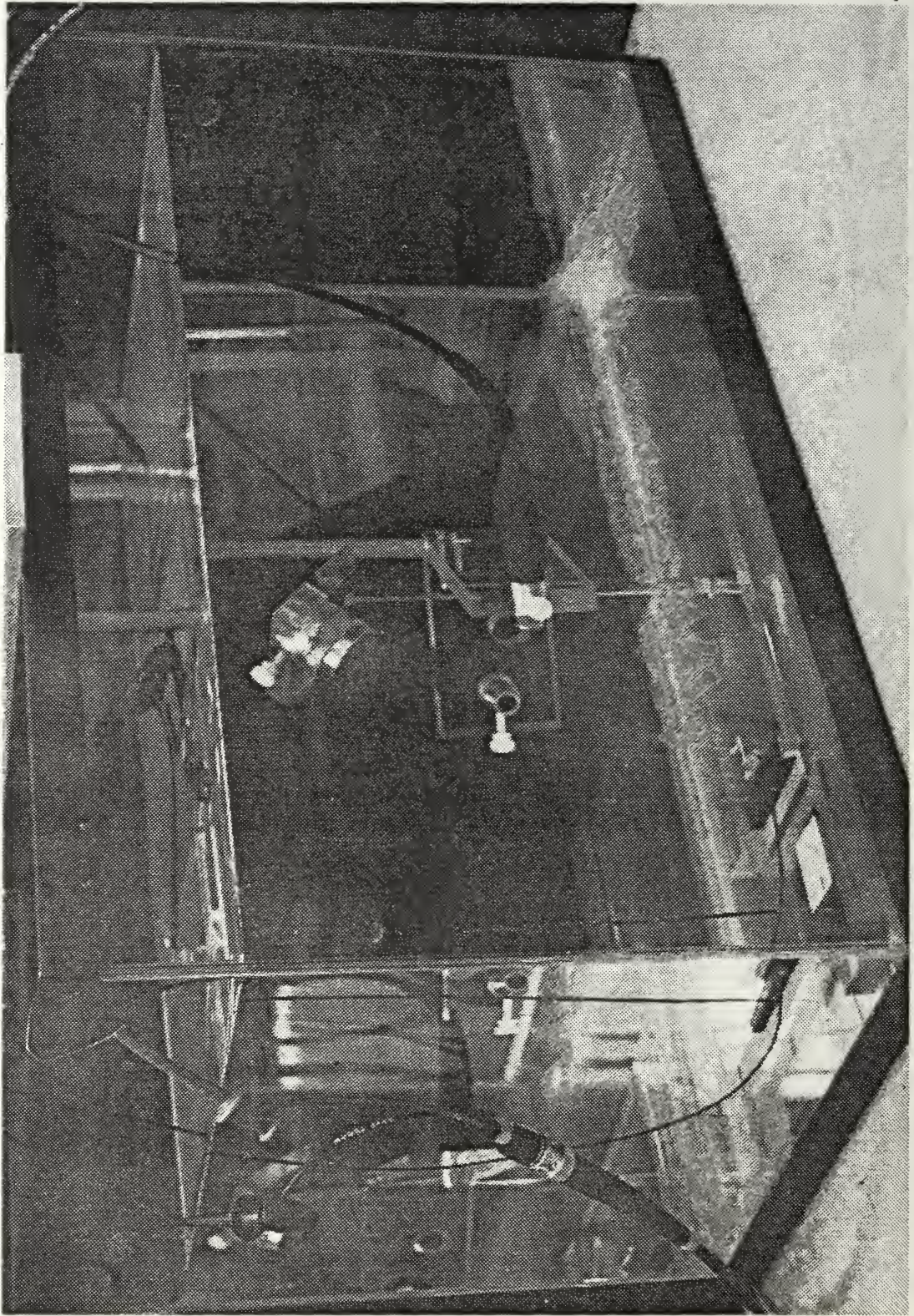
Figure 14. Imaging (Far Field), Receive, and Downward Looking Pump (AQDPIFF) in Aquarium
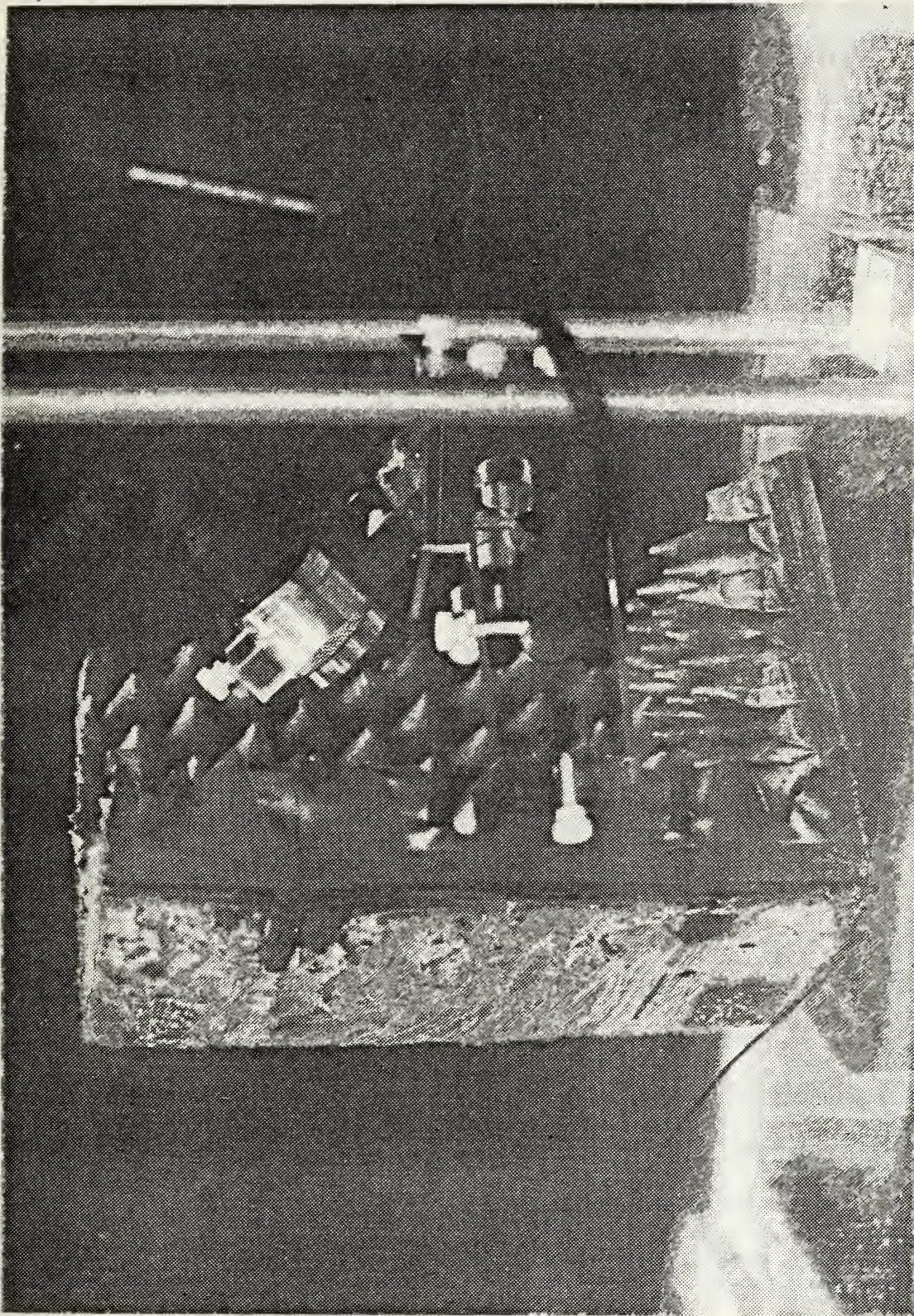
Figure 15. Single System Large Acoustic Tank Transducer Arrangement in Aquarium (LTDPIFF)

the primary and sideband sound pressure levels in the frequency domain. The limiting equipment in the receive process was the 27 dB pre-amplifier, which had a 50 kHz low-frequency cut-off. The 50 kHz low-frequency cutoff was not a problem when measuring dual-freqeuncy sideband levels, but it was a complication when measuring low-frequency transducer responses or fundamental bubble resonance levels.

The image transducer was driven by a HP 3314A Function Generator. This function generator could provide imaging signal frequencies up to 10 MHz and input levels up to 10 volts zero to peak with little distortion.

The pump transducer was provided input signals from a Wavetek Model 22 Sweep Generator. The signal was amplified ten times (x 10) through a HP 467A power amplifier. The amplifier was added after a conversation with P. M. Shankar of Drexel University revealed the need for sweeping the pump frequency range with higher pressure amplitudes than were originally used [Ref. 21]. All the equipment used during the experiment is pictured in Figure 10. Data from each phase was recorded and plotted from the spectrum analyzer using a HP 7090 plotter.

1. Phase One— Initial Measurements in Fresh Water

The ten-gallon aquarium was filled with fresh deionized water to conduct initial measurements and calibrations. Fresh water was used so that the possibility of electrical "cross-talk" between transducers would be reduced during these initial measurements. The

receive transducer was taken from its mount and used to test for electrical cross–talk by removing only the transducer face from the water. In this position, the receive transducer detected only a small portion of the imaging signal present in the water. By sliding the transducer in and out of the water, it was determined that the signal detected was not electrical cross–talk but was mostly noise picked up by the receiver through the sides of the transducer casing.

The use of deionized fresh water did create a problem for bubble generation by electrolysis. The fresh water did not have enough conductivity to support electrolysis. Therefore, a small amount of table salt was added to increase the conductivity of the water. This proved adequate for the generation of small bubble clouds.

Two different types of bubble clouds were investigated during this phase. The first bubble cloud was generated off a coil of brass wire which contained two different diameters of wire. Higher voltages were used and the bubble cloud was large and dense. Large bubble clouds appeared to make data collection difficult due to the large amount of bubble screening that occurred outside the sample volume. For this reason, a second, smaller bubble cloud was used. The second type of bubble cloud was a narrow stream of bubbles passing through the sample volume. It was created by a small, single–diameter piece of exposed brass wire at lower voltages. The bubble stream was still fairly dense, as shown in Figure 16, but did not appear to produce as much screening. These results will be discussed further in Chapter 5.
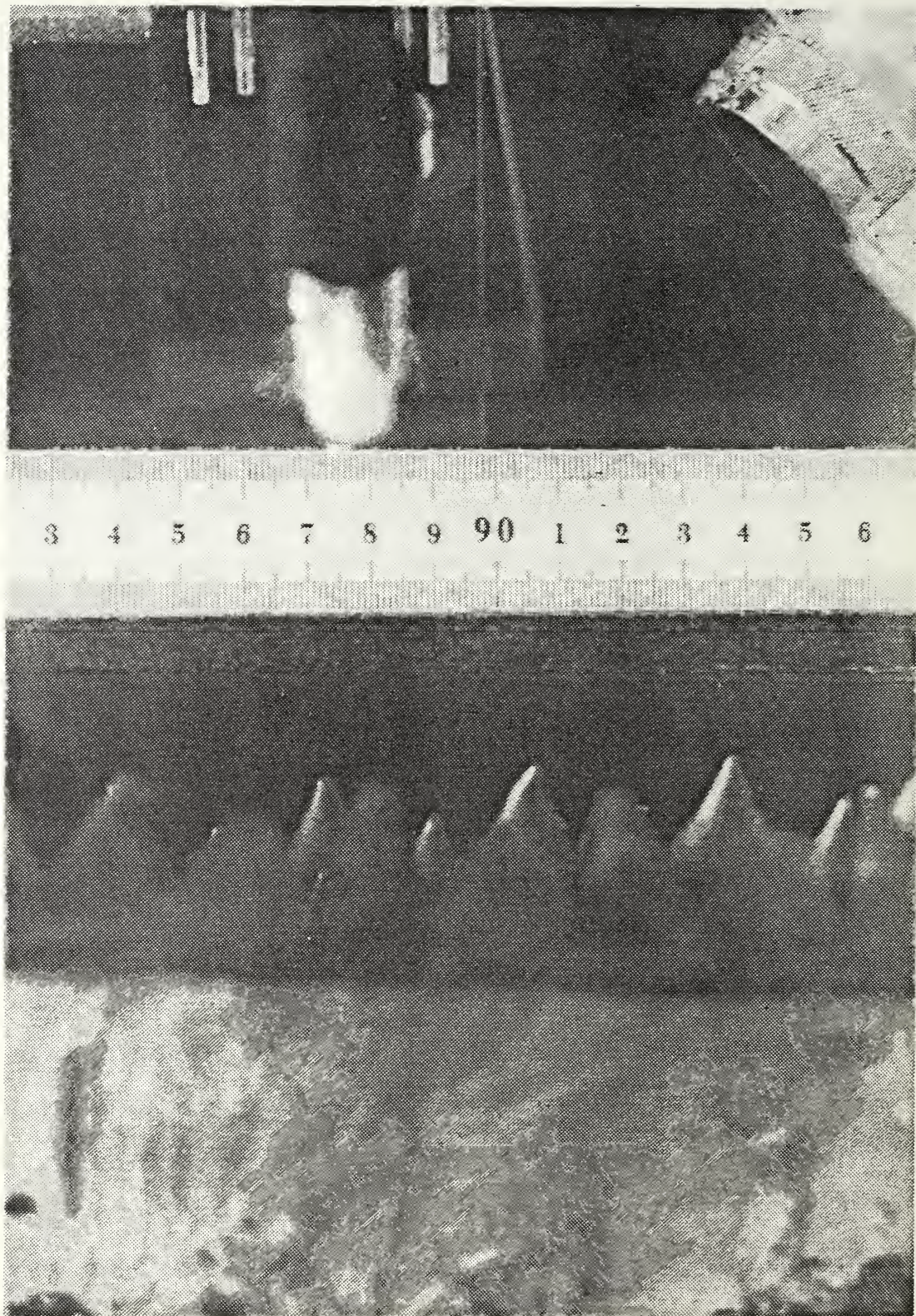
Figure 16. Narrow Bubble Stream in Aquarium

82

The small, narrow bubble stream was used throughout the remainder of the experiment for all data collection.

Transducer frequency response checks were done on both the imaging and pump transducers using both a calibrated Celesco LC-10 and a Naval Postgraduate School MA-1 hydrophone. The imaging transducer investigation was done to check for proper operation and to get an approximate idea of what frequency produced the highest imaging pressure amplitudes. The MA-1 was placed in the far field of the imaging transducer's beam pattern, as shown in Figure 17. The frequency response was measured for imaging frequencies ranging from 2.20 MHz to 2.55 MHz at a far-field distance of 6.7 centimeters. Imaging sound pressure amplitudes (p_i) are calculated in Appendix E from the measured sound pressure levels. The pump transducer frequency response was carefully checked at several distances using the LC-10 hydrophone as shown in Figure 18. The near field frequency response was recorded at one, two, four, and seven centimeters. The far field frequency response was recorded at ten and fourteen centimeters. The pump transducer frequency responses collected at various distances from the transducer face reflect the pump sound pressure amplitudes (p_p) available. The pump sound pressure p_p was calculated as shown in Appendix D. The best distance appeared to be a balance between the pump pressure amplitude available and the far field considerations discussed in Chapter II. Therefore, for most of the data runs, the sample volume was placed at a distance of ten centimeters from the pump transducer
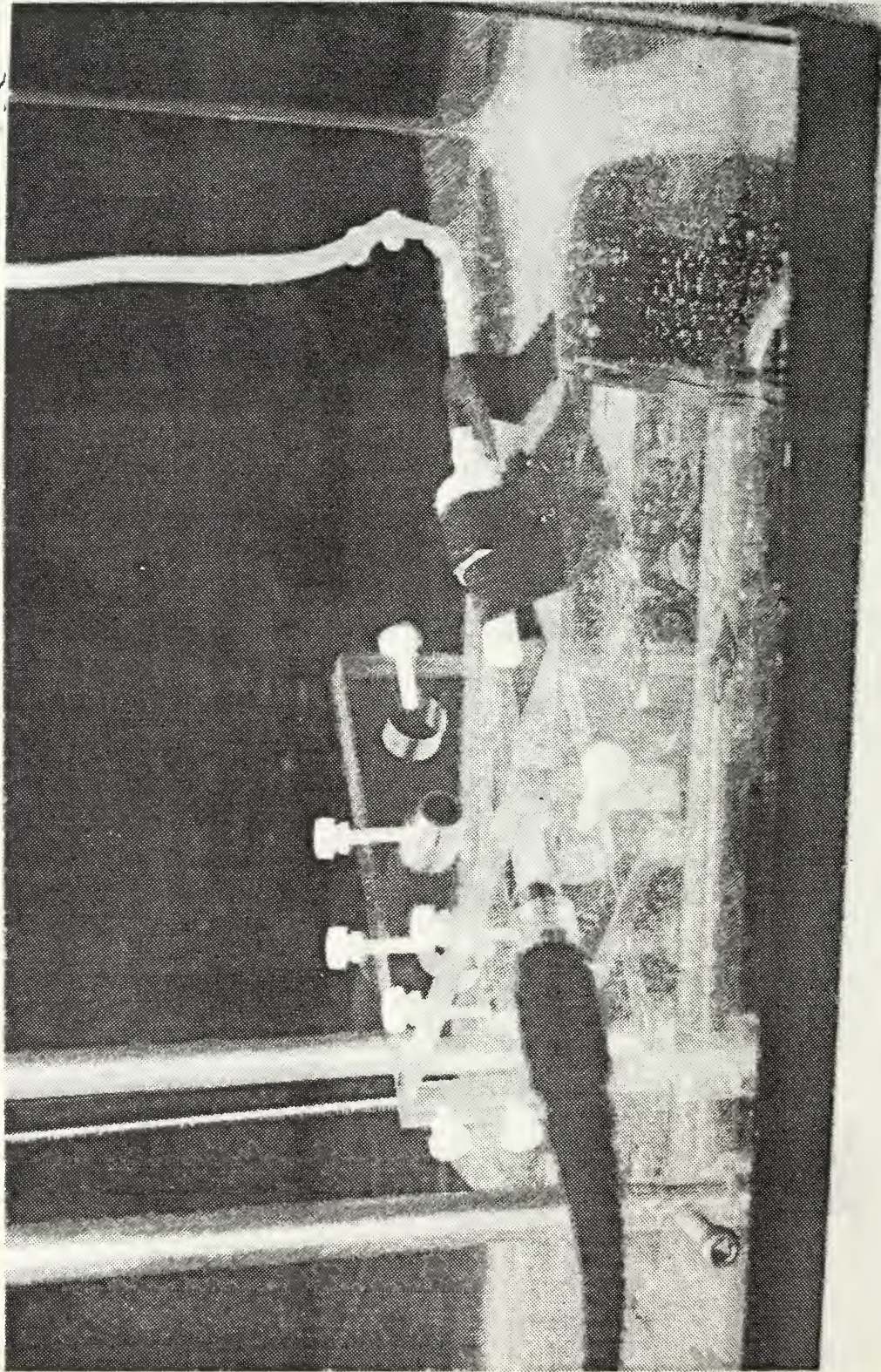
Figure 17. Calibrated MA-1 Hydrophone For Measuring
Imaging Transducer Frequency Response

84
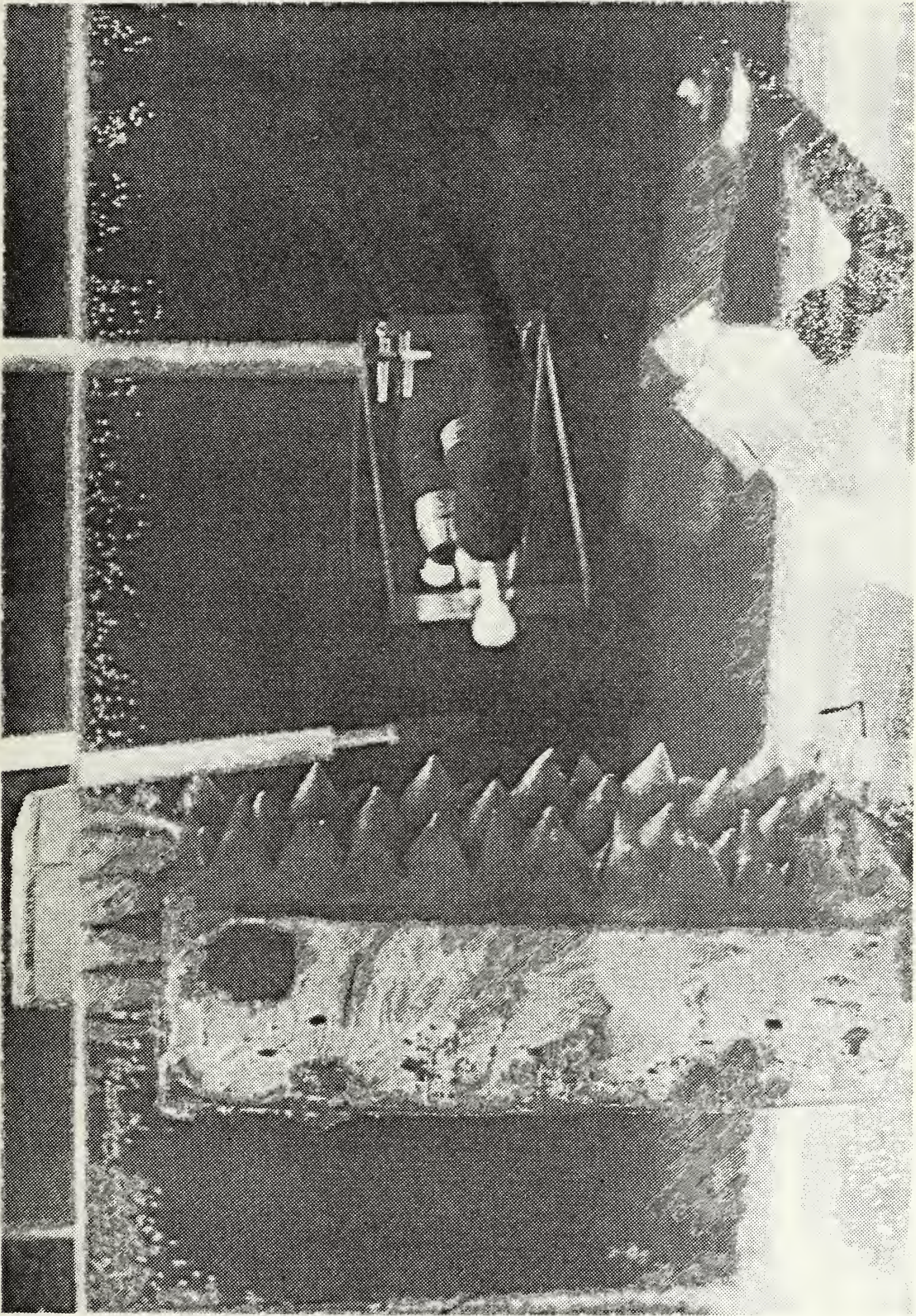
Figure 18. Calibrated LC-10 Hydrophone For Measuring Pump Transducer Frequency Response

85

face, which is in the far field for freqeuncies up to approximately 300 kHz.

A second check concerning the pump sound pressure versus frequency sweep time was also run. The LC-10 was placed ten centimeters from the pump transducer face and the frequency response measured at four different sweep times. A sizeable difference in pump sound pressure levels was recorded between the 0.01-second sweep time and the higher sweep times. The most favorable sweep time appeared to be 0.10 seconds. The measurements for the various distances and sweep time frequency responses are also available in Appendix D. Since the highest sound pressure levels (SPL) resulted with the sweep time of 0.10 seconds, that time was used throughout.

The entire group of three transducers was placed in the aquarium such that standing waves and reflections produced a minimum amount of noise at the receive transducer. Absorptive material was placed in front of the transducers and at the surface of the water. This was done to help eliminate reflections and break up standing waves. An arrangement using absorptive material is shown in Figure 19.

The placement of the pump, imaging, and receive transducers relative to each other was investigated using three different arrangements. The first two arrangements were with the pump transducer in an upward-facing position (UP) and the sample volume at a distance of ten centimeters from the pump transducer face. The
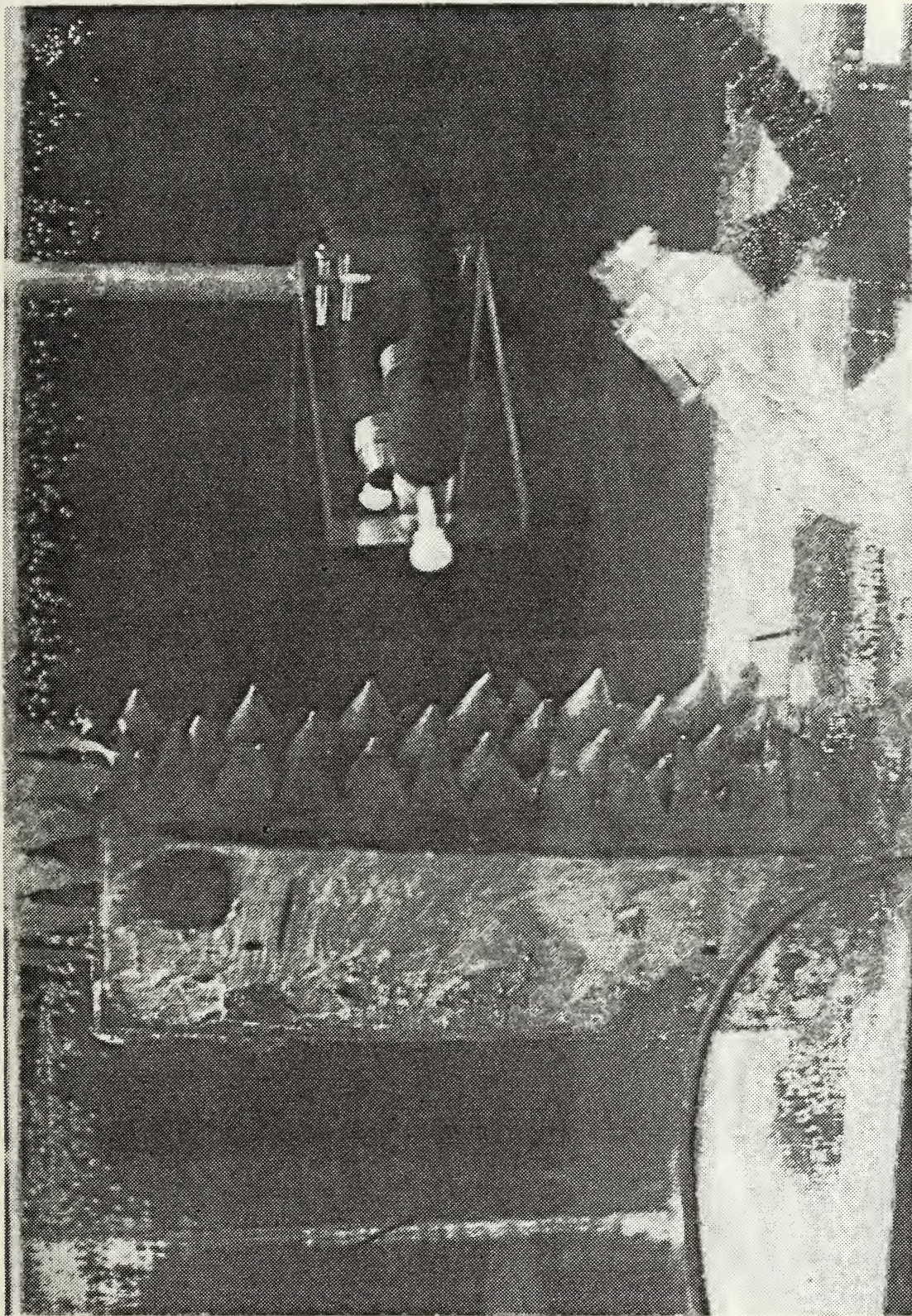
Figure 19. Phase One Set-up With Absorptive Material

87

sample volume was placed in either the near (Image Far Field or IFF) or far fields (Image Near Field or INF) of the imaging and receive transducers. The third transducer arrangement was with the pump transducer in a downward-facing position (DP). Here, the sample volume was put in only the far field of the imaging and receive transducers. Several sets of data were collected for each transducer arrangement.

In all cases, the sample volume, bubble stream, and pump transducer sound fields for each arrangement were aligned using the LC-10 hydrophone. The pump transducer input level was 42 volts peak to peak and the imaging transducer input level was 6.0 volts (zero to peak), unless otherwise noted.

Phase one data collection began with a fresh-water electrical cross-talk check. A pre-amplifier ground check provided a baseline noise level. The pump transducer was aimed directly into the face of the receive transducer to check for modulation and sidebands in the presence of no bubbles. A second "no-bubble test" to check for false sideband pressure amplitudes was conducted using an aluminum rod, or dowel, which acted as a reflector within the sample volume. The aluminum rod test is shown in Figure 20. Neither test produced dual-frequency sidebands. Finally, the receive transducer frequency response was recorded using bubbles as a reflector in the near field. This last check was used later to determine a more ideal image frequency which would avoid lower-frequency harmonics.
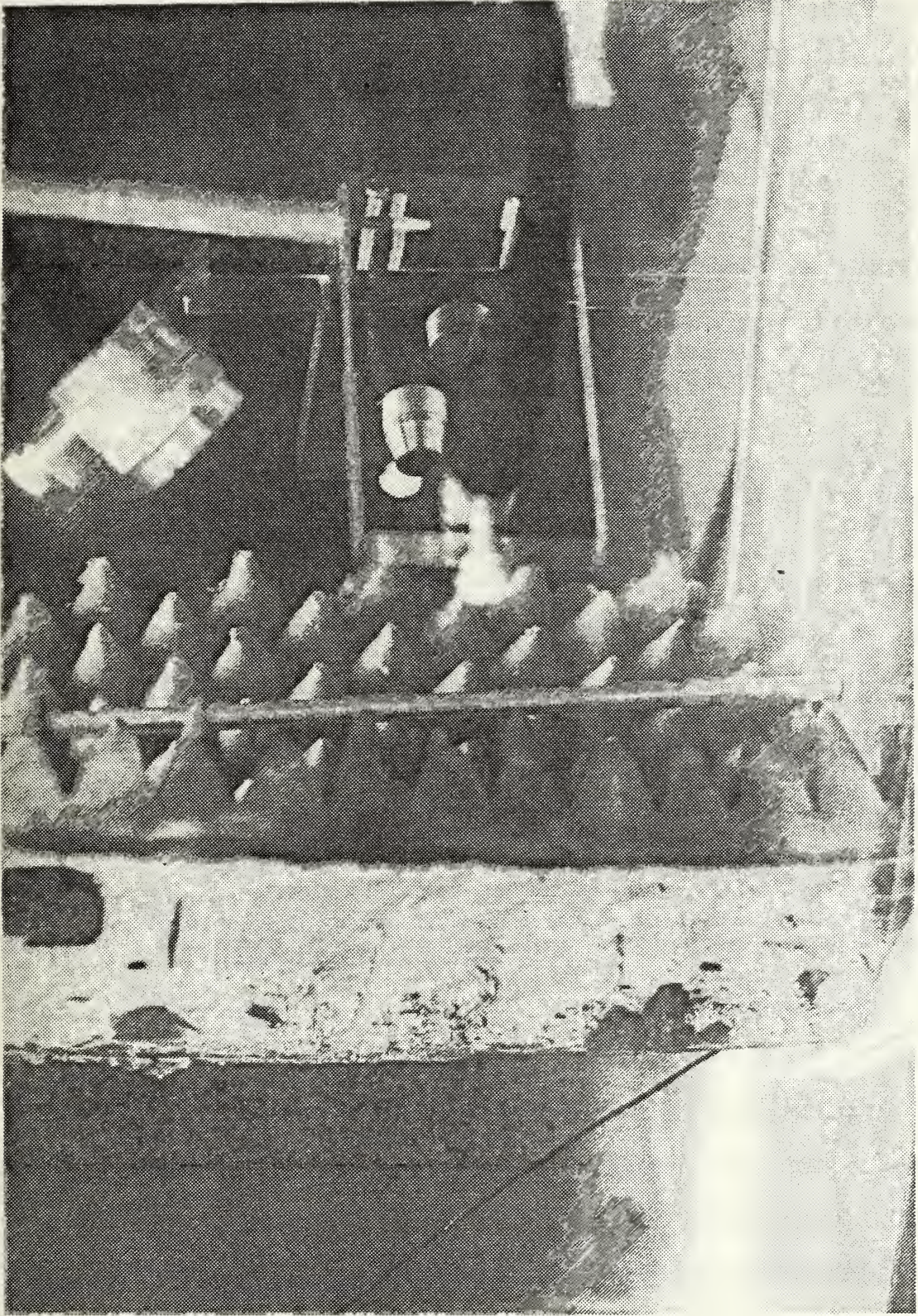
Figure 20. Aluminum Dowel Reflector Test Set-up

89

The first fresh-water transducer arrangement used to record data was the Aquarium Upward Pump Image Far Field$_f$, designated AQUPIFF$_f$, where the subscript stands for fresh water. This arrangement placed the pump transducer face 10 centimeters from the sample volume and maintained the far field for the high-frequency receiver. The following data runs were recorded using the AQUPIFF$_f$:

1. Wide Spectrum Analyzer Frequency Window—Pump and imaging sound fields for bubbles present versus no bubbles present. Pump sweep frequencies 15 kHz to 310 kHz. Imaging frequency 2.25 MHz.

2. Wide Spectrum Analyzer Frequency Window—Bubbles always present for imaging sound field only versus both pump and imaging sound fields. Pump sweep frequency 15 kHz to 310 kHz. Imaging frequency 2.25 MHz.

3. Narrow Spectrum Analyzer Frequency Window—A "close-up" of the dual-frequency sidebands P_+ and P_- with pump sweep frequencies of 15 kHz to 310 kHz. Imaging frequency 2.25 MHz.

4. Repeat of run number three (3) with reduced pump power, i.e., less than 42 volts peak to peak for the pump power supply. Imaging frequency 2.25 MHz. Pump sweep frequencies of 15 kHz to 310 kHz.

5. Narrow Spectrum Analyzer Frequency Window—A "close-up" of the imaging sidebands P_+ and P_- with an expanded pump sweep range of 15 kHz to 500 kHz. Imaging frequency 2.25 MHz.

The second fresh-water transducer arrangement was the Aquarium Upward Pump Image Near Field$_f$, designated AQUPINF$_f$. This arrangement was used to record any increased signal sensitivity that could be gained by moving the receiver closer to the bubble cloud or stream. The pump transducer face was still maintained at a distance of ten centimeters from the sample volume so the sample

volume would remain in the far field of the pump transducer beam pattern. The following data was recorded using the $AQUPINF_f$:

1. Narrow Spectrum Analyzer Frequency Window—Bubbles present and radiated by both pump and imaging sound fields. Pump sweeping frequencies of 15 kHz to 310 kHz. Imaging frequency 2.25 MHz.

2. Narrow Spectrum Analyzer Frequency Window—Bubbles present and radiated by both pump and imaging sound fields. Reduced image level to 3.0 volts and expanded pump sweep frequencies of 15 kHz to 420 kHz to study effects of harmonics. Imaging frequency 2.25 MHz.

3. Repeat run two (2) except used receive transducer response data to move imaging frequency to more favorable 2.51 MHz to better avoid harmonics. Image level 3.0 volts. Pump sweep frequencies of 15 kHz to 420 kHz.

The third and last fresh-water aquarium arrangement was the Aquarium Downward Pump Imaging Far Field$_f$, designated $AQDPIFF_f$. This arrangement was used to investigate any advantage gained by having the pump sound field oppose the bubble flow and by having the pump transducer face closer to the sample volume. A single set of data was recorded using the $AQDPIFF_f$:

Wide Spectrum Analyzer Frequency Window—Bubbles Present—Imaging sound field versus imaging plus pump sound fields, and the difference. Pump frequencies swept 15 kHz to 310 kHz. Imaging frequency 2.25 MHz.

2. Phase Two—Seawater Testing

The ten-gallon aquarium was filled with seawater. The electrical cross-talk checks conducted in phase one were repeated. The same procedure of immersing the transducer up to the transducer face and noting the response on the spectrum analyzer was used. The imaging transducer frequency response was again measured

91

in salt water using the MA-1 hydrophone. It did not differ from that measured in fresh water.

Phase two data collection repeated that of phase one with the bubble sample volume in the imaging and receive transducer far field. The pump transducer was upward facing and the transducer face was at a distance of ten centimeters from the sample volume. In salt water, this configuration is designated AQUPIFF$_s$. This data was collected for comparison with the fresh-water phase one data and, therefore, was run using the same variations. Data collected using the AQUPIFF$_s$ configuration includes:

1. Wide Spectrum Analyzer Frequency Window—Bubbles present—Imaging sound field only versus imaging plus pump sound fields, and the difference. Pump sweep frequencies of 15 kHz to 310 kHz. Imaging frequency 2.25 MHz.

2. Narrow Spectrum Analyzer Frequency Window—Single plot of bubbles radiated by both pump and imaging sound fields. Pump sweep frequencies of 15 kHz to 310 kHz. Imaging frequency 2.25 MHz.

The aquarium filled with seawater was also used for the initial testing of the final transducer arrangement. This final arrangement was designed to be used in a large (3.0 meters deep) acoustically insulated tank. The Large Tank Downward Pump Image Far Field$_s$, designated LTDPIFF$_s$, is shown in Figure 15. The subscript "s" denotes the phase two use of salt water. The sample volume for this arrangement is approximately 7.0 centimeters from the pump transducer face. Appendix D also calculates the pump pressure amplitude (p_p) for this distance. The pump pressure amplitude at 7.0 centimeters distance compares favorably with the pressure amplitude at 10 centimeters

distance. As mentioned previously, the imaging and receive transducers place the sample volume in the far field of the beam pattern.

The following data runs were taken with the LTDPIFF$_s$:

1. Wide Spectrum Analyzer Frequency Window— Bubbles present— Imaging sound field versus imaging plus pump sound fields, and the difference. Pump sweep frequencies of 15 kHz to 310 kHz. Imaging frequency 2.25 MHz.

2. Wide Spectrum Analyzer Frequency Window— Bubbles present— Imaging and pump sound fields. Imaging frequency shifted up to 2.50 MHz to avoid harmonics. Pump sweep frequencies of 15 kHz to 310 kHz.

3. Wide Spectrum Analyzer Frequency Window— Bubbles present— Same set-up and format as run (1)— Extra imaging level to 9.83 volts to bring out dual-frequency sidebands. Pump sweep frequencies of 15 kHz to 310 kHz. Imaging frequency 2.25 MHz.

3.   Phase Three— Large Acoustically Insulated Tank

The third and final phase uses a large fresh-water tank, which is acoustically insulated, to investigate the possibility of reflections causing excessive noise in the aquarium (phases one and two). The large tank provided an acoustically quiet environment due to its size, insulation, and the relatively low amplitude of the imaging and pump sound signals. The transducer arrangement was the same one used in the later portion of phase two. The Large Tank Downward Pump Image Far Field$_f$ (LTDPIFF$_f$), was used in the large tank with the same equipment rack as was used in the first two phases of the experiment. Figures 21 and 22 show the phase three experiment arrangements.
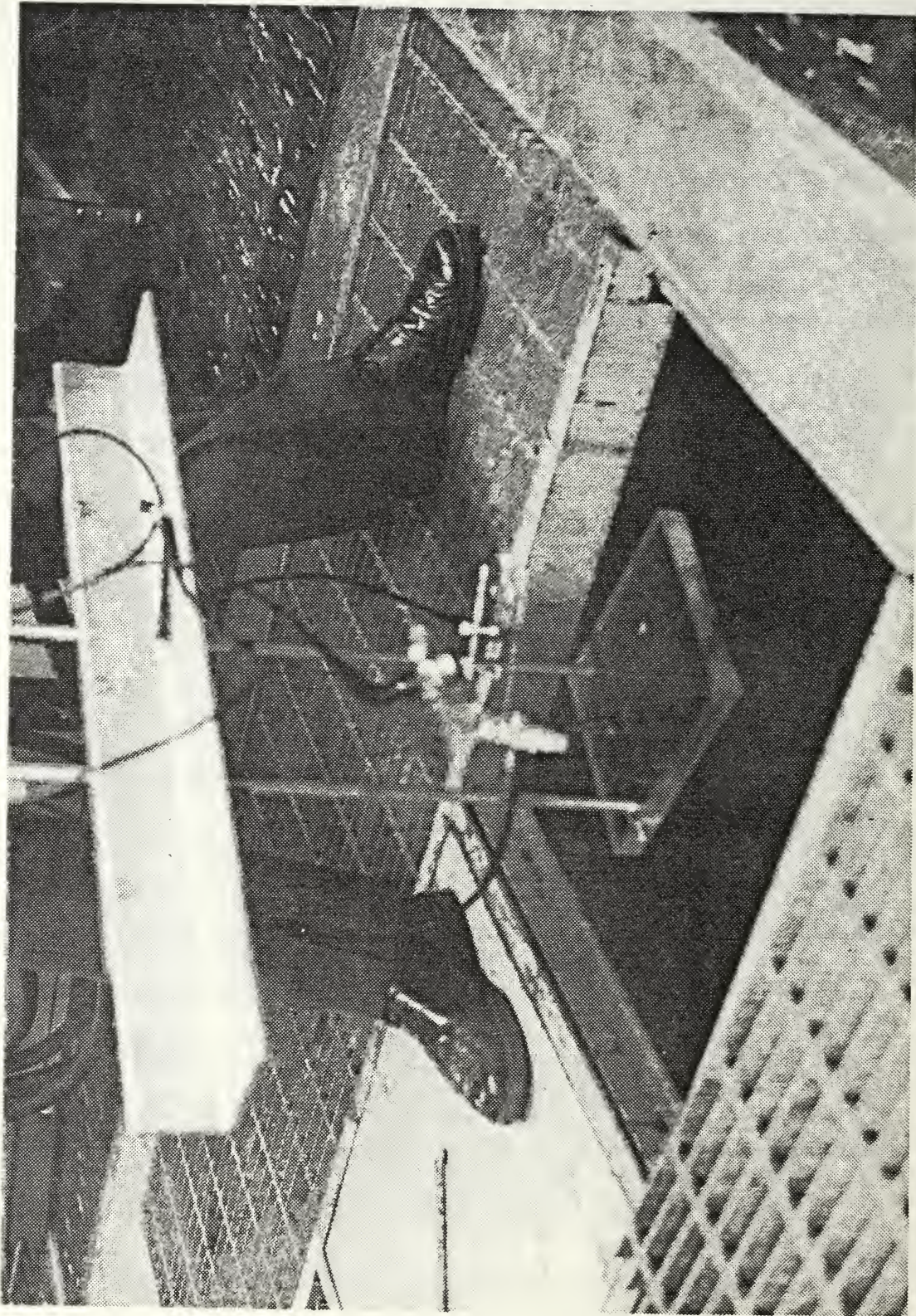
Figure 21. Large Tank Transducer Arrangement (LTDPIFFf) and Large Tank Access

94
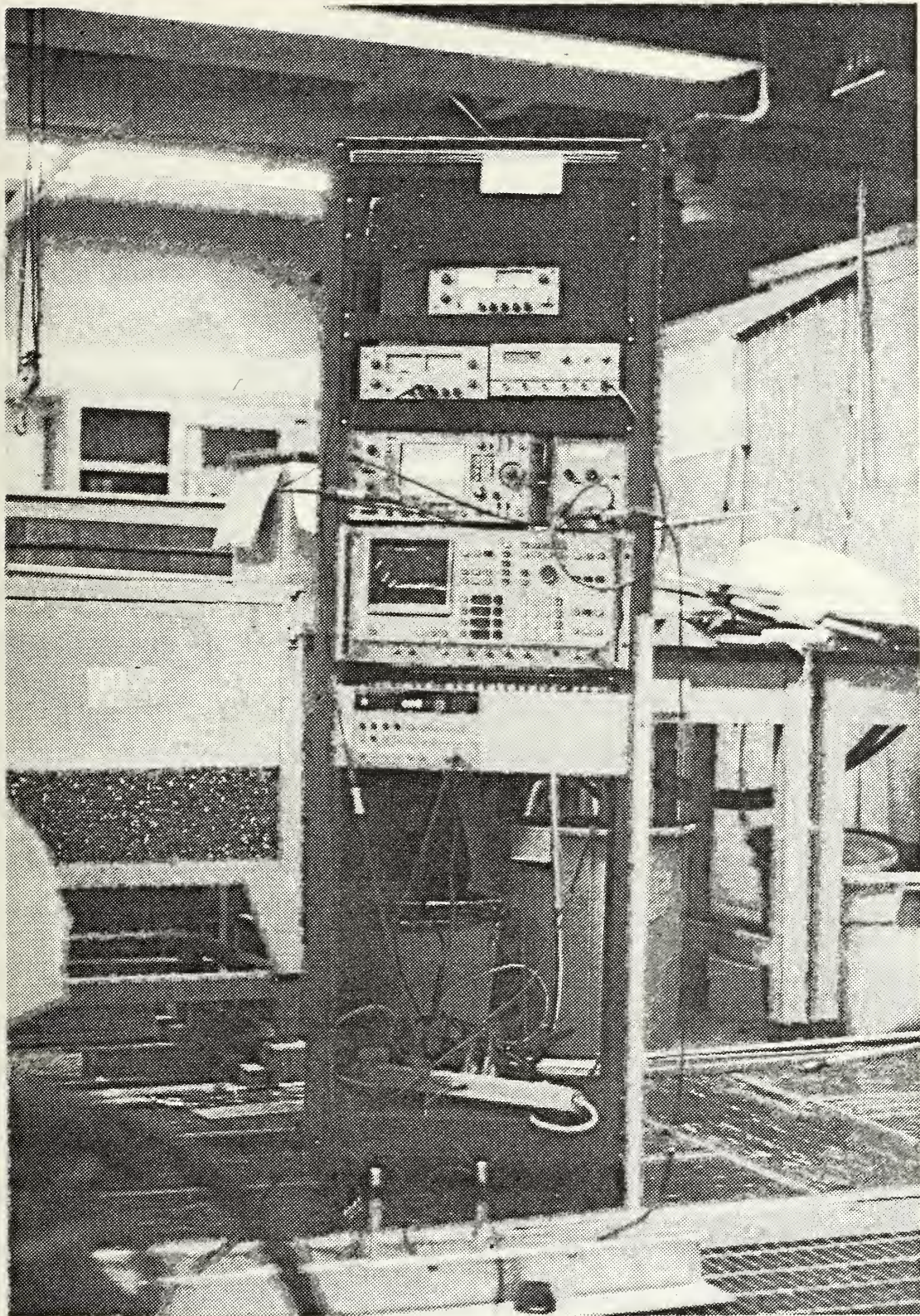
Figure 22. LTDPIFF$_f$ and Equipment Set-up Operational in Large Acoustically Insulated Tank

95

The LTDPIFF$_f$ data runs include the following:

1. Wide Spectrum Analyzer Frequency Window— Bubbles present— Imaging sound field only versus imaging plus pump sound fields, and the difference. Pump sweep frequencies of 15 kHz to 310 kHz. Imaging frequency 2.25 MHz.

2. Narrow Spectrum Analyzer Frequency Window— Sum Sideband (P_+)— Bubbles present— Imaging sound field only versus imaging plus pump sound fields, and the difference Pump sweep frequencies of 15 kHz to 310 kHz.

The data and results for all data runs conducted in phases one, two, and three will be presented and briefly discussed in Chapter IV.

IV. RESULTS

The results of the data collected during the course of the experiment are presented in this chapter. The figures that are the result of the data runs discussed in the Experimental Procedure section of Chapter III are plots of the HP3585A Spectrum Analyzer CRT display. The actual figures were reproduced from the analyzer by the HP 7090 Measurement Plotting System. Each figure is a plot of sound pressure level (dB re 1.0 mW) versus frequency (MHz). The sound pressure levels can be easily converted to pressure amplitudes using the same methods described in Appendices D and E. The resolution bandwidth (RBW) from the CRT display is shown on each figure.

This chapter is organized to present the results in the order that the data was taken during the experiment. A general discussion of each data run is included. The first data sets are for electrical cross-talk checks (both fresh and seawater), amplifier noise level measurements, measurement of the optimum receiver frequency response using bubbles as a reflector in the sample volume, a frequency modulation investigation using direct radiation of pump sound field energy, and comparison of the signals received by the receive transducer for bubbles versus a solid reflecting object in the sample volume. The data runs from phases one, two, and three of the experimental procedure follow the discussion of the initial calibrations.

Electrical cross-talk checks were conducted in both fresh water and seawater to determine if the increased conductivity of seawater

would cause a portion of the electrical signal to be transmitted from the imaging transducer to the receive transducer. Figures 23a and 23b are measurements of the signals received via the casing of the receive transducer at 2.25 MHz. Both figures are in terms of sound pressure levels (SPLs). Both figures are the difference between the 2.25 MHz signal being present and the noise when no signal is present. The signal spike at 2.25 MHz is approximately 16 dBm for both fresh water and seawater. It is concluded, therefore, that electrical cross–talk must be minimal and is the same for both fresh water and seawater. A more likely source of the signal spike is energy that is transmitted acoustically through the receive transducer casing.

A baseline noise measurement was performed by grounding the pre–amplifier input. The results are plotted in Figure 24. The noise level from 150 kHz up to 3.50 MHz is constant at approximately –103 dB re 1.0 mW.

The receive transducer frequency response using swept frequencies of the sound field reflected from a bubble stream in the sample volume is plotted in Figure 25. Figure 25 was used to determine the adjustment of the imaging frequency (f_i) from 2.25 MHz to 2.50 MHz in order to better avoid harmonics of the pump sound field and resonating bubbles. Figure 25 shows that the receive transducer frequency response begins to fall off after 2.50 MHz.

A frequency modulation check in fresh water was conducted to investigate the effects of direct radiation of the pump sound field on the face of the receive transducer. The pump transducer was pointed directly at the receive transducer and the difference between the
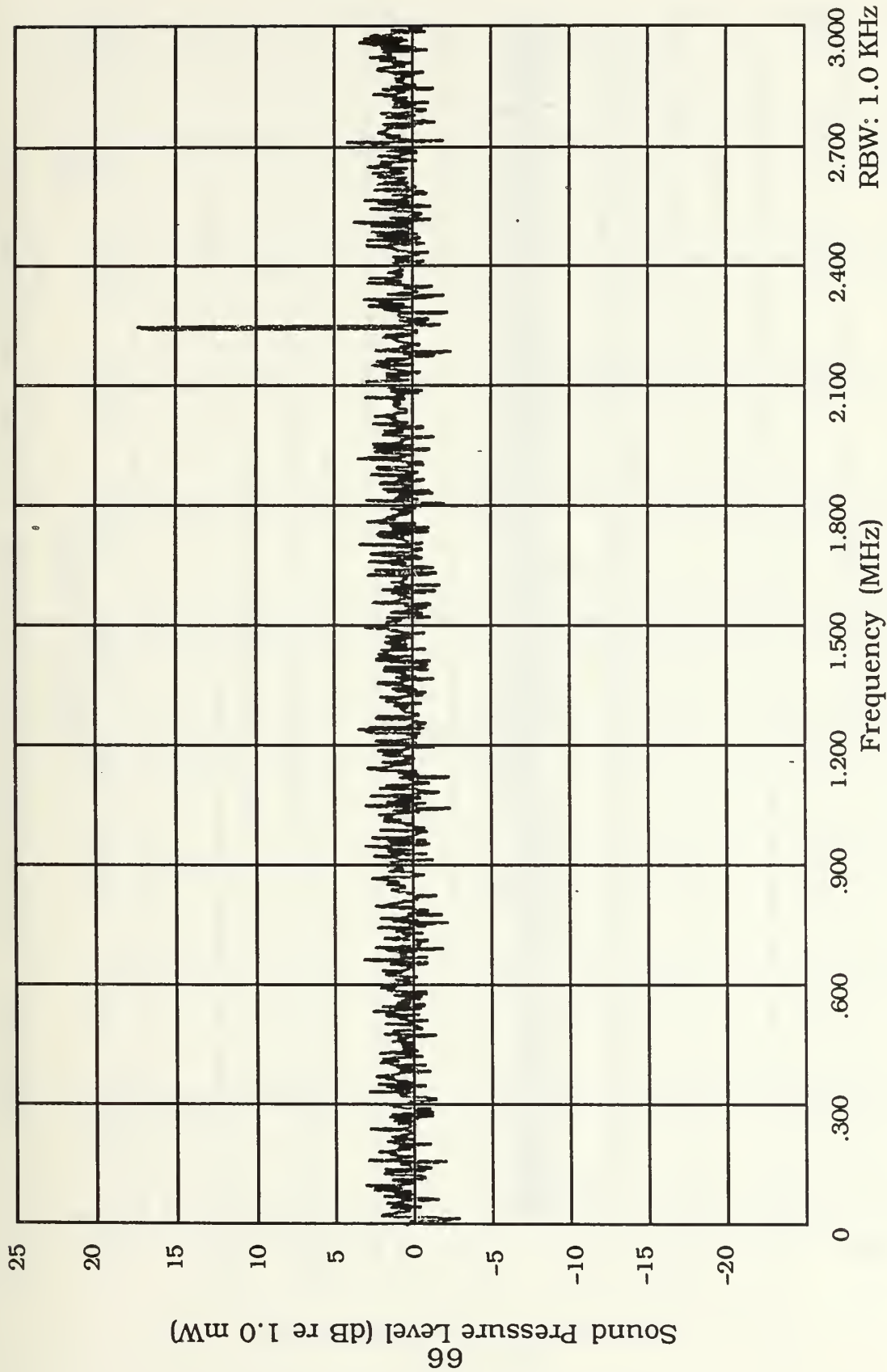
Figure 23a. Fresh Water Electrical Cross–Talk Check at Imaging Frequency

RBW: 1.0 KHz

Frequency (MHz)

Sound Pressure Level (dB re 1.0 mW)

99
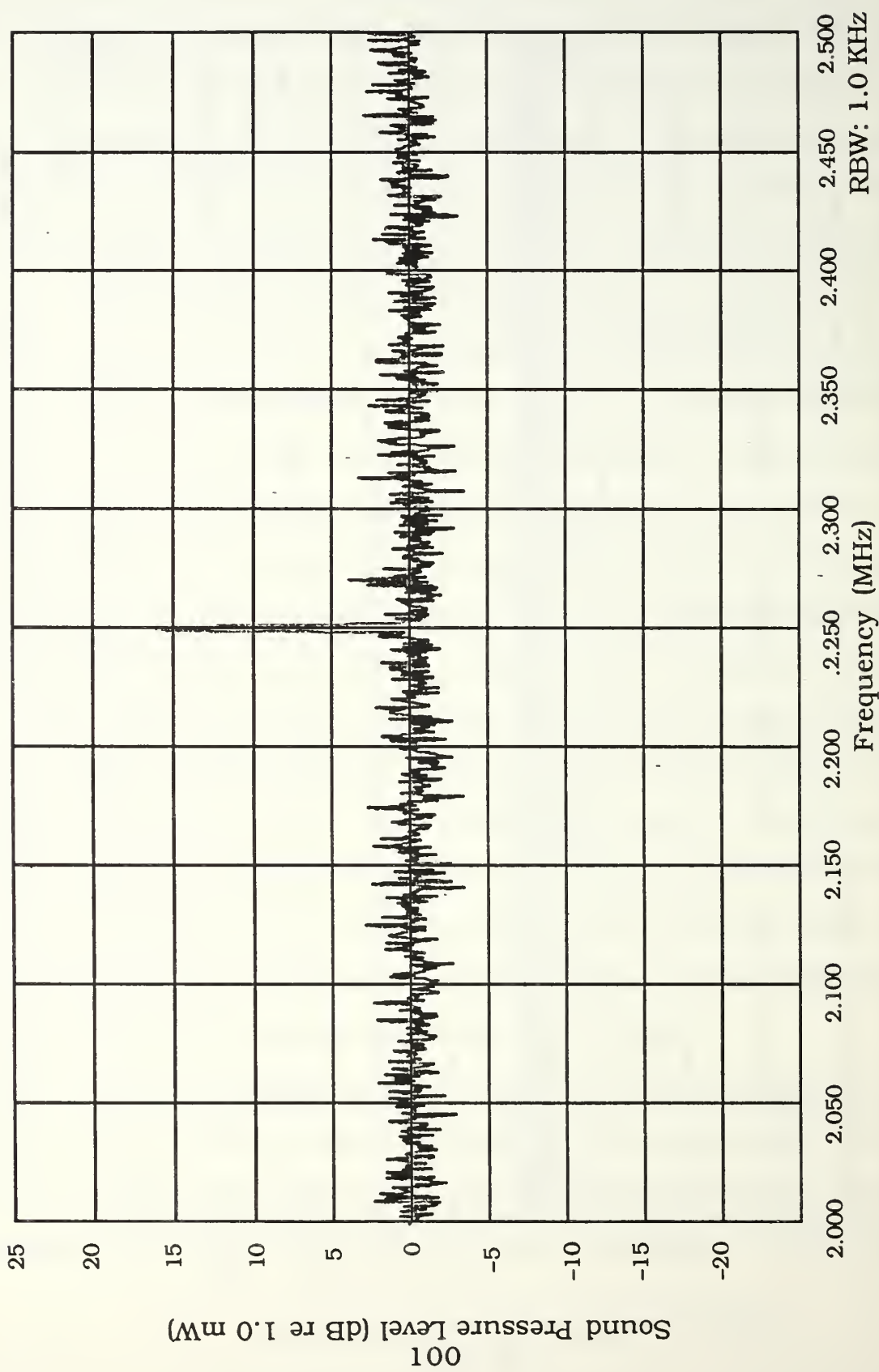
Figure 23b. Salt Water Electrical Cross-Talk Check at Imaging Frequency

RBW: 1.0 KHz

Frequency (MHz)

Sound Pressure Level (dB re 1.0 mW)

100
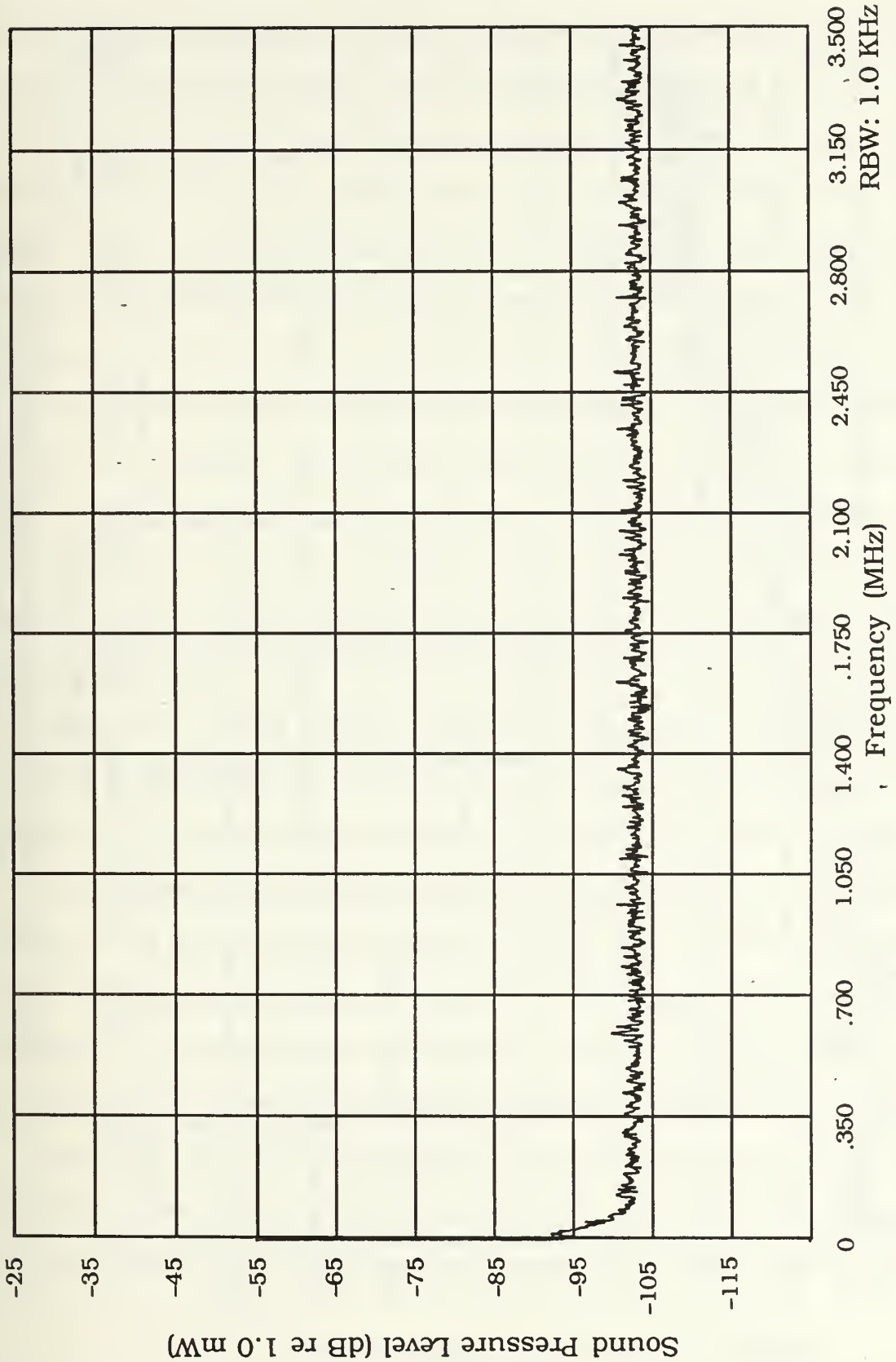
Figure 24. Baseline Noise Measurement

RBW: 1.0 KHz

Frequency (MHz)

Sound Pressure Level (dB re 1.0 mW)

101
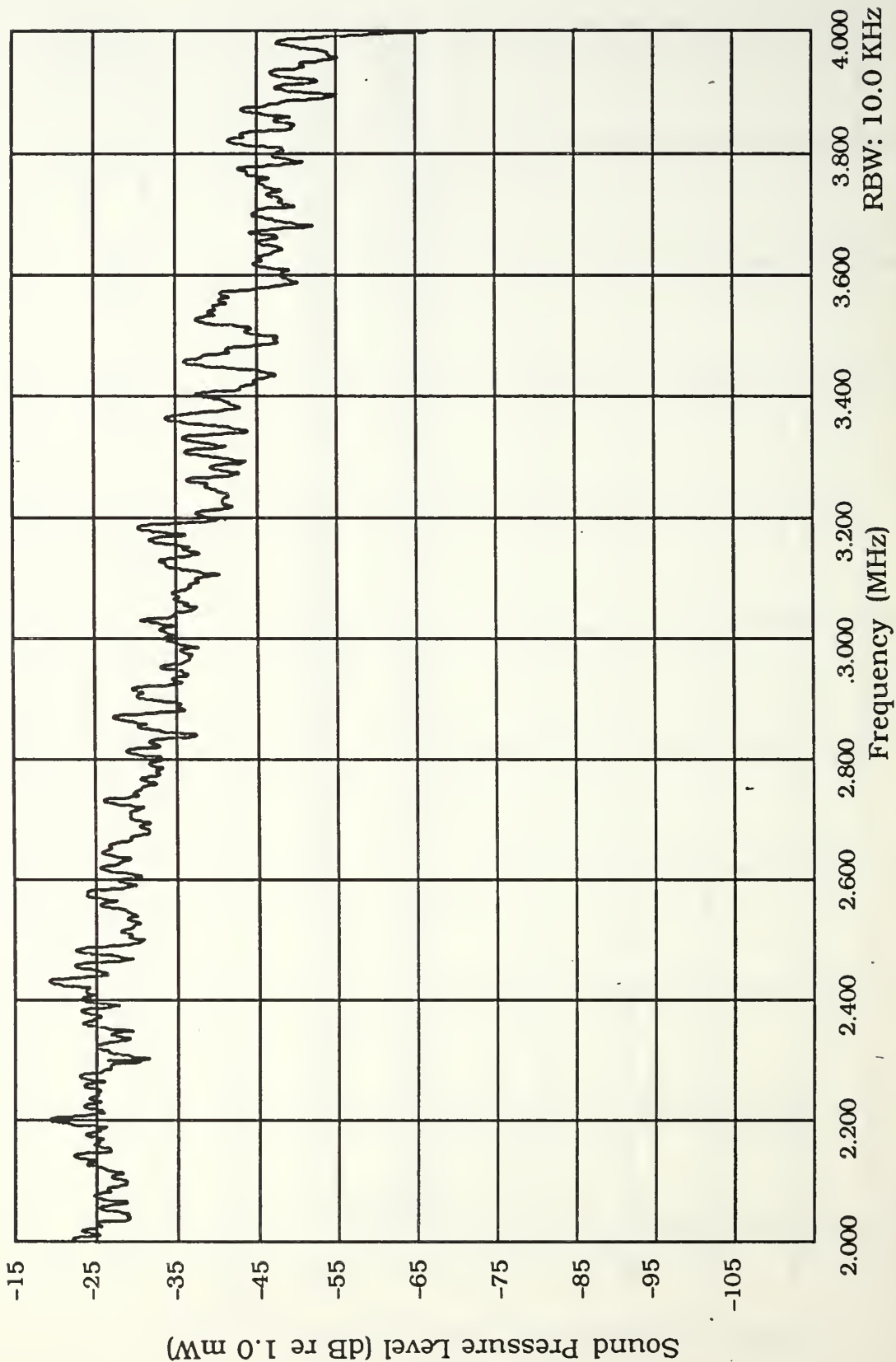
Figure 25. Receive Transducer Frequency Response Due to Reflected Imaging Sound Fields (Swept Frequencies)

RBW: 10.0 KHz

Frequency (MHz)

Sound Pressure Level (dB re 1.0 mW)

102

signal and noise plotted in Figure 26. This figure demonstrates that harmonics of the pump (f_p = 15 kHz to 310 kHz) exist throughout the frequency spectrum and higher than the imaging frequency of 2.25 MHz. The pump transducer was driven at a maximum input level of 42 volts peak to peak. This did produce very low pressure levels at the sidebands about the imaging frequency, but they were considered insignificant to bubble detection because it required direct pump sound field radiation to cause modulation and produce those low–level sidebands.

The final calibration check was to measure the sound pressure levels of the imaging and pump sound fields as they were reflected from a solid aluminum dowel placed in the sample volume. The purpose was to see if the combined sound fields would modulate if reflected from a solid. Figure 27a is the noise measurement of only the imaging sound field as it is reflected to the receive transducer. The amount of sound energy reflected at the peak (2.25 MHz) was adjusted to be similar to the same level as that reflected by a bubble stream (SPL approximately –27 dB re 1.0 mW). Figure 27b is a plot of both the imaging and pump sound fields reflected by the dowel. Figure 27c is a plot of the difference between the reflected dual sound field and the imaging "noise" sound field. Figure 27c shows no sidebands or harmonics created by the aluminum dowel, which is as expected since the dowel is solid and does not resonate.

All of the previously mentioned initial measurements were conducted to prove that the signals received in the data sets of phases one, two, and three were caused by bubbles that produced legitimate

103
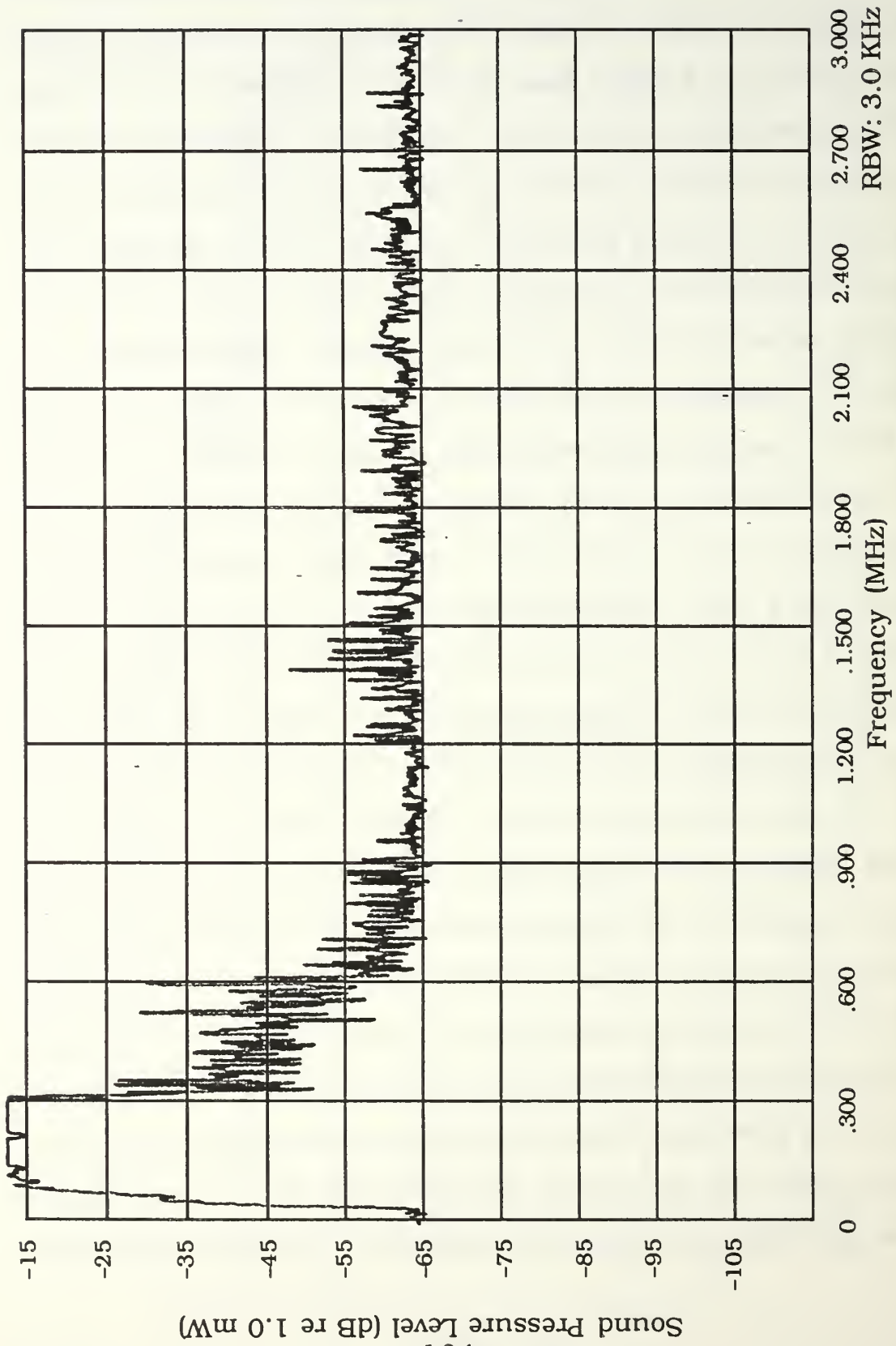
Figure 26. Frequency Modulation Due to Direct Radiation of Pump Sound Field
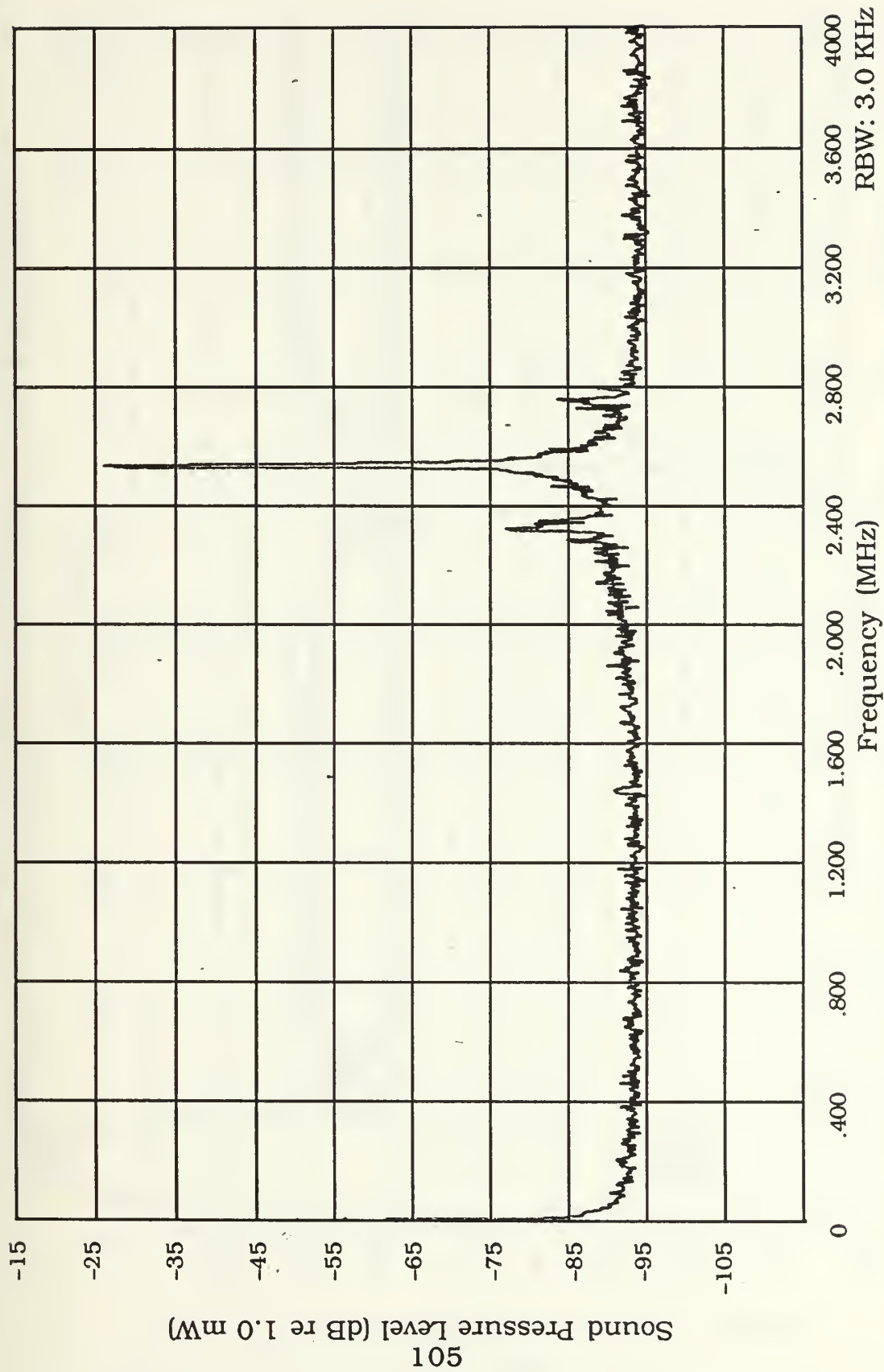
Figure 27a. Sideband and Harmonic Investigation Using Solid Reflector—Imaging Sound Field

105
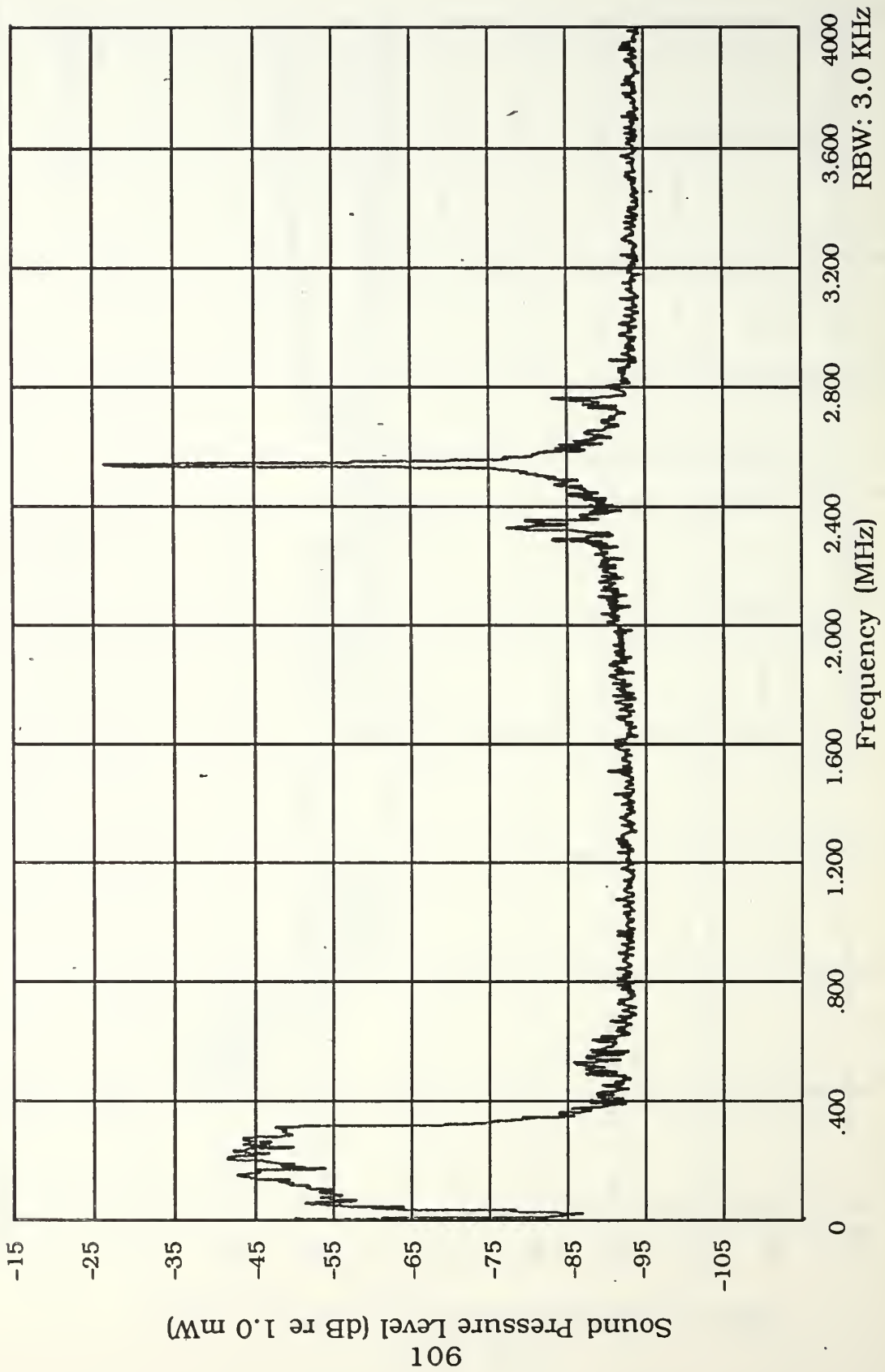
Figure 27b. Sideband and Harmonic Investigation Using Solid Reflector—
Imaging and Pump Sound Fields
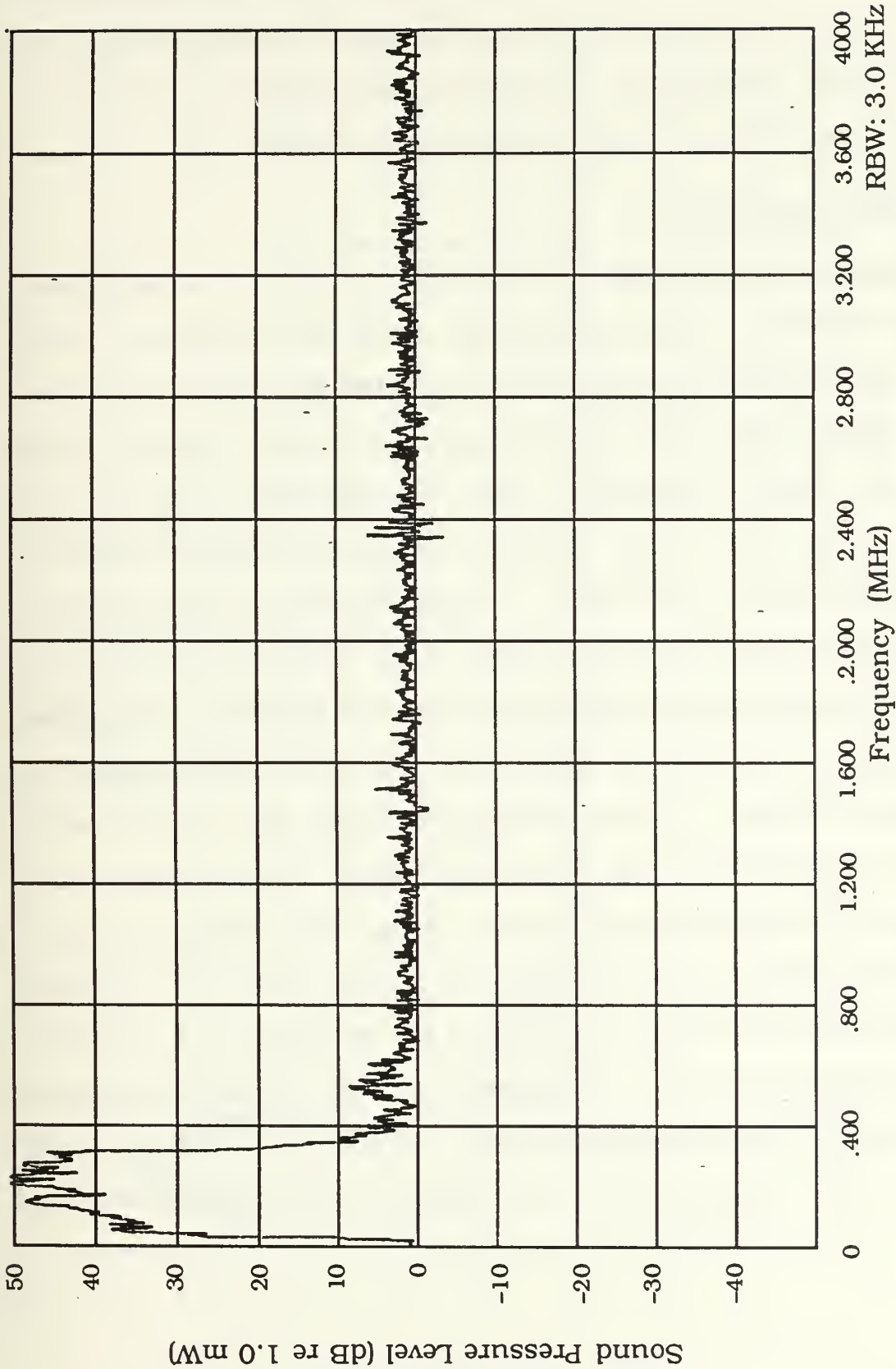
Figure 27c. Sideband and Harmonic Investigation Using Solid Reflector—
Imaging and Pump/Imaging Only Difference

107

sidebands about the imaging frequencies. The following sections present the data as it was taken during the experimental procedure and provide some observations. The same abbreviations for transducer arrangements used in Chapter III apply here in Chapter IV.

A. PHASE ONE DATA

Figures 28a, 28b, and 28c represent a baseline measurement which compares the received imaging, pump, and resonating bubble sound signals in the presence of bubbles versus the absence of bubbles. These figures show data for the Aquarium Upward Looking Pump Image Far Field$_f$ (AQUPIFF$_f$), where the subscript "f" is for fresh water, set-up and a wide HP3585A spectrum analyzer frequency window (0.0 MHz to 2.75 MHz). Figure 28a shows sound pressure levels for the pump sound field being swept from f_p = 15 kHz to 310 kHz and a sharp imaging sound level "spike" at 2.25 MHz. No bubbles are present in the sample volume and, therefore, these signals are considered "noise." Figure 28b demonstrates the change when bubbles are introduced into the sample volume. Harmonics are now evident in the frequency spectrum almost up to the imaging frequency (f_i). Sharp sideband levels appear on either side of the imaging frequency (f_i) and extend up and down the spectrum to f_i ±310 kHz. It can be noted here that the signal-to-noise ratio for the imaging sound pressure level is approximately 70 dB re 1.0 mW above the "noise" level. Figure 28c is the signal difference between the

108
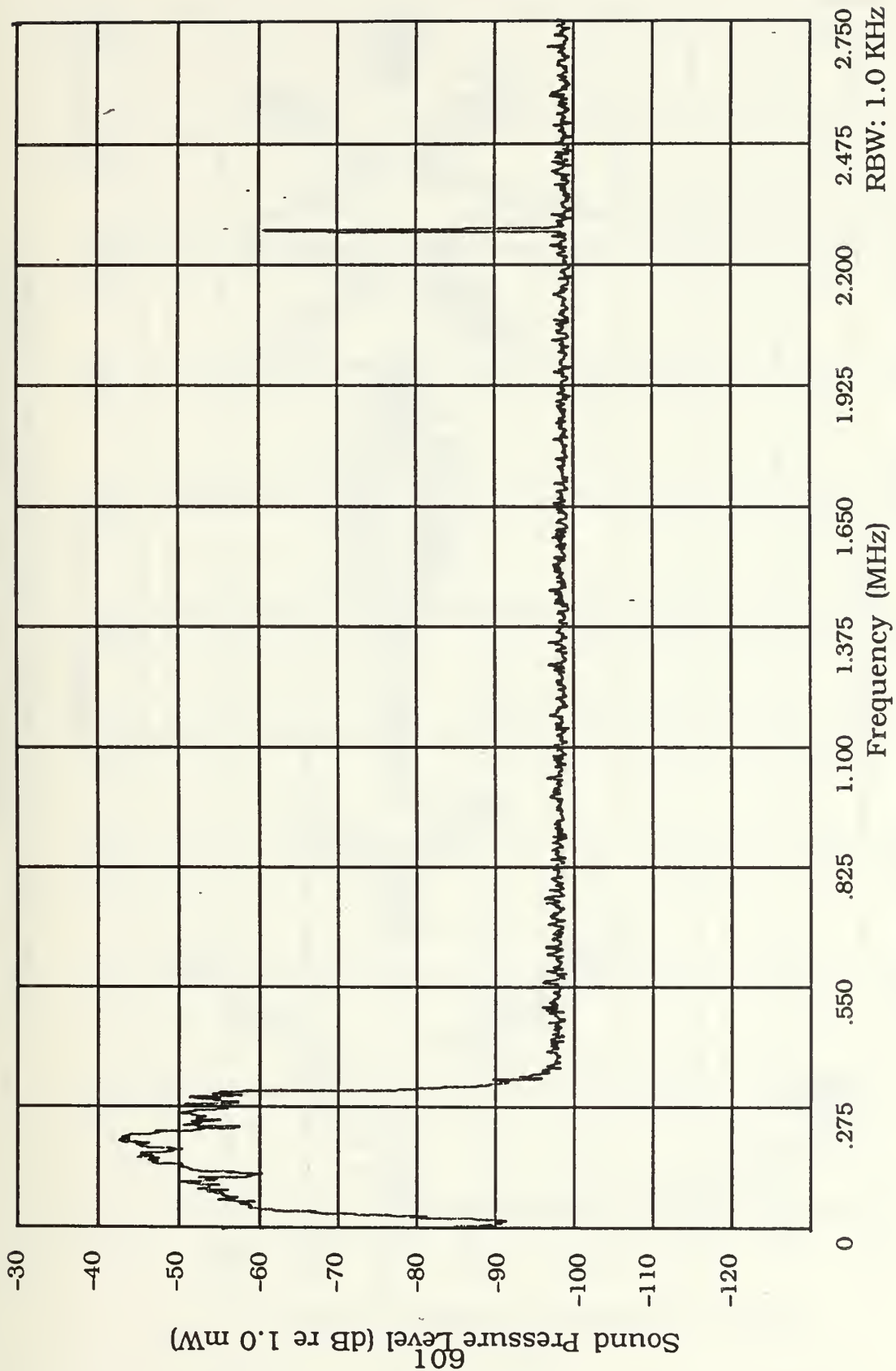
Figure 28a. Wide Spectrum Analyzer Window—AGUPIFF$_f$—
Imaging and Pump Sound Fields—No Bubbles
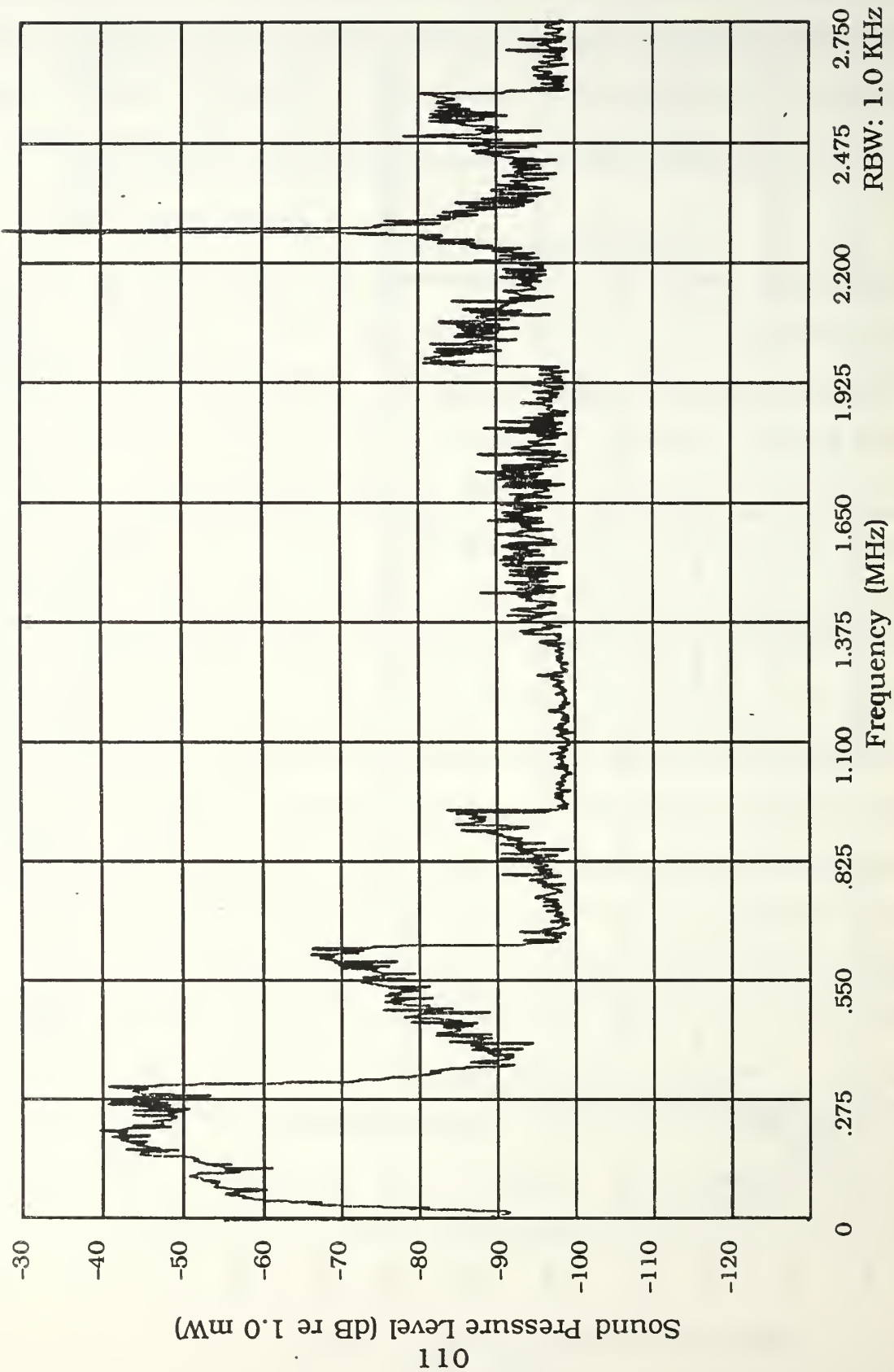
Figure 28b. Wide Spectrum Analyzer Window—AQUPIFR—Imaging and Pump Sound—Bubbles Present

RBW: 1.0 KHz

Frequency (MHz)

Sound Pressure Level (dB re 1.0 mW)

110
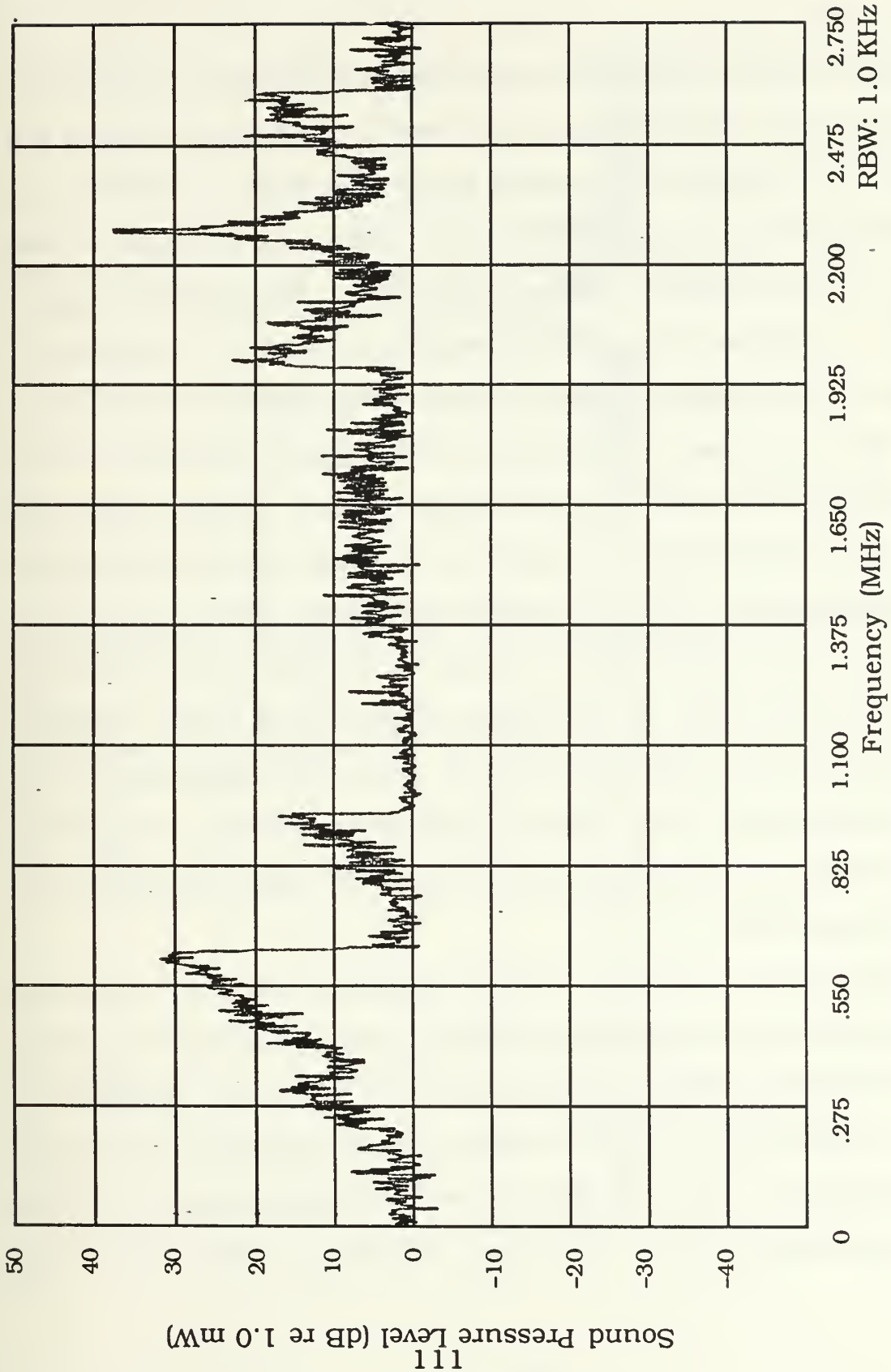
Figure 28c. Wide Spectrum Analyzer Window—AGUPIFFf—
Bubble/No Bubbles Difference

111

the presence of bubbles (Figure 28b) and the absence of bubbles (Figure 28a).

Figure set 29 is the result of constantly maintaining the bubbles as reflectors in the sample volume and shows the difference between the presence and absence of the pump sound field while the bubbles are irradiated by the imaging sound field. Data was collected in this manner for the duration of the experiments. The objective was to provide a constant target in the sample volume and maintain a constant peak imaging sound pressure level signal-to-noise ratio. Figure 29a is a "noise" measurement of the imaging sound field as it is reflected off of the bubbles in the sample volume. In Figure 29b, the pump sound field had been turned on and created distinct harmonics and dual-frequency sideband pressure levels (that can be converted to P_+ and P_-). Note again that the harmonics go high up the frequency spectrum to the point of the imaging frequency (f_i), which suggests that increasing the imaging frequency above 2.25 MHz would help avoid the harmonics. Figure 29c is a plot of the difference in signal for the presence of both imaging and pump sound fields versus only the imaging sound field.

Figure 30 is a narrow spectrum analyzer window with both imaging and pump sound fields present, creating the dual-frequency sideband sound pressure levels (P_+ and P_-) about the imaging fre-quency pressure level. Figure 30 shows a sizeable signal-to-noise ratio of approximately 12 to 15 dB for these sidebands (at $f_i \pm f_p$). The sideband pressure levels have sharp cut-offs on either side of the
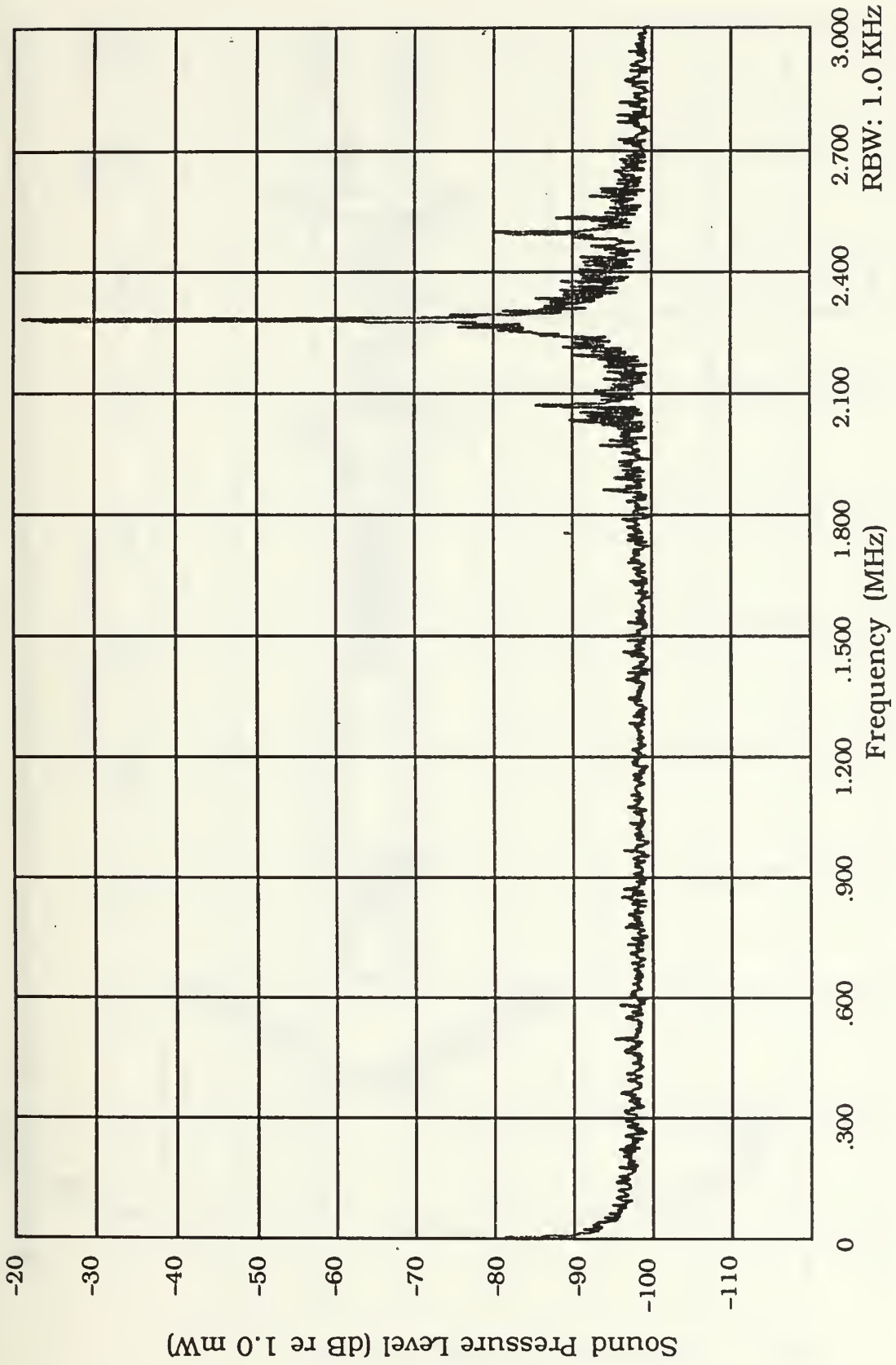
Figure 29a. Wide Spectrum Analyzer Window—AQUPIFF$_f$—Imaging Sound Field Only

RBW: 1.0 KHz

Frequency (MHz)

Sound Pressure Level (dB re 1.0 mW)

113
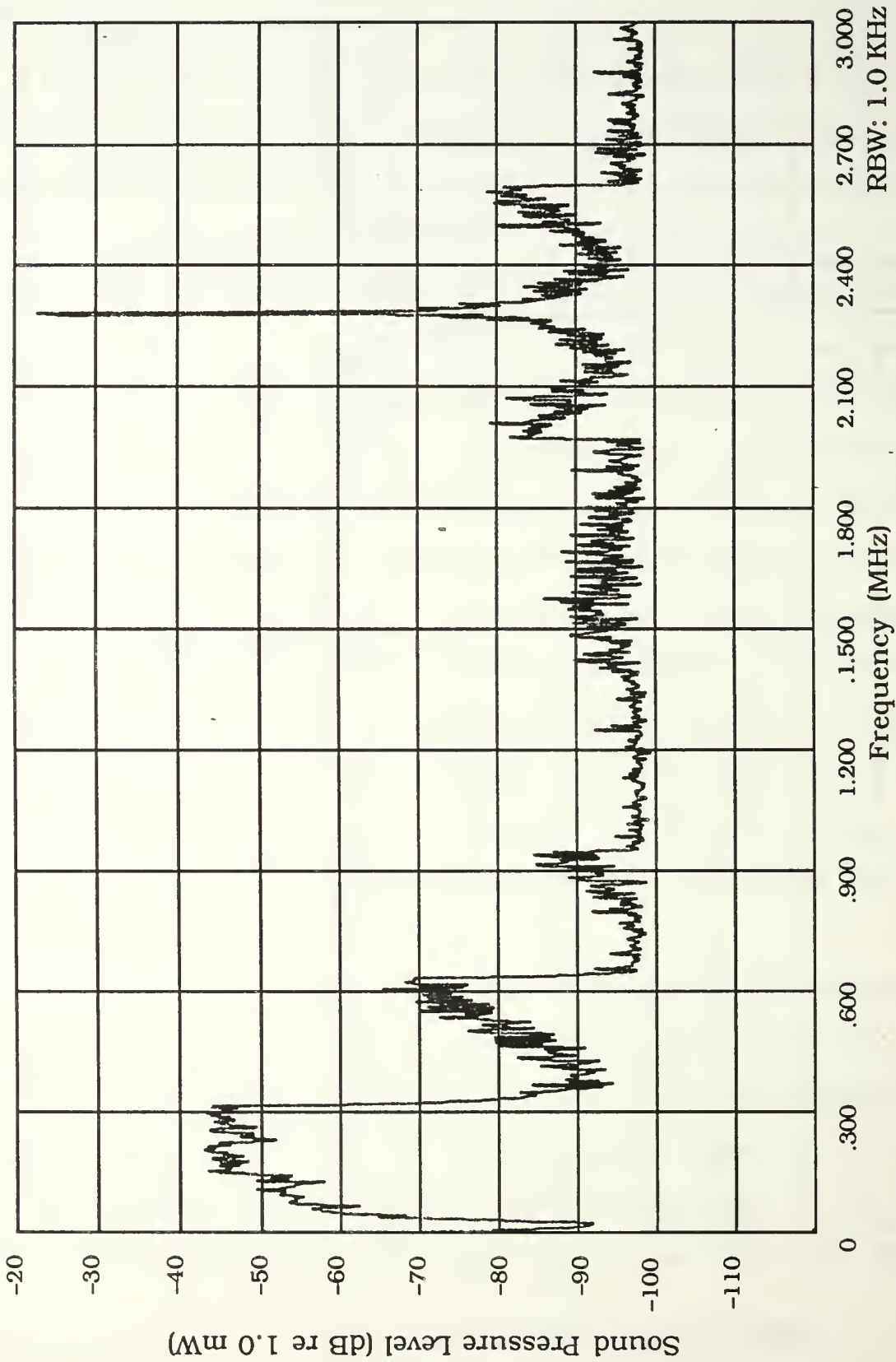
Figure 29b. Wide Spectrum Analyzer Window—AQUPIFF₁—Imaging and Pump Sound Fields

114
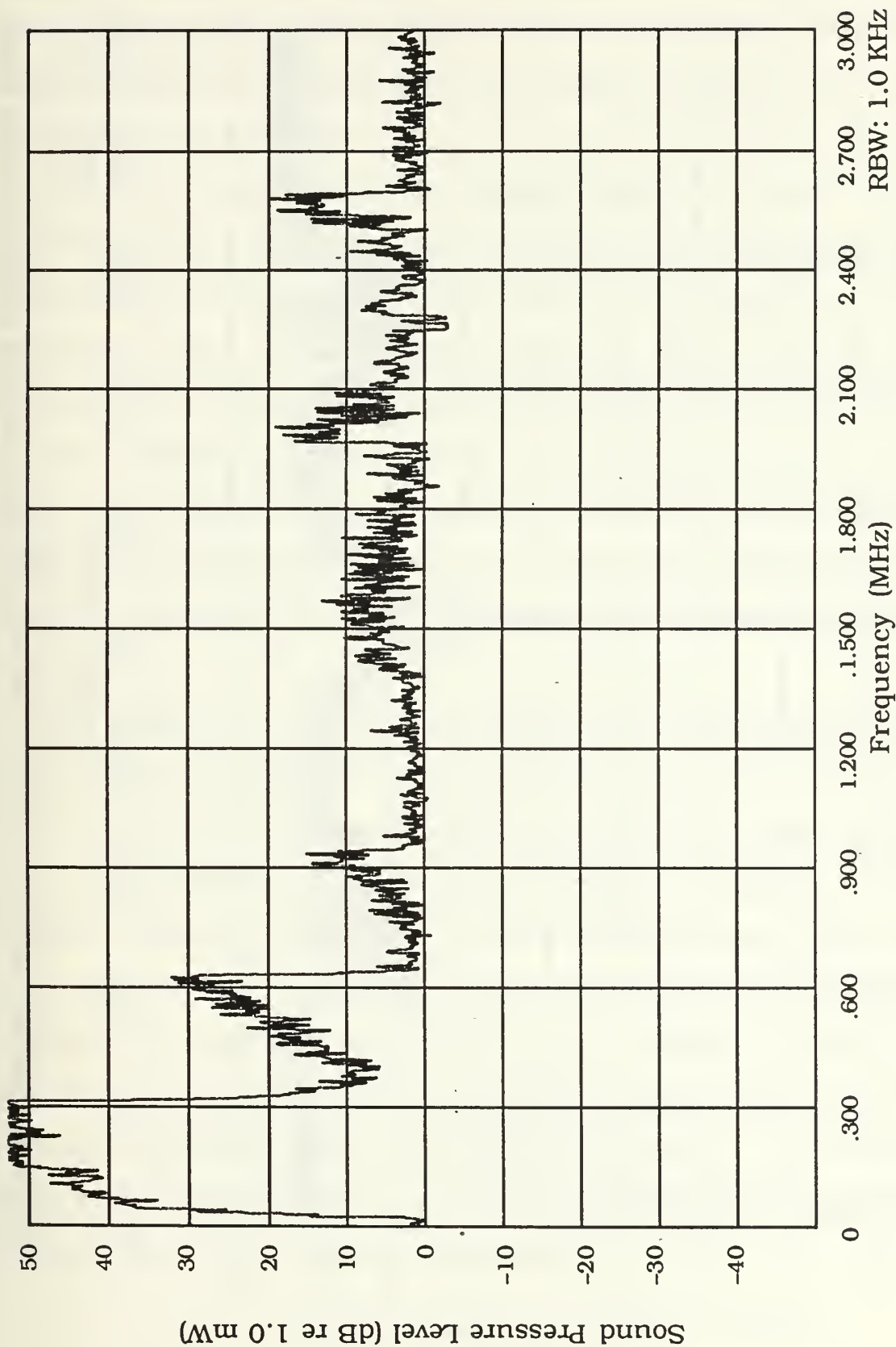
Figure 29c. Wide Spectrum Analyzer Window—AGUPIFF$_f$—
Imaging and Pump/Imaging Only Difference

115
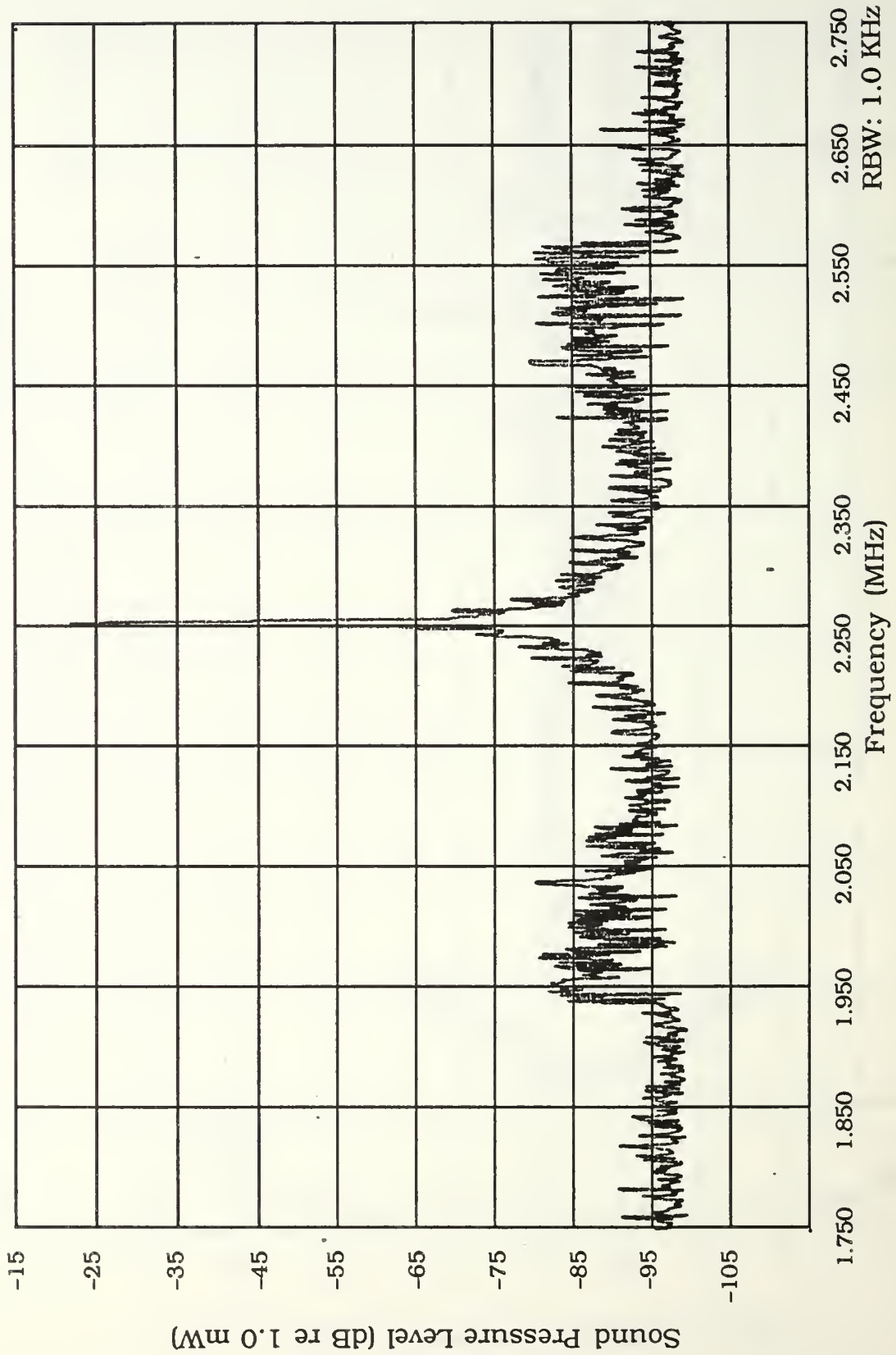
Figure 30. Narrow Spectrum Analyzer Window—AGUPIFR—Imaging and Pump Sound Fields

RBW: 1.0 KHz

Frequency (MHz)

Sound Pressure Level (dB re 1.0 mW)

116

imaging pressure level "spike" at $f_i \pm f_p$ where the pump sound field comes to the end of its sweep (f_p = 310 kHz in this case). This sharp cutoff indicates the presence of even smaller bubbles than those resonated at 310 kHz.

Figure 31 represents the same data as Figure 30, except that the pump frequency sweep range was expanded so that the pump sound field was swept from f_p = 15 kHz to 500 kHz at a normal level of 42 volts peak to peak. This was done to study the effects of pump sound field harmonics. The previous figures show sharp sideband cutoffs at f_i ±310 kHz, indicating that bubble sizes exist beyond the 310 kHz resonance range. Figure 31 shows the effect, or trade-off, of the expanded pump sweep frequencies (f_p) since the harmonics carry beyond the imaging frequency (f_i) and cover the sideband ($f_i \pm f_p$) pressure levels with noise.

The possibility of reducing the pump sound field harmonics discussed in the previous paragraph exists at reduced pump sound field power. Figures 32a and 32b are the plots of the results when reducing the pump transducer input from 42 volts peak to peak to 20 volts (Reduced Pump Power (1)) and 10 volts (Reduced Pump Power (2)), respectively. This power reduction lowered the pump pressure amplitude (p_p) supplied to the bubbles and, therefore, reduced the harmonics. Reducing the pump pressure amplitudes also lowered the pressure amplitudes of the dual-frequency sideband. The expanded pump sweep frequencies of f_p = 15 kHz to 500 kHz were maintained for the plotting of both Figures 32a and 32b.

Figure 31. Narrow Spectrum Analyzer Window—AGUPIFF$_f$—
Imaging and Expanded Pump Sound Field

118

Sound Pressure Level (dB re 1.0 mW)

Frequency (MHz)
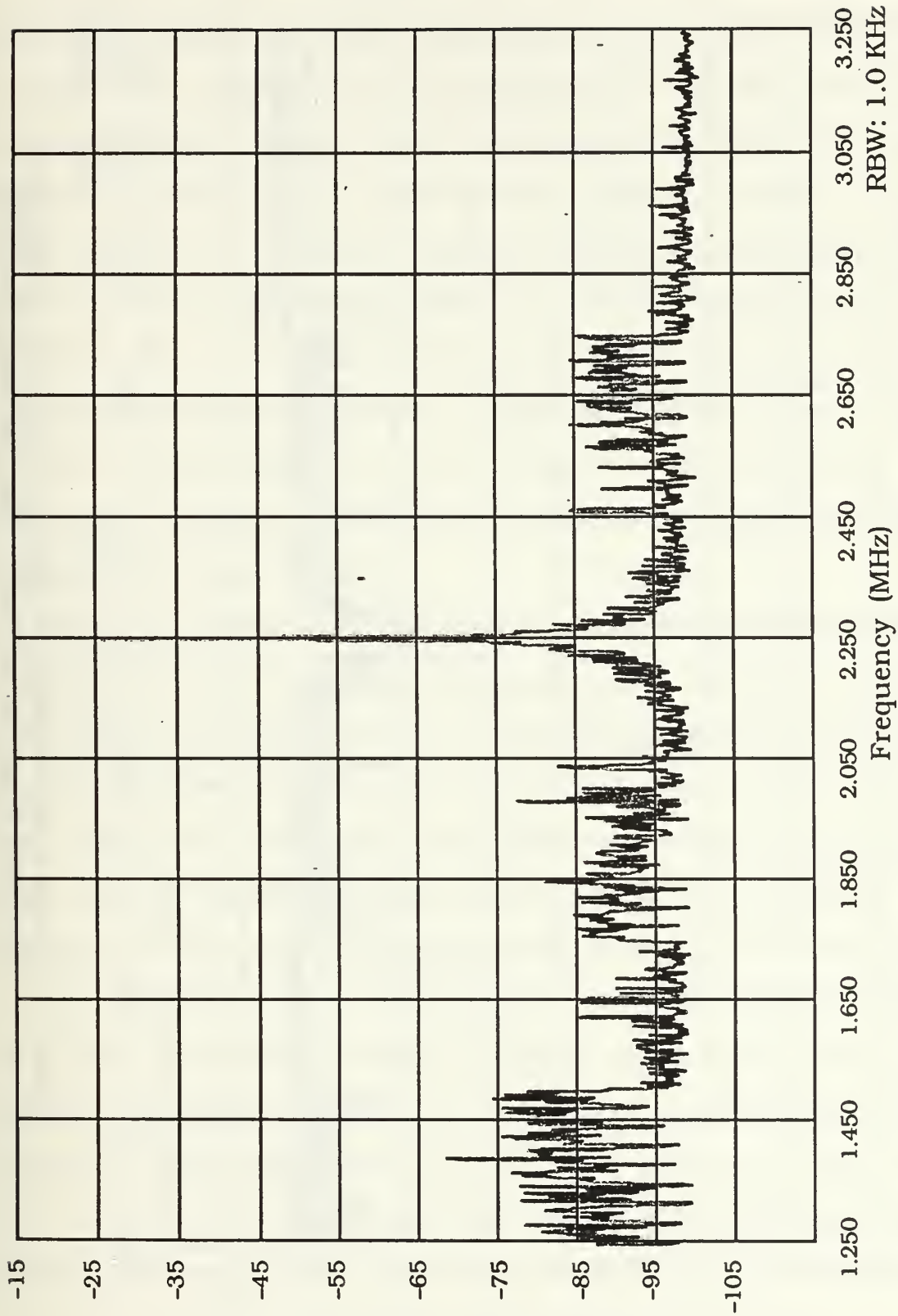
RBW: 1.0 KHz

Figure 32a. Narrow Spectrum Analyzer Window—AQUPIFF$_f$ —Imaging and
Expanded Pump Sound Fields—Reduced Pump Power (1)

119
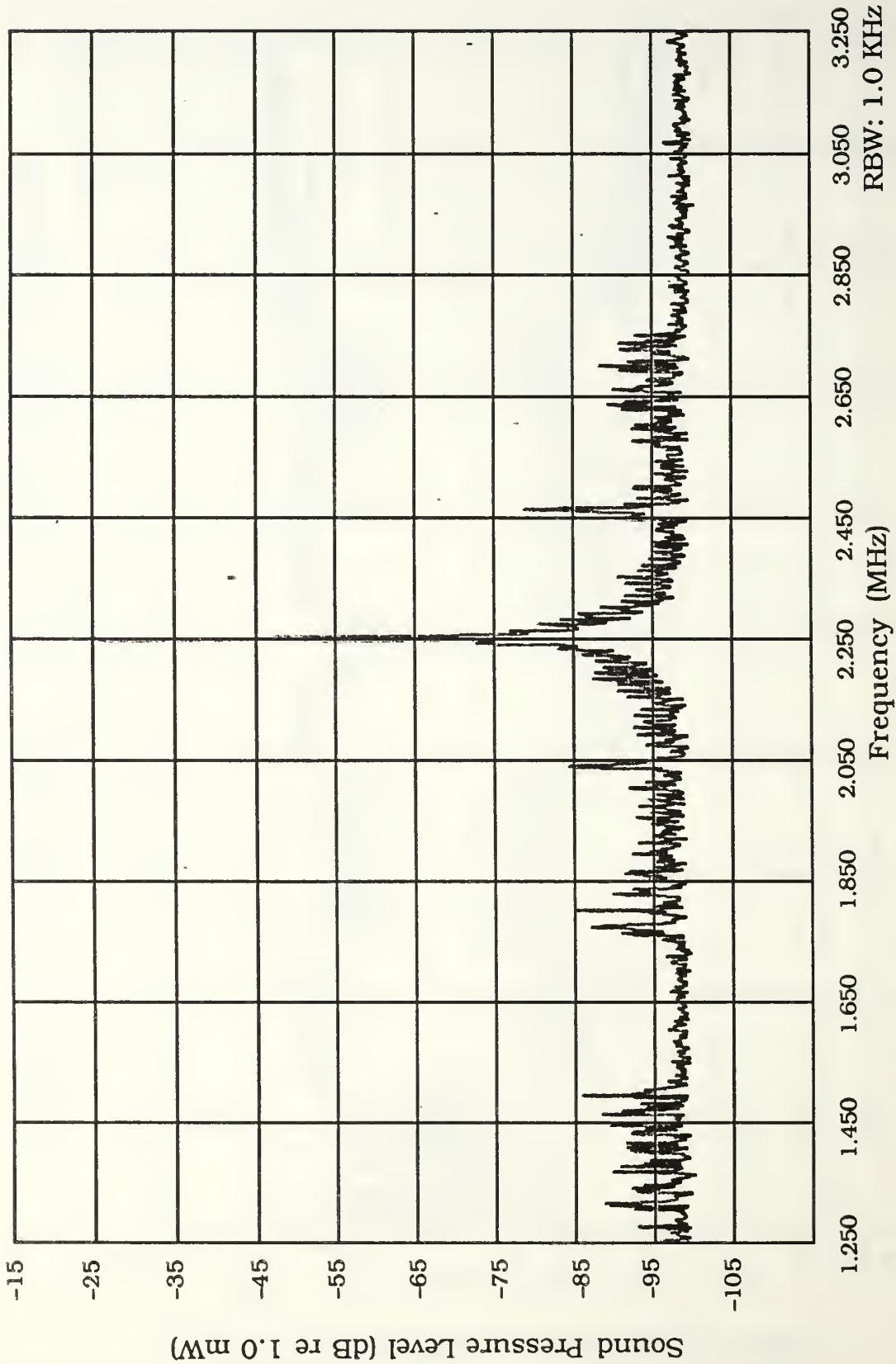
Figure 32b. Narrow Spectrum Analyzer Window—AQUPIFF₁—Imaging and Expanded Pump Sound Fields—Reduced Pump Power (2)

120

The transducer arrangement was changed to the Aquarium Upward Looking Pump Image Near Field in fresh water, designated the AQUPINF$_f$. This was done to investigate the receive transducer sensitivity and the imaging transducer power inputs when the sample volume was in the near field. Figure 33 is a narrow spectrum analyzer window plot of the sideband pressure levels and associated noise levels for the normal imaging level of 6 volts and imaging frequency (f_i) of 2.25 MHz. The pump frequency (f_p) was swept from 15 kHz to 310 kHz at 42 volts peak to peak. The sideband pressure levels shown in Figure 33 show a clear cut-off at $f_i \pm 310$ kHz, indicating the termination of the pump frequency sweep, not the lack of smaller bubbles in the sample volume.

Since the bubble sizes present in the sample volume extend beyond the 310 kHz resonance frequency range, Figure 34 is plotted for the AQUPINF$_f$ with the input to the imaging transducer reduced to 3.0 volts and the pump frequencies (f_p) expanded to range from 15 kHz to 420 kHz. The imaging input level was reduced to check the effects on the harmonics created by the resonating bubbles and demonstrate the direct relationship of the imaging sound field (p_i) to the sidebands (P_+). Figure 34 shows that the sidebands ($f_i \pm f_p$) are still present at the reduced image transducer input level, however, the resonance harmonics still go higher up the frequency spectrum beyond the upper sideband ($f_i \pm f_p$) pressure level at 2.67 MHz. Note that reducing the imaging pressure amplitudes lowers the dual-frequency sideband pressure amplitudes (see Figure 33 for comparison).
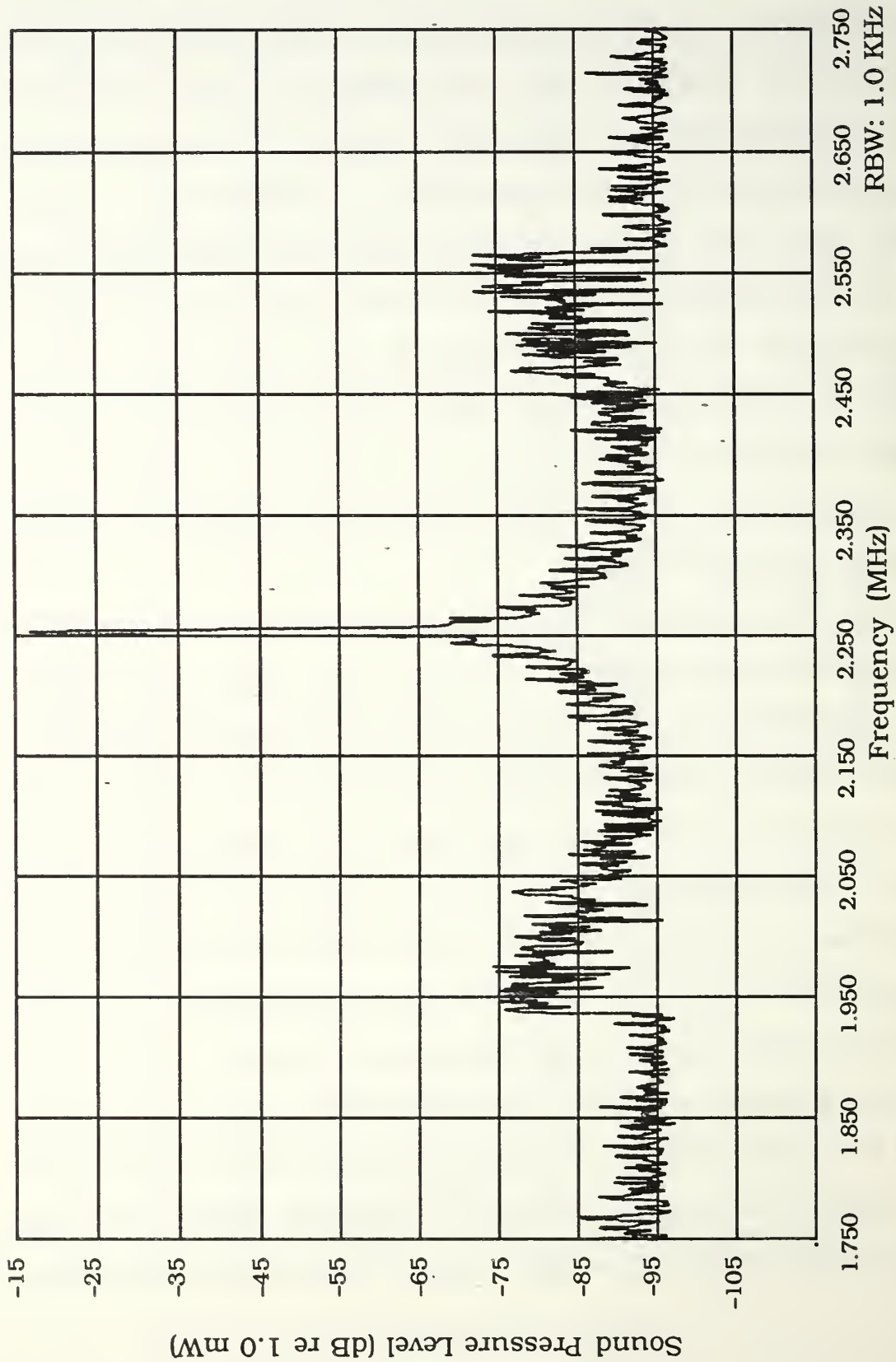
Figure 33. Narrow Spectrum Analyzer Window—AQUPINF$_f$—Imaging and Pump Sound Field

122

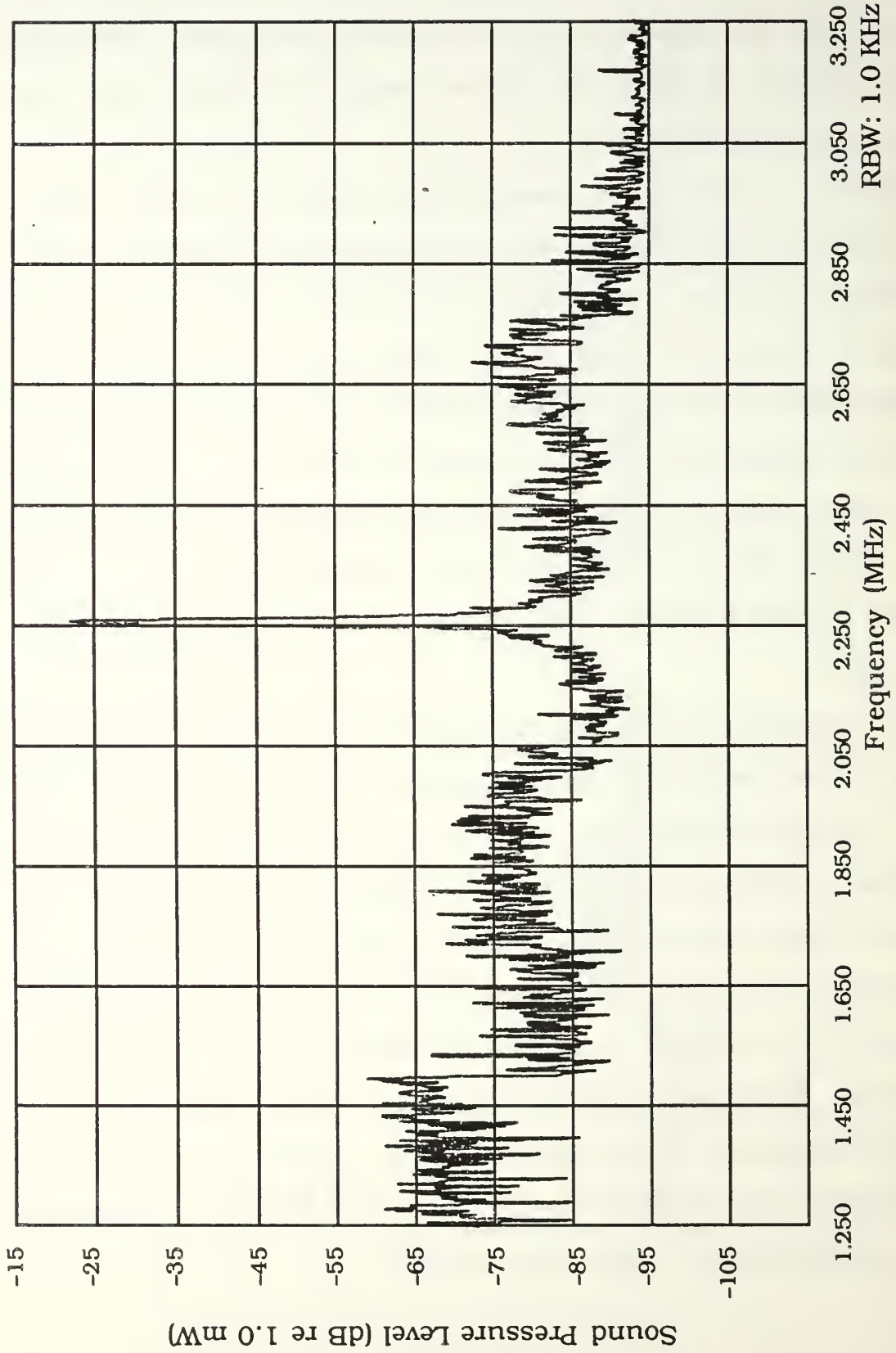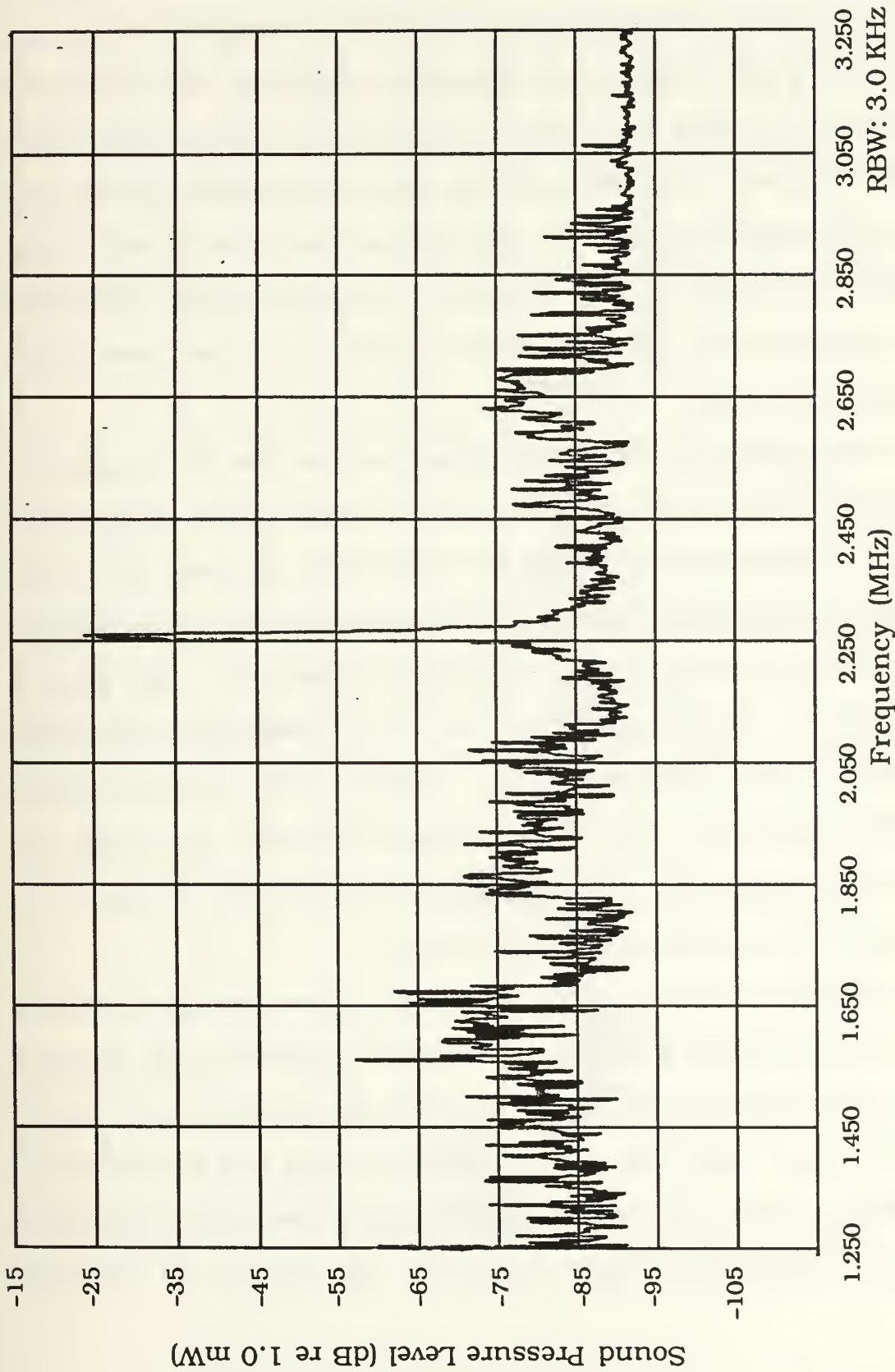Figure 34. Narrow Spectrum Analyzer Window—AGUPINF$_f$—Imaging and Expanded Pump Sound Field—Reduced Image Power

123

In an effort to avoid the noise caused by harmonics, the imaging frequency (f_i) was increased to 2.51 MHz, moving the imaging pressure level peak further up the frequency spectrum. The results of this frequency increase are plotted in Figure 35. The imaging input level is still reduced to 3.0 volts and the pump frequencies (f_p) are still expanded to range from 15 kHz to 420 kHz so that a comparison with Figure 34 can be made. Note in Figure 35 that the upper sideband pressure levels (at $f_i + f_p$ = 2.67 MHz) are now free of the resonating bubble harmonic noise.

The final data set collected in phase one was for the Aquarium Downward Looking Pump Image Far Field in fresh water, designated AQDPIFF$_f$. This data set is plotted in Figures 36a, 36b, and 36c. The downward–looking pump transducer experiment was for comparison with the upward–looking pump transducer experiment. The transducer inputs are: imaging transducer at f_i = 2.50 MHz and input level at 6.0 volts; pump transducer at f_p = 15 kHz to 310 kHz and input level at 42 volts peak to peak. The imaging frequency (f_i) is high on the frequency spectrum to better avoid the harmonics induced by resonating bubbles and the pump sound field.

Figure 36a is a wide spectrum analyzer window plot of the imaging sound field reflected from a small stream of bubbles in the sample volume. Figure 36a is the "noise" level for the downward–looking pump data runs. Figure 36b is a plot of the imaging and pump sound fields interacting with the bubble stream. Figure 36c is the difference between the signal levels plotted in Figures 36b and 36a. It appears
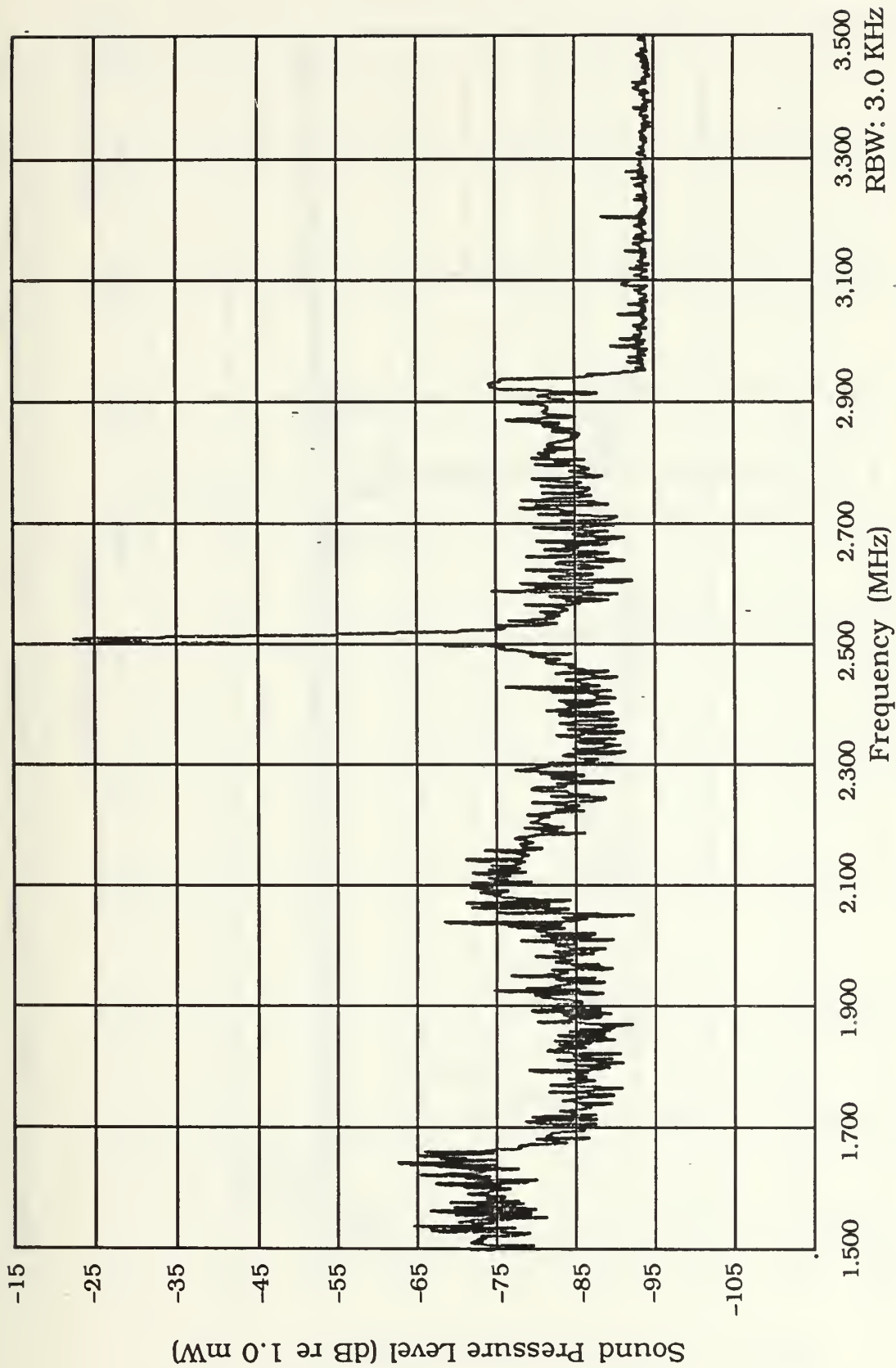
Figure 35. Narrow Spectrum Analyzer Window—AQUPINF$_f$—High Imaging and Expanded Pump Sound Field—Reduced Image Power

125
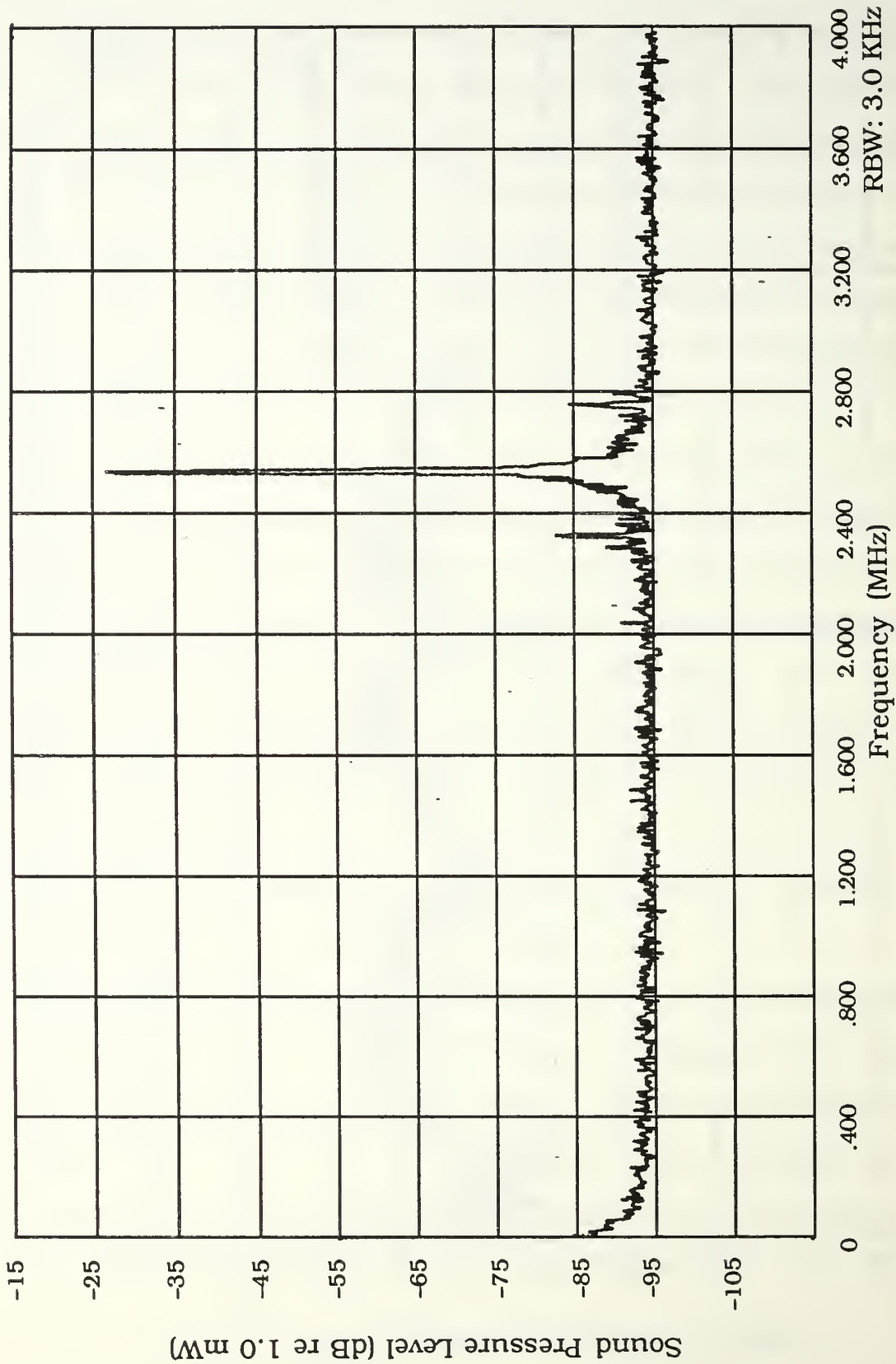
Figure 36a. Wide Spectrum Analyzer Window—A9DPIFFf—High Imaging Sound Field Only

126

Figure 36b. Wide Spectrum Analyzer Window—AQDPIFF̄ —High Imaging and Pump Sound Fields

127

Figure 36c. Wide Spectrum Analyzer Window—AODPIFF$_f$—High Imaging and Pump/High Imaging Only Difference

RBW: 3.0 KHz

Frequency (MHz)

Sound Pressure Level (dB re 1.0 mW)

128

from the pressure levels plotted in Figures 36b and 36c that the downward-looking pump transducer provides the same signal-to-noise ratios as the upward-looking pump transducer.

B.   PHASE TWO DATA

Phase two was conducted in the ten-gallon aquarium with sea-water and two different transducer arrangements. Further transducer arrangements were not used in this phase because the primary purpose of phase two was only to show the compatibility of the dual-frequency bubble density measurement technique with seawater and the ship wake bubble density problem. To draw a comparison between fresh water and seawater, the Aquarium Upward Looking Pump Image Far Field$_s$ (AQUPIFF$_s$) (the subscript "s" designates each experiment conducted in seawater) transducer arrangement was used to repeat the previous fresh-water data runs.   The second transducer arrangement used in seawater was the Large Tank Downward Looking Pump Image Far Field$_s$ (LTDPIFF$_s$) mount designed for use in the large, acoustically insulated tank (approximately three meters deep). This second transducer arrangement was initially tested in seawater and, because it closely approximated the fresh water downward-looking pump transducer mount (AQDPIFF$_f$), was used to compare the downward-looking pump in seawater versus fresh water.

The first seawater data plotted was obtained using the AQUPIFF$_s$ transducer arrangement. A wide spectrum analyzer window, with standard imaging and pump transducer inputs (f_i = 2.25 MHz at 6.0 volts, f_p = 15 kHz to 310 kHz at 42 volts peak to peak), was used to

plot Figures 37a, 37b, and 37c. As before, Figure 37a was plotted with only the imaging sound field reflected from the bubble stream, and is considered the "noise" level. Figure 37b plots the received signal resulting from bubbles being irradiated by both imaging and pump sound fields. Figure 37c is the difference between the signal received from the bubbles with both sound fields present (Figure 37b) and the imaging noise (Figure 37a). The sideband pressure levels present at the sideband frequencies $(f_i \pm f_p)$ correspond to the pump frequencies that were swept, however, there appears to be a lower signal-to-noise ratio for both imaging and sideband pressure levels in seawater. Figure 38 is a plot using a narrow spectrum analyzer window, or "close-up," of the sideband pressure levels shown in Figure 37b. Figure 38 data also shows the slightly lower imaging and sideband signal-to-noise ratio when compared to the same data of Figure 30 for fresh water.

The second transducer arrangement used in phase two of the experiment was the LTDPIFF$_s$ in the aquarium. Figures 39a, 39b, and 39c again show harmonics which result from resonating bubbles under the influence of the pump sound field (sweeping frequencies $f_p = 15$ kHz to 310 kHz), and the sideband pressure levels which result from dual-frequency bubble excitation. Figure 39a is a plot of the "noise" signal received when the bubbles are irradiated by only the imaging sound field. Figure 39b is a plot of the received signal from the bubbles when both imaging and pump sound fields are present. Figure 39c is a plot of the reflected imaging "noise" subtracted from the imaging and resonating bubble sound fields. Figure 40 is a

Figure 37a. Wide Spectrum Analyzer Window—AGUPIFFs—Imaging Sound Field Only
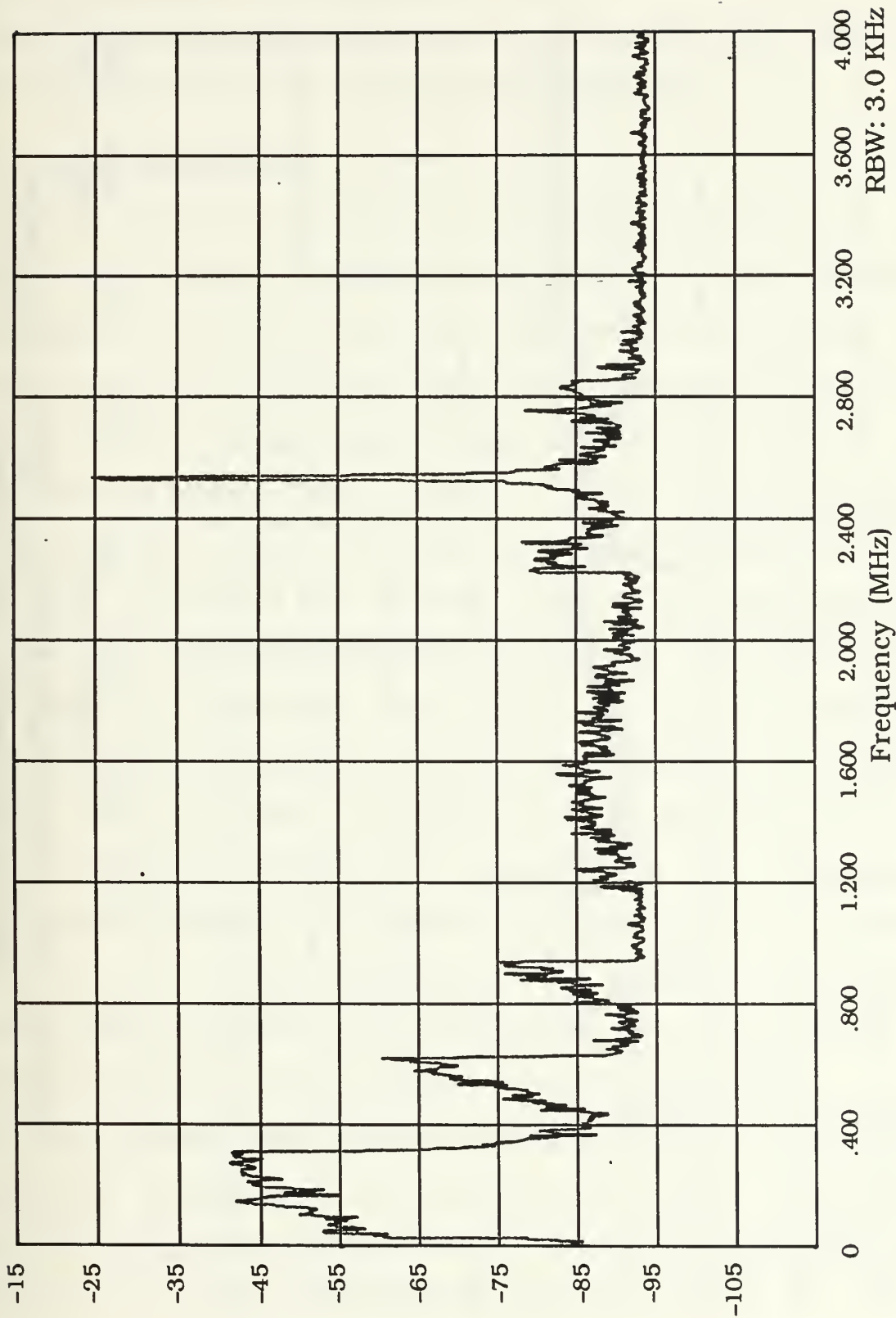
RBW: 3.0 KHz

131
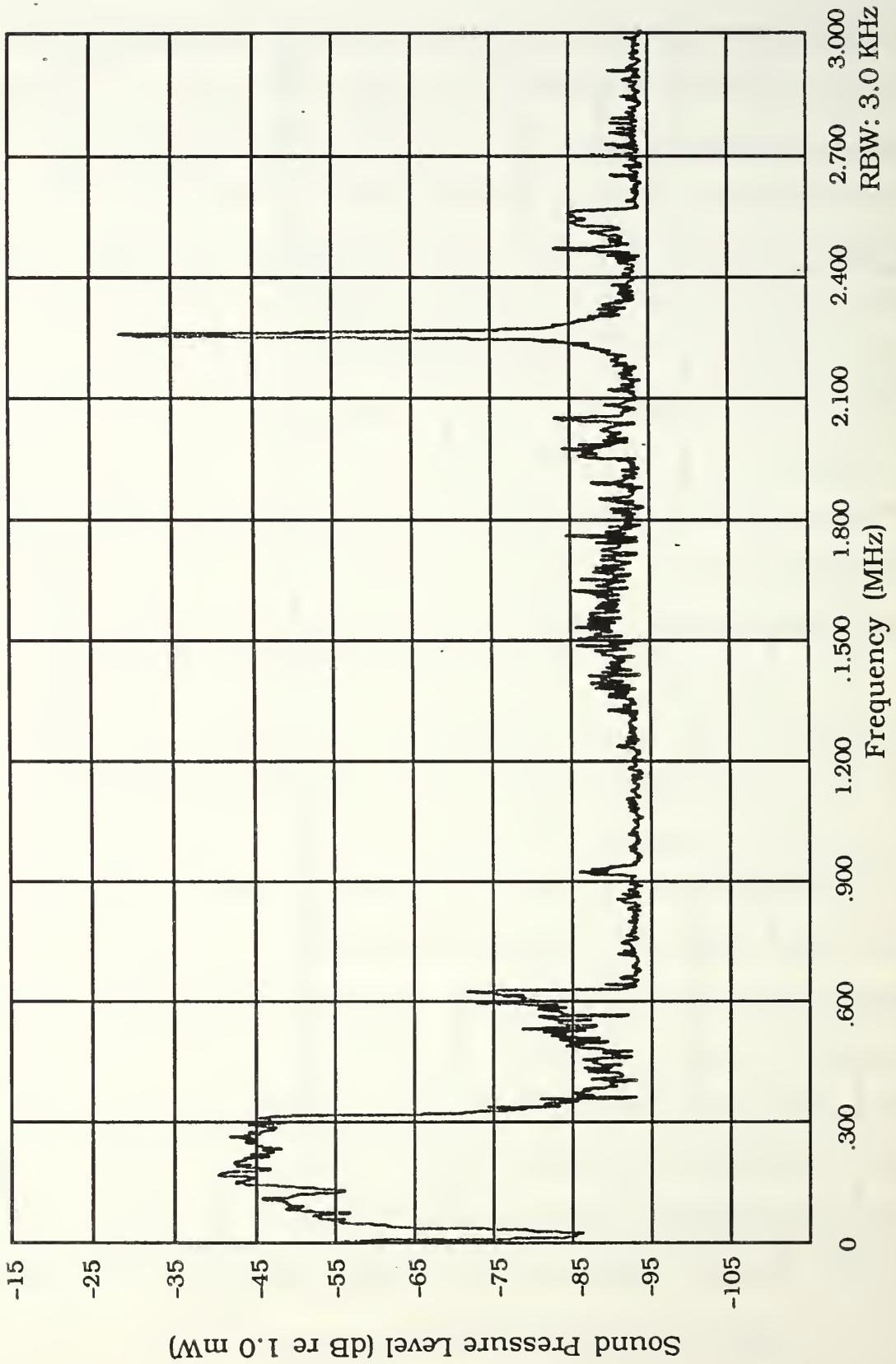
Figure 37b. Wide Spectrum Analyzer Window—AQUPIFF$_s$—Imaging and Pump Sound Fields

132
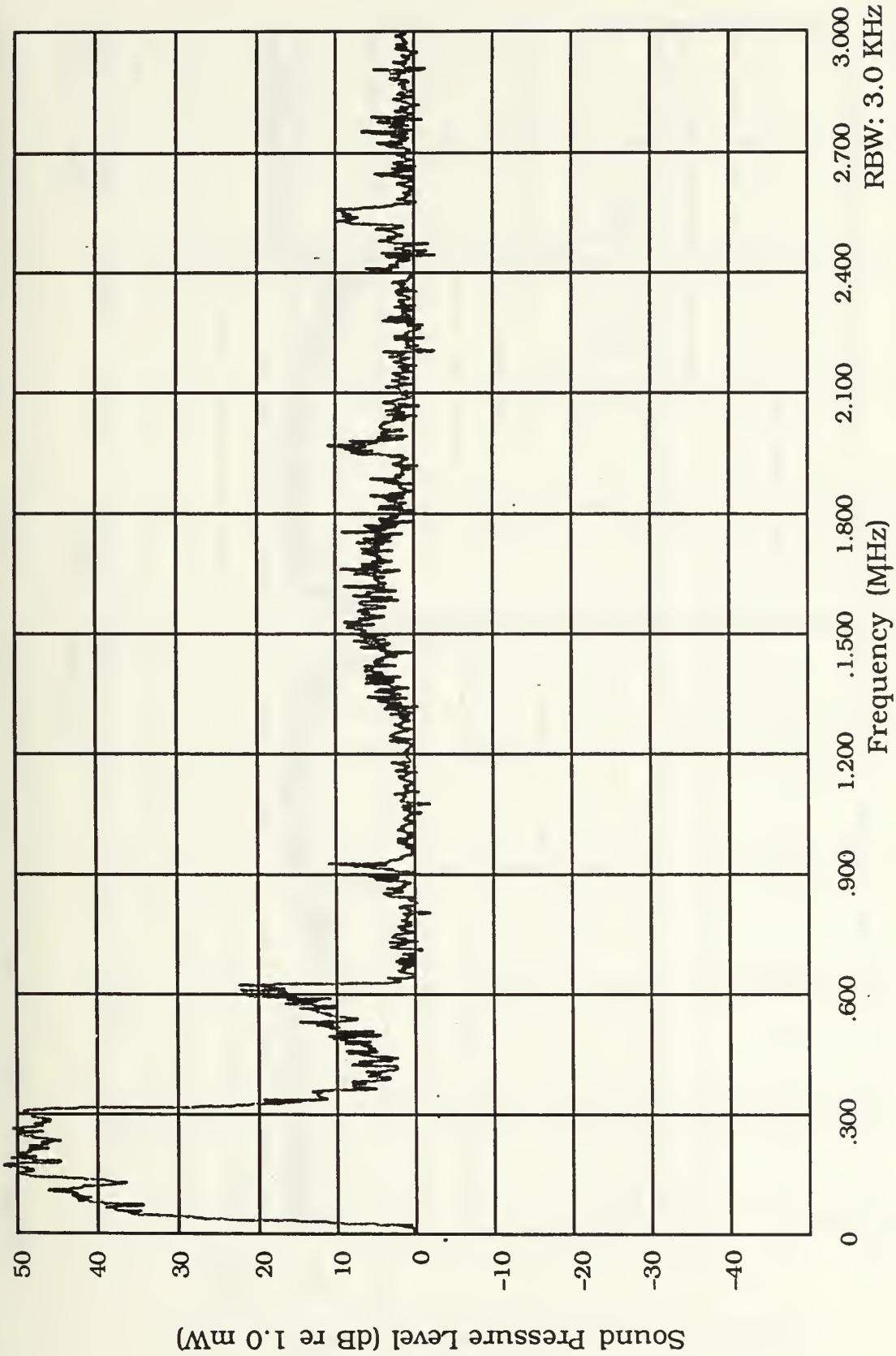
Figure 37c. Wide Spectrum Analyzer Window—AQUPIFF$_s$—
Imaging and Pump/Imaging Only Difference

RBW: 3.0 KHz

Frequency (MHz)

Sound Pressure Level (dB re 1.0 mW)

133
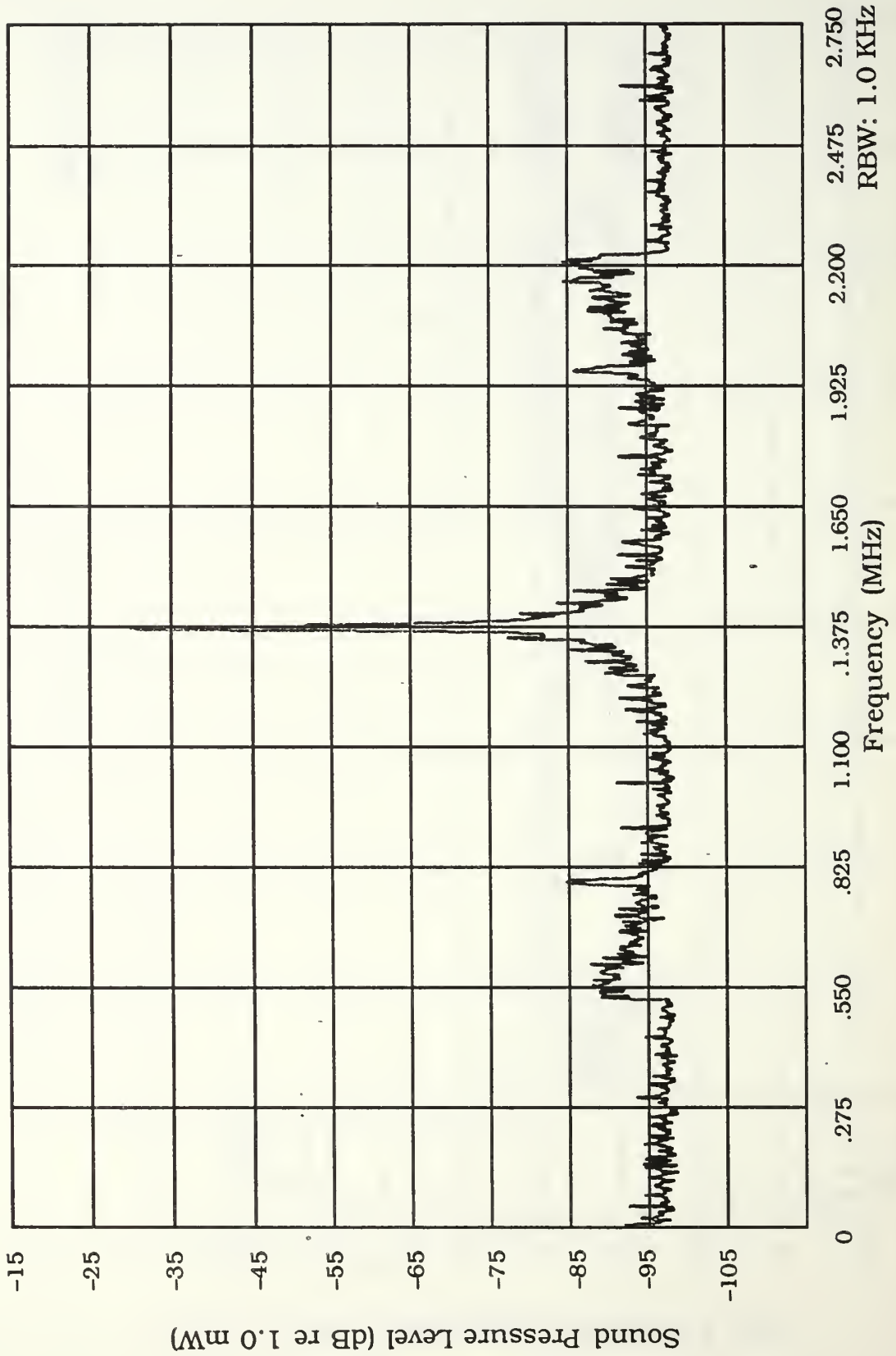
Figure 38. Narrow Spectrum Analyzer Window—AQUPIFF$_s$—Imaging and Pump Sound Fields

134
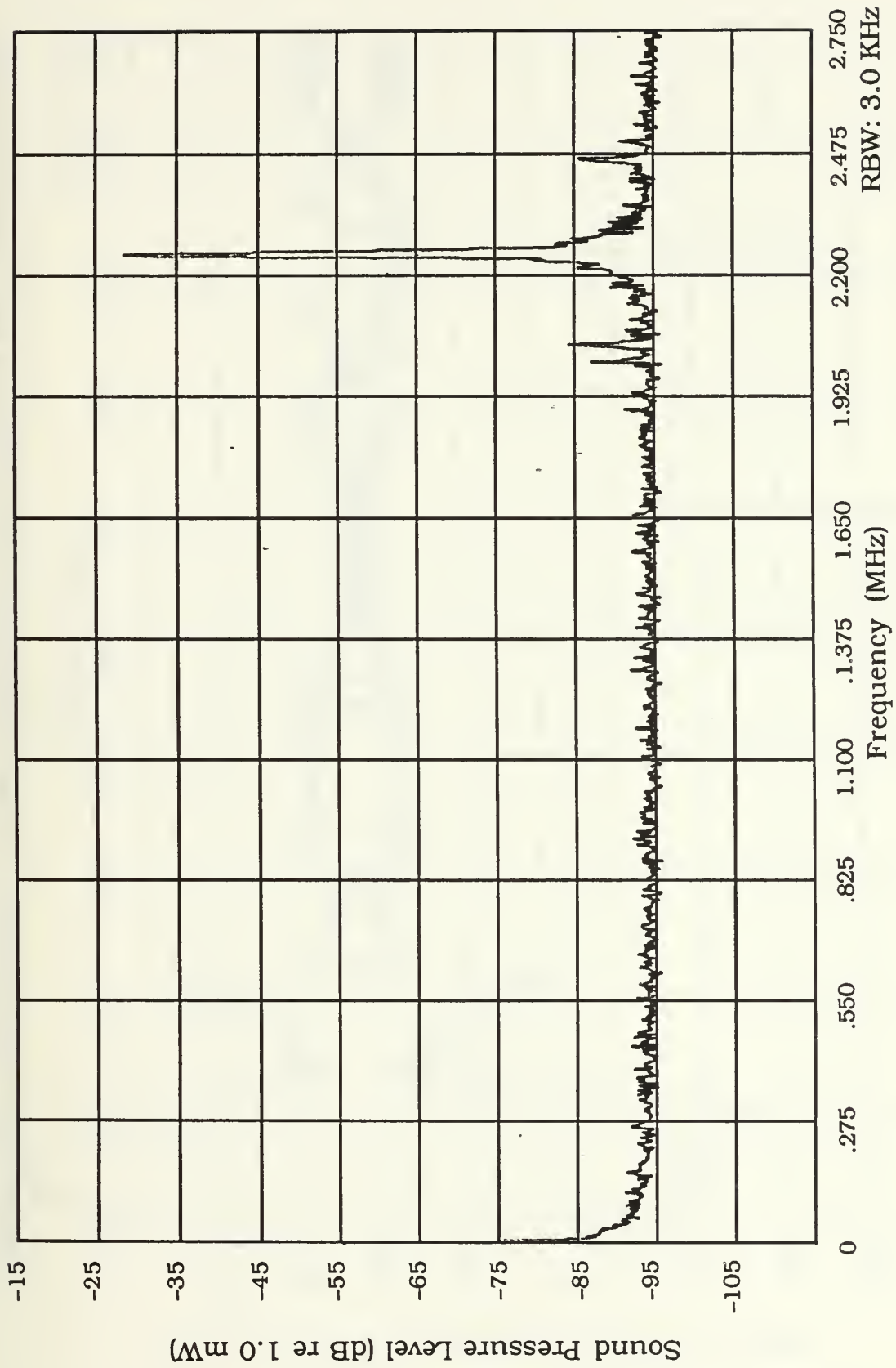
Figure 39a. Wide Spectrum Analyzer Window—LTDPIFFs—Imaging Sound Field Only

135
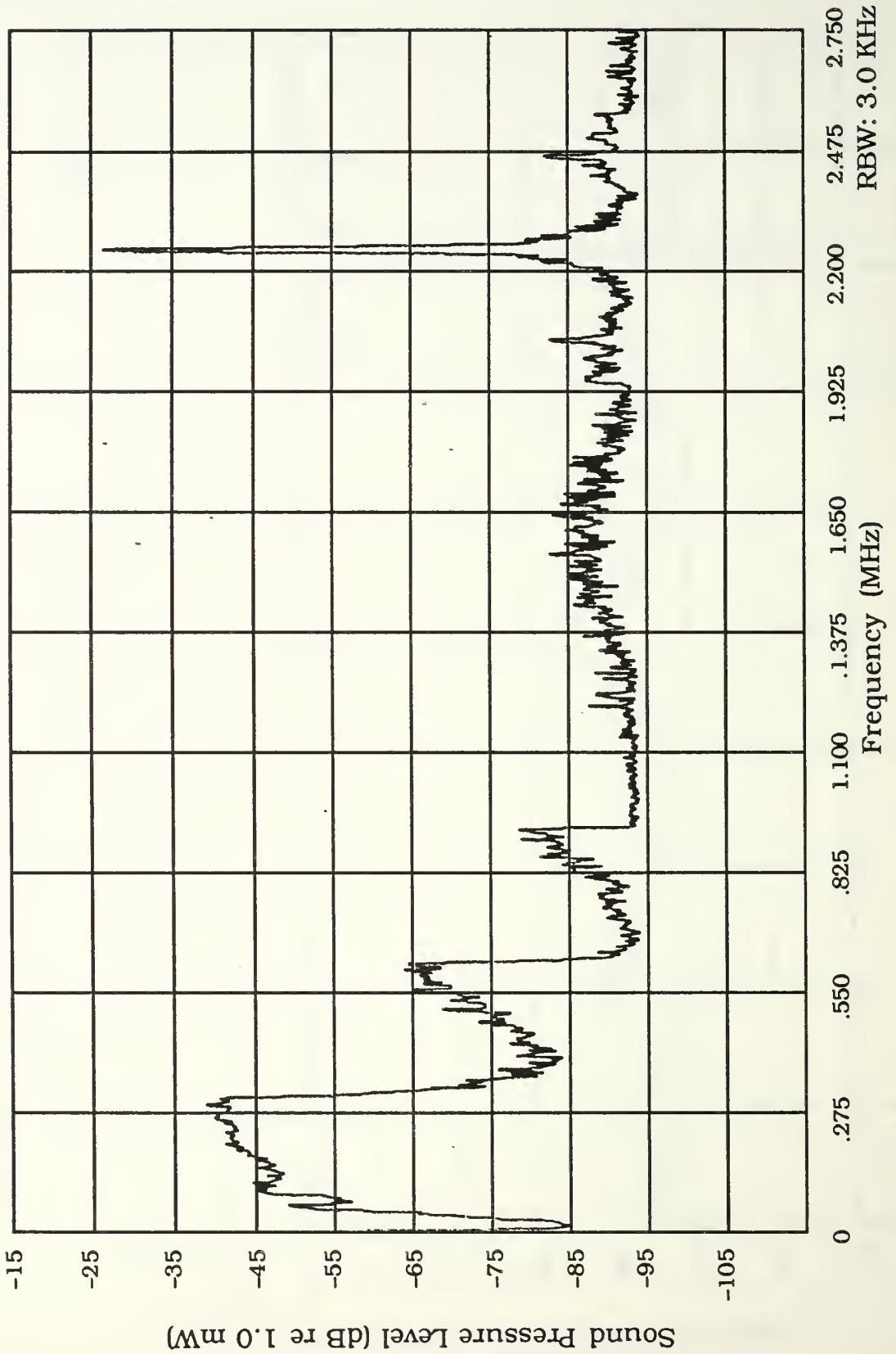
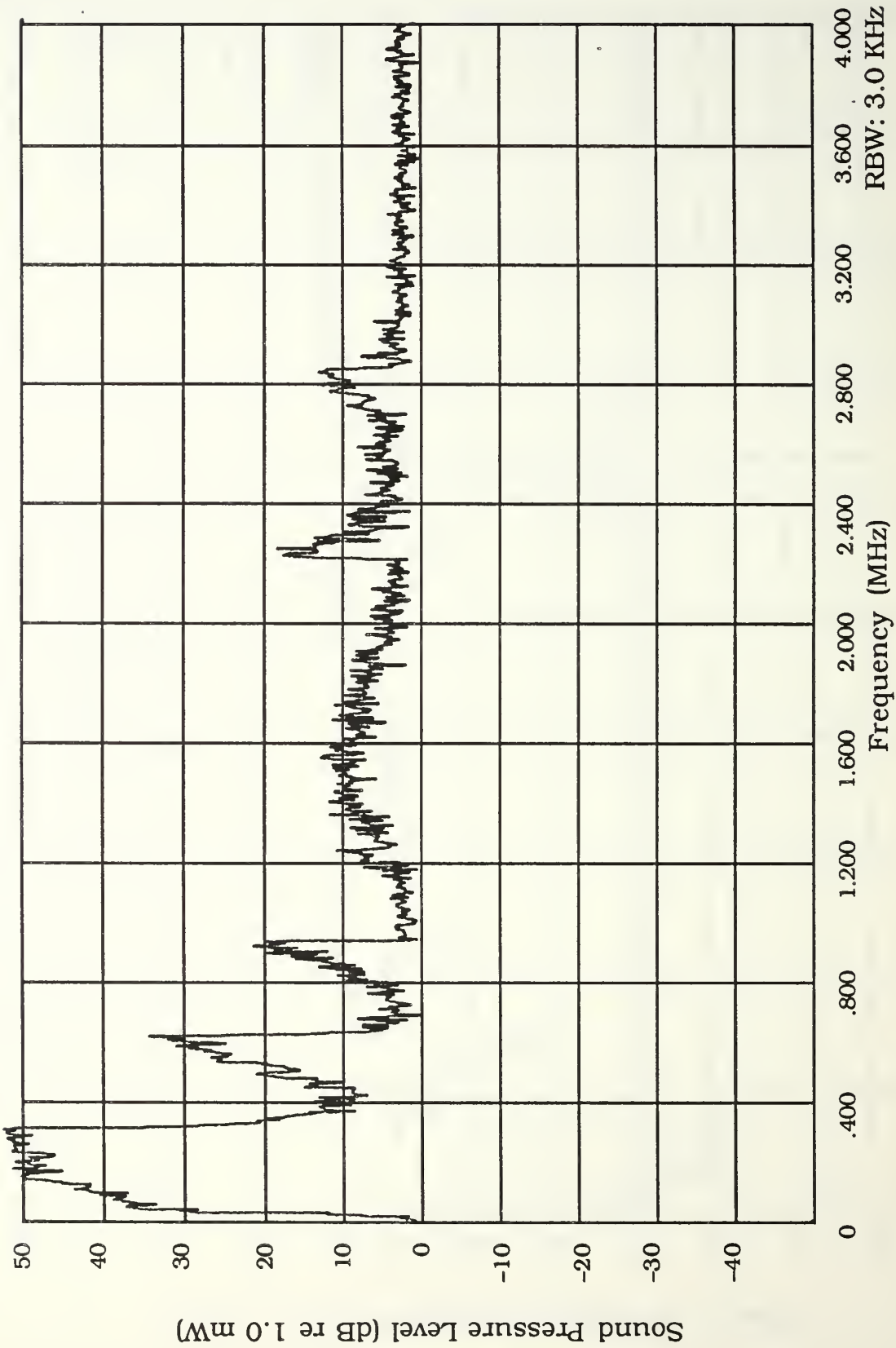**Figure 39b. Wide Spectrum Analyzer Window—LTDPIFFs—Imaging and Pump Sound Fields**

136
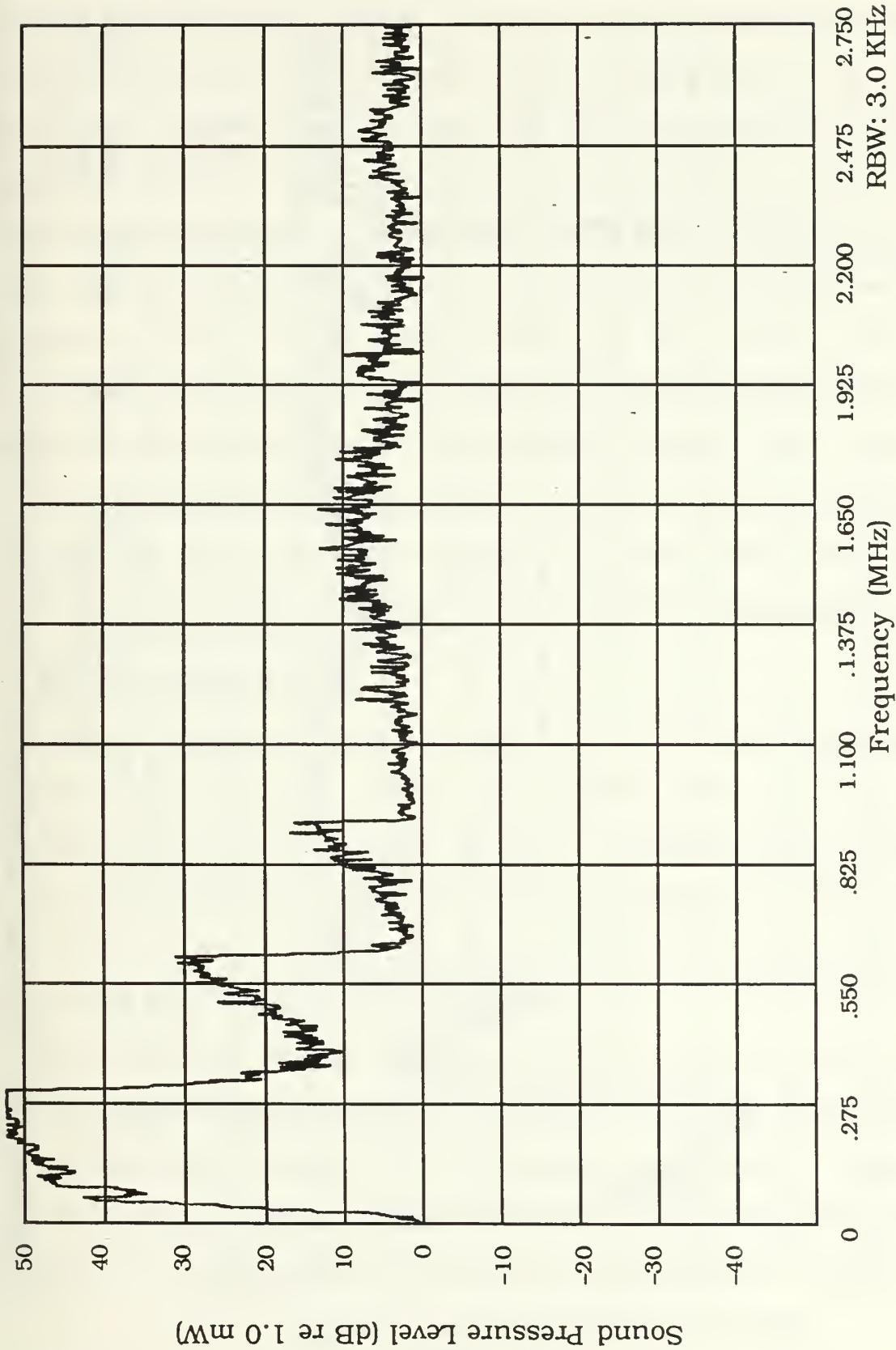
Figure 39c. Wide Spectrum Analyzer Window—LTDPIFFs—
Imaging and Pump/Imaging Only Difference

137
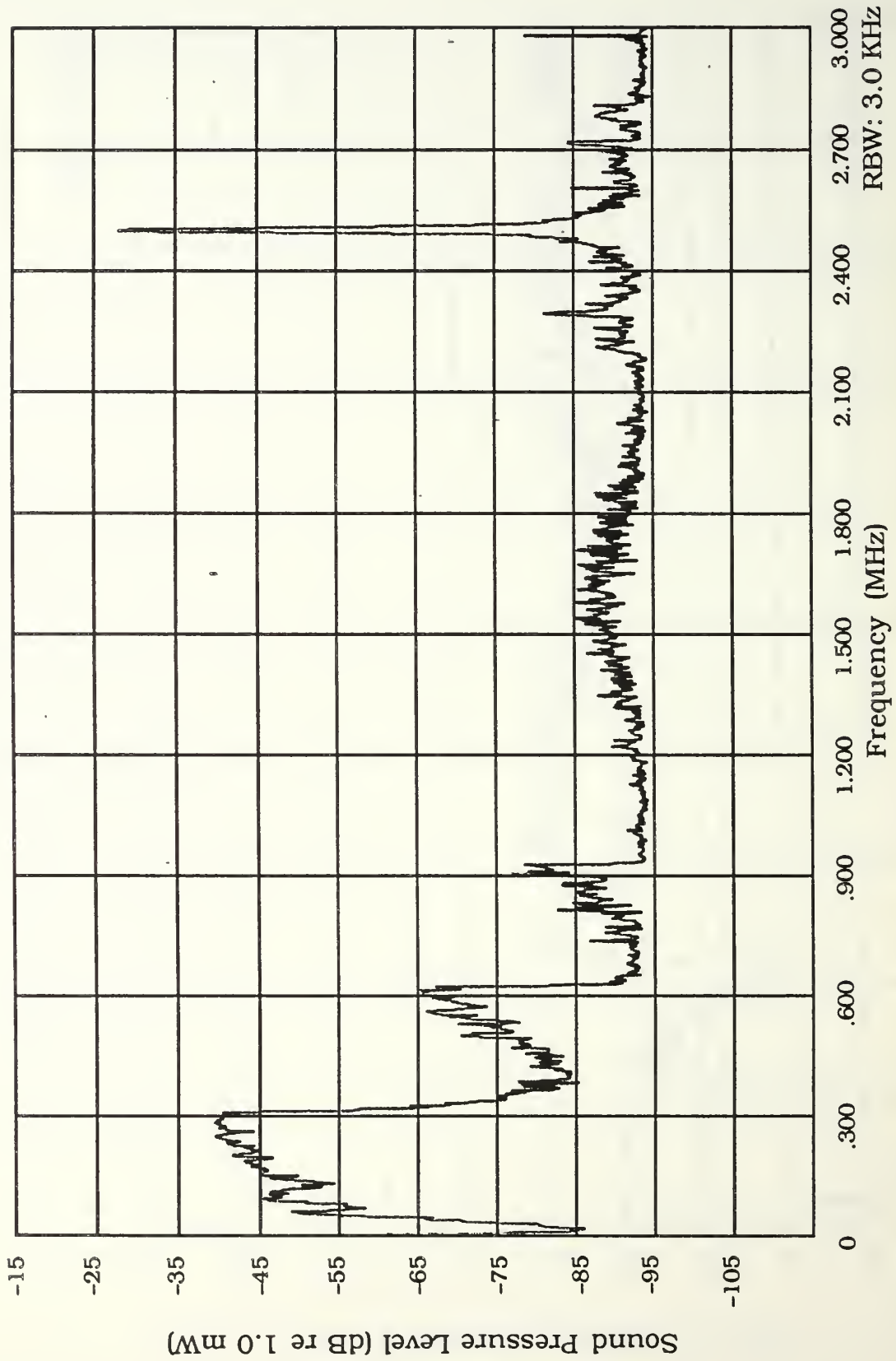
Figure 40. Wide Spectrum Analyzer Window—LTDPIFFs—High Imaging and Pump Sound Fields

138

wide-spectrum analyzer window repeat of Figure 39b, except the plot shows a change in the imaging frequency to 2.50 MHz so as to move the dual-frequency sidebands away from the resonance harmonics. The plots in Figures 39a, 39b, and 39c were all recorded using an imaging frequency at 2.25 MHz at 6.0 volts of transducer input, and swept pump frequencies of 15 kHz to 310 kHz set at 42 volts peak to peak transducer input. Again, the dual-frequency sideband sound pressure levels in both Figures 39b and 40, while both at approximately -90 dB re 1.0 mW, appear to be slightly lower than the levels recorded in fresh water. The sideband pressure levels plotted in Figure 40 do have a better signal-to-noise ratio than those plotted in Figure 39b due to the higher imaging frequency used. The higher imaging frequency avoids the resonance harmonics of the bubbles.

C. PHASE THREE DATA

Phase three was conducted in one of the Naval Postgraduate School's large, fresh water, acoustically insulated tanks. The object of this phase was to investigate the effects of a reflection-free environment on the dual-frequency sideband sound pressure level signal-to-noise ratios. The Large Tank Downward Pump Image Far Field$_f$ in fresh water was used in the non-reflecting tank.

The first series of data is plotted in Figures 41a, 41b, and 41c. The same data format of phases one and two is repeated here. Figure 41a is a plot of the received reflected imaging signal from the bubbles and is considered "noise." Figure 41b is the received signal from the bubbles with both imaging and pump sound fields present. Figure 41c
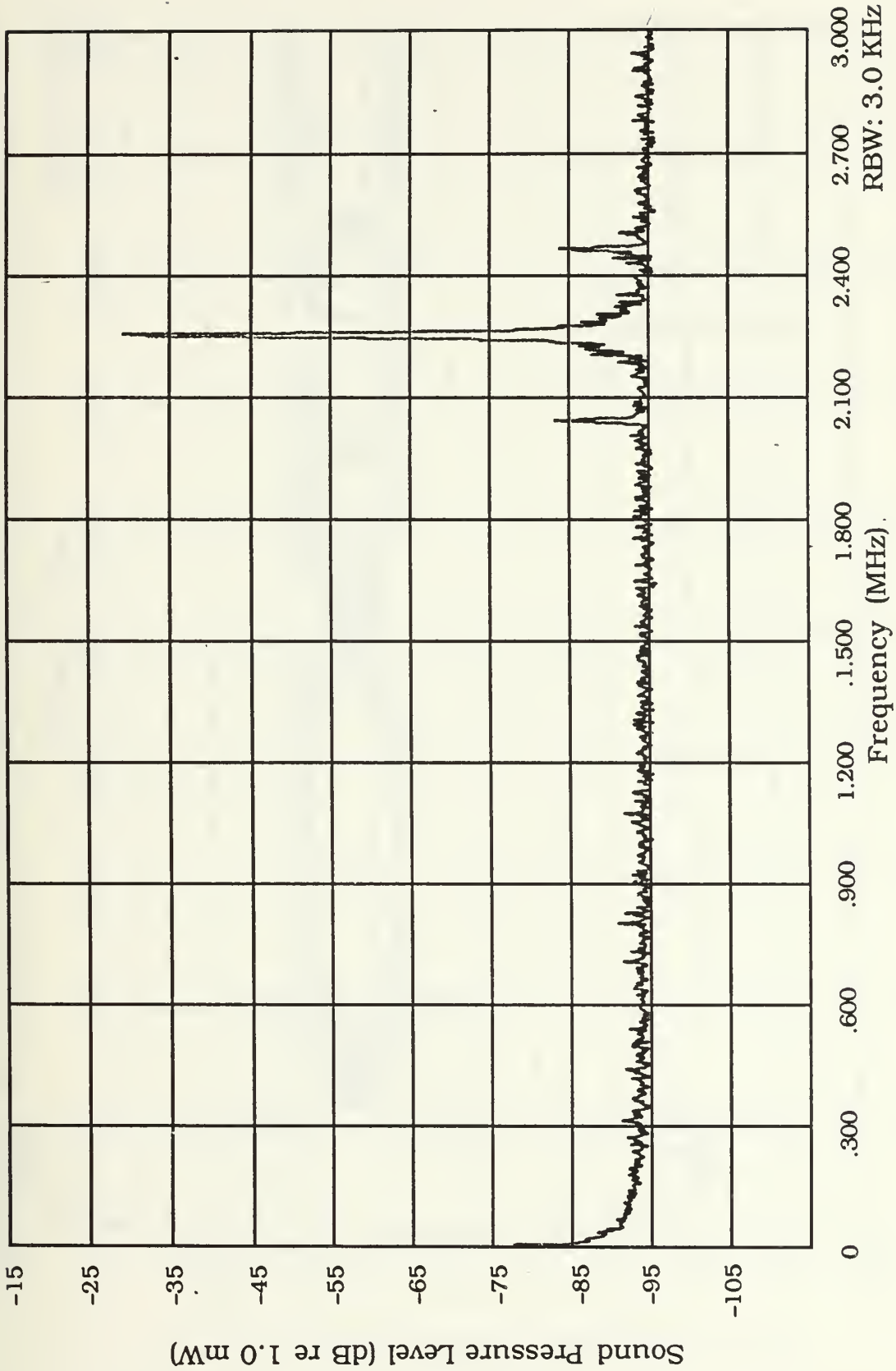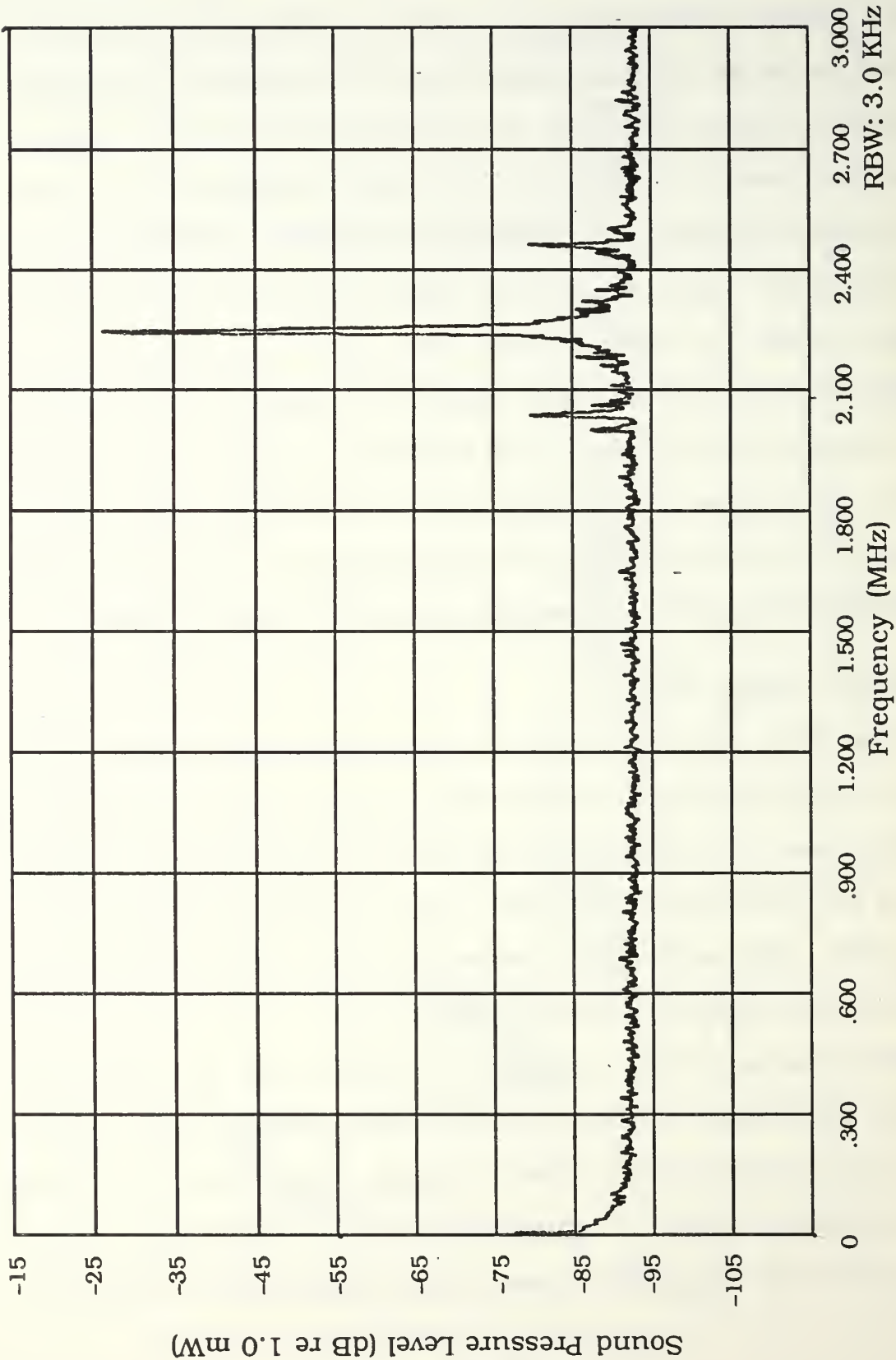
Figure 41a. Wide Spectrum Analyzer Window—LTDPIFF$_f$—Imaging Sound Field Only

140
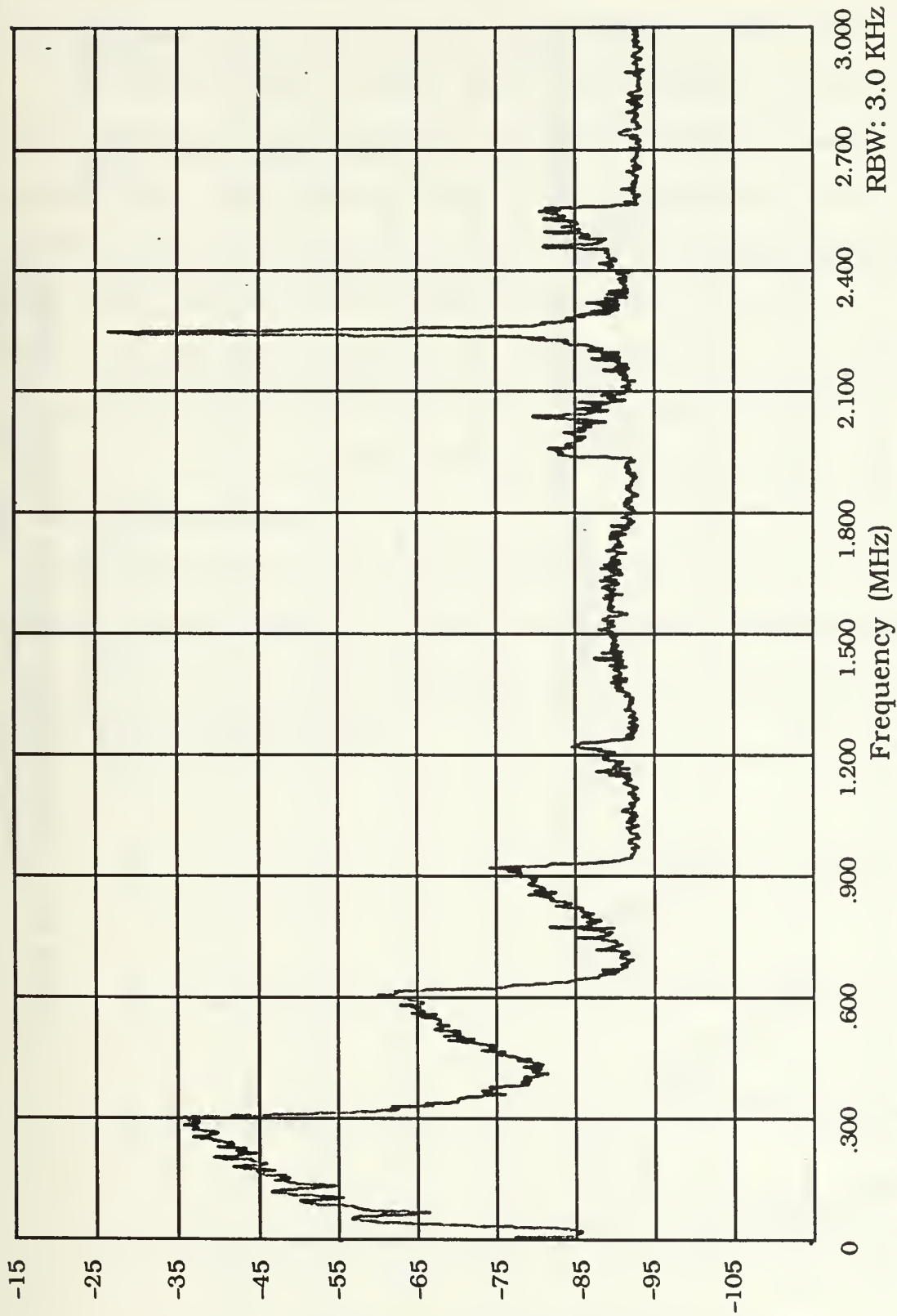
Figure 41b. Wide Spectrum Analyzer Window—LTDPIFf—Imaging and Pump Sound Fields

141
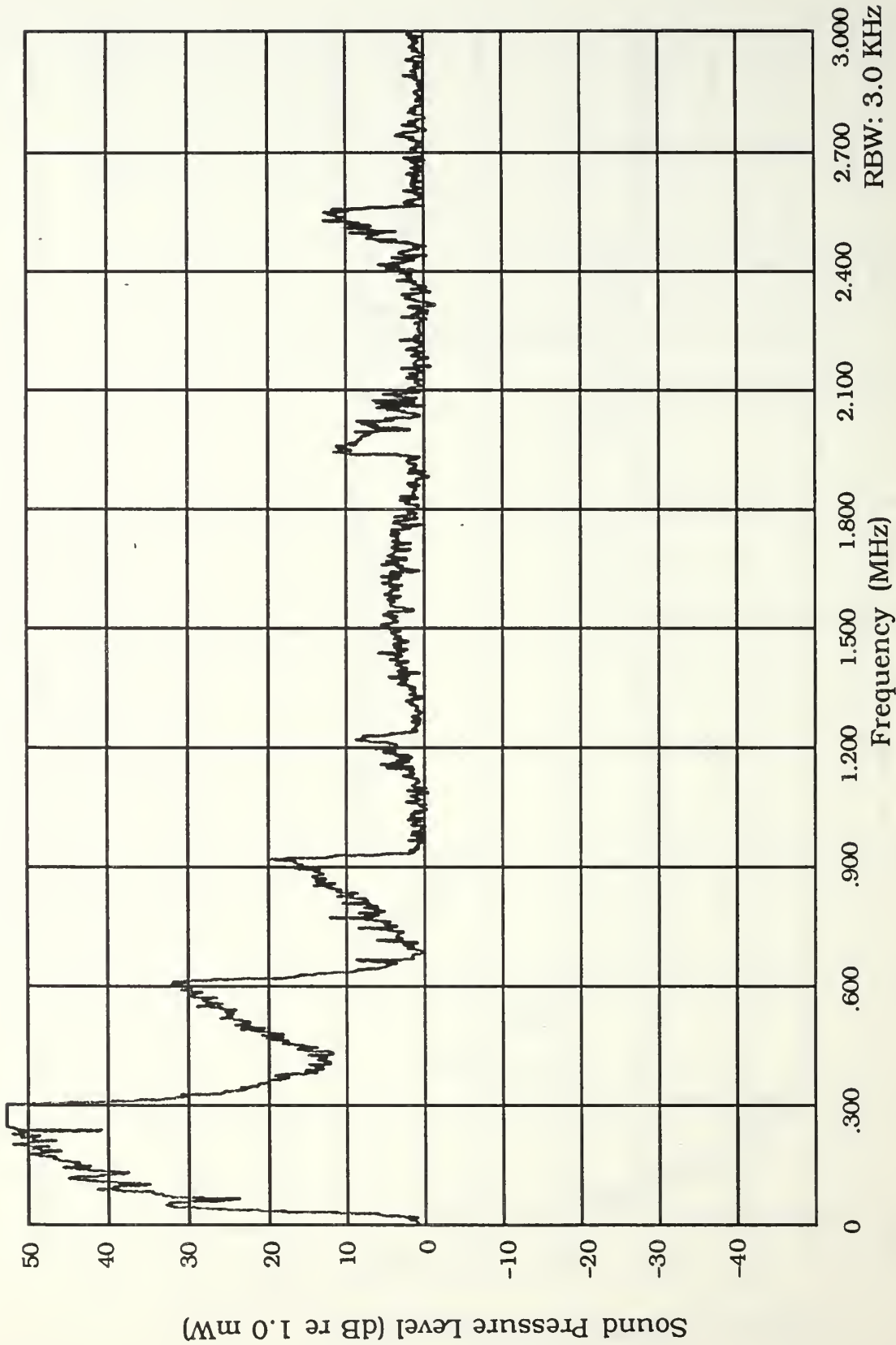
Figure 41c. Wide Spectrum Analyzer Window—LTDPIFF$_f$—
Imaging and Pump/Imaging Only Difference

142

is the difference between the signal from the bubbles in the presence of imaging and pump sound fields and the imaging "noise" only.

The second series of phase three data, plotted in Figures 42a, 42b, and 42c, is a narrow spectrum analyzer window, or "close-up," of the first series. Figure 42a is a plot of the imaging noise. Figure 42b is plotted with both imaging and pump sound fields radiating the bubbles, and Figure 42c is the difference between the latter two. All phase three experiments utilized an imaging frequency of 2.25 MHz at a transducer input level of 6.0 volts. The pump frequencies were swept from 15 kHz to 310 kHz. The pump transducer input level was 42 volts peak to peak.

The results from all three experimental phases has been briefly discussed in this chapter. Chapter V, Conclusions and Recommendations, will use these results and further discuss the implications of the data in a more general sense.
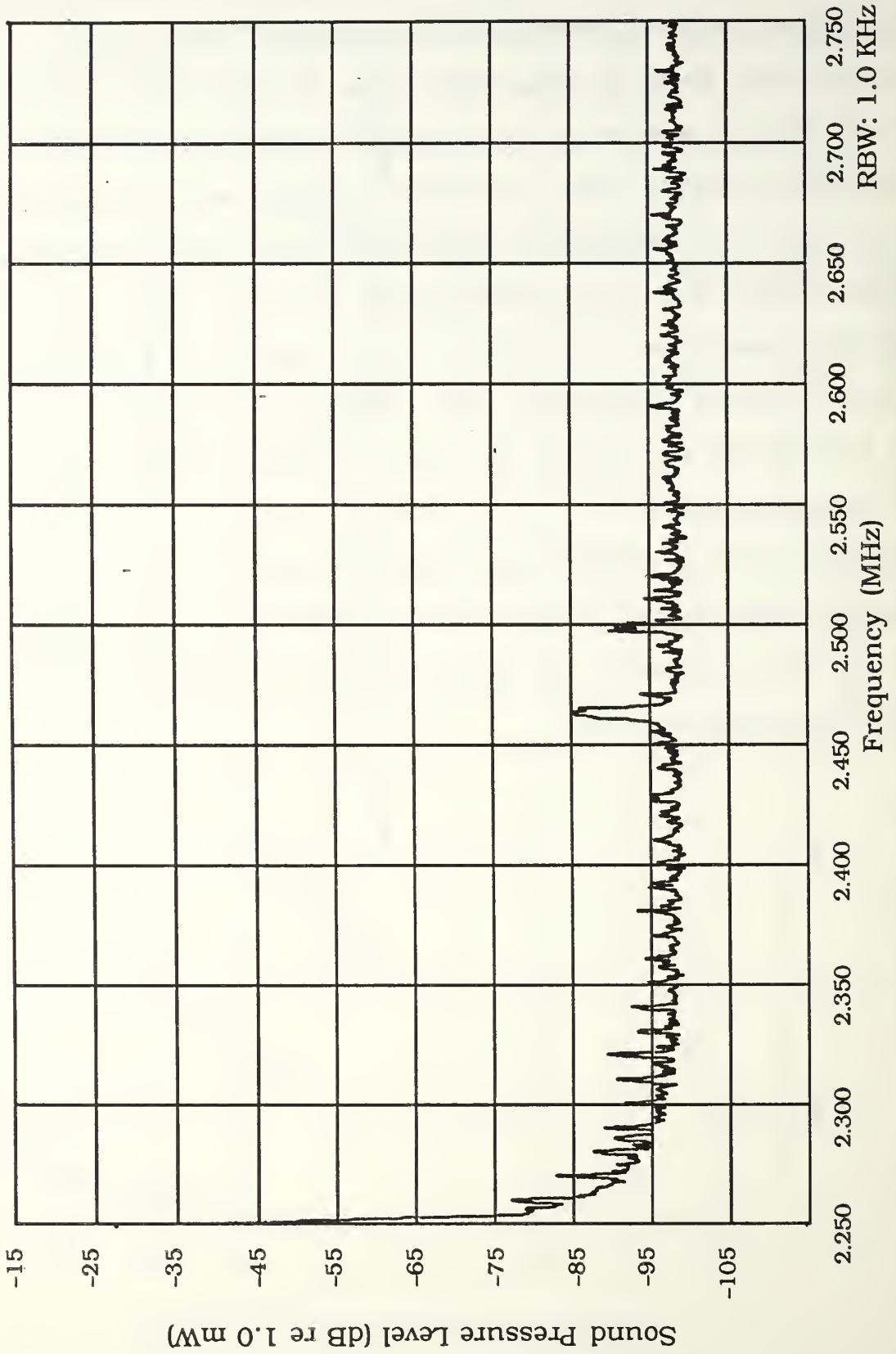
Figure 42a. Narrow Spectrum Analyzer Window—LTDPIFF$_f$—
Upper Sideband—Imaging Sound Field Only

144
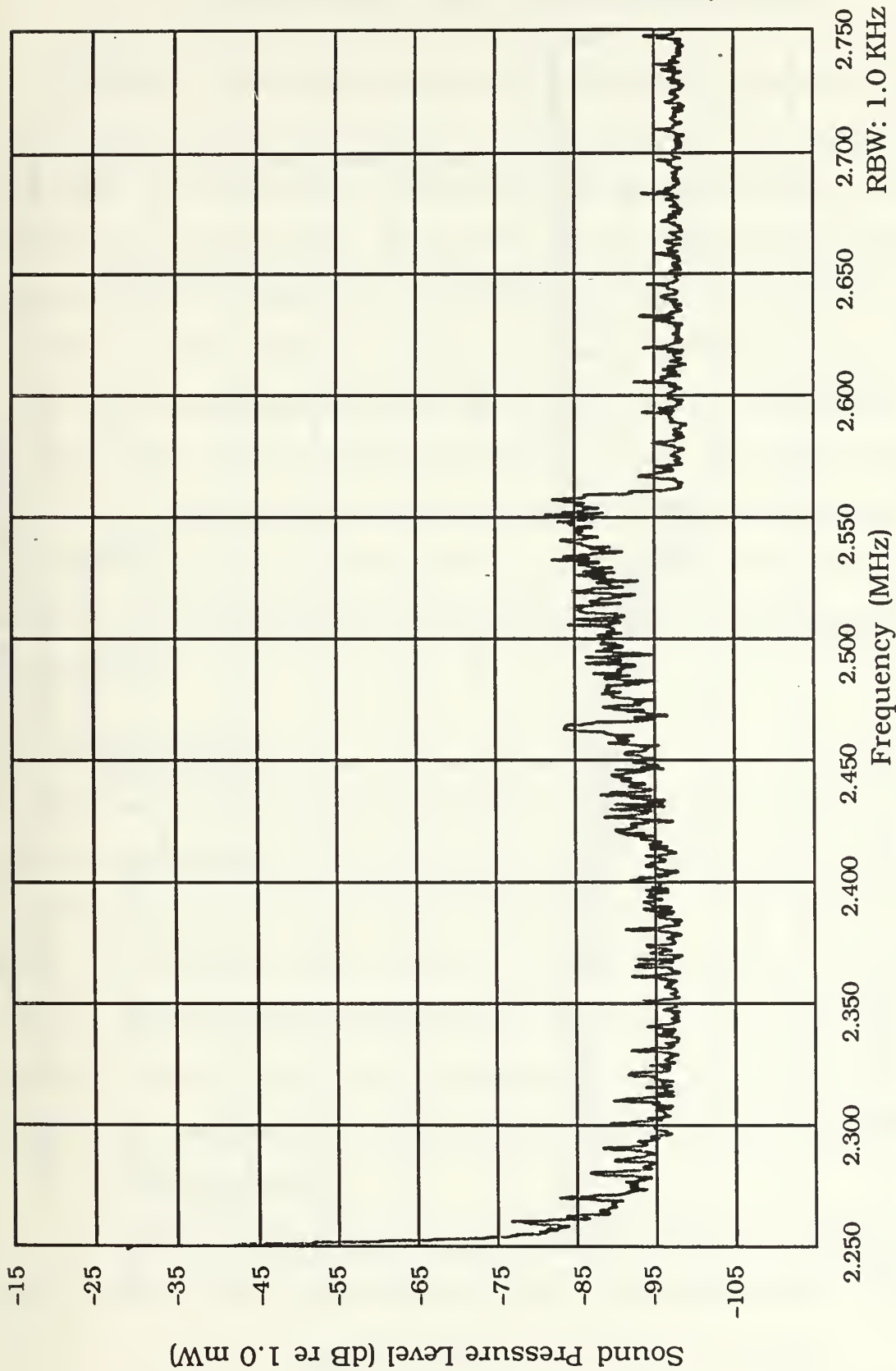
Figure 42b. Narrow Spectrum Analyzer Window—LTDPIFF$_f$—
Upper Sideband—Imaging and Pump Sound Fields

145
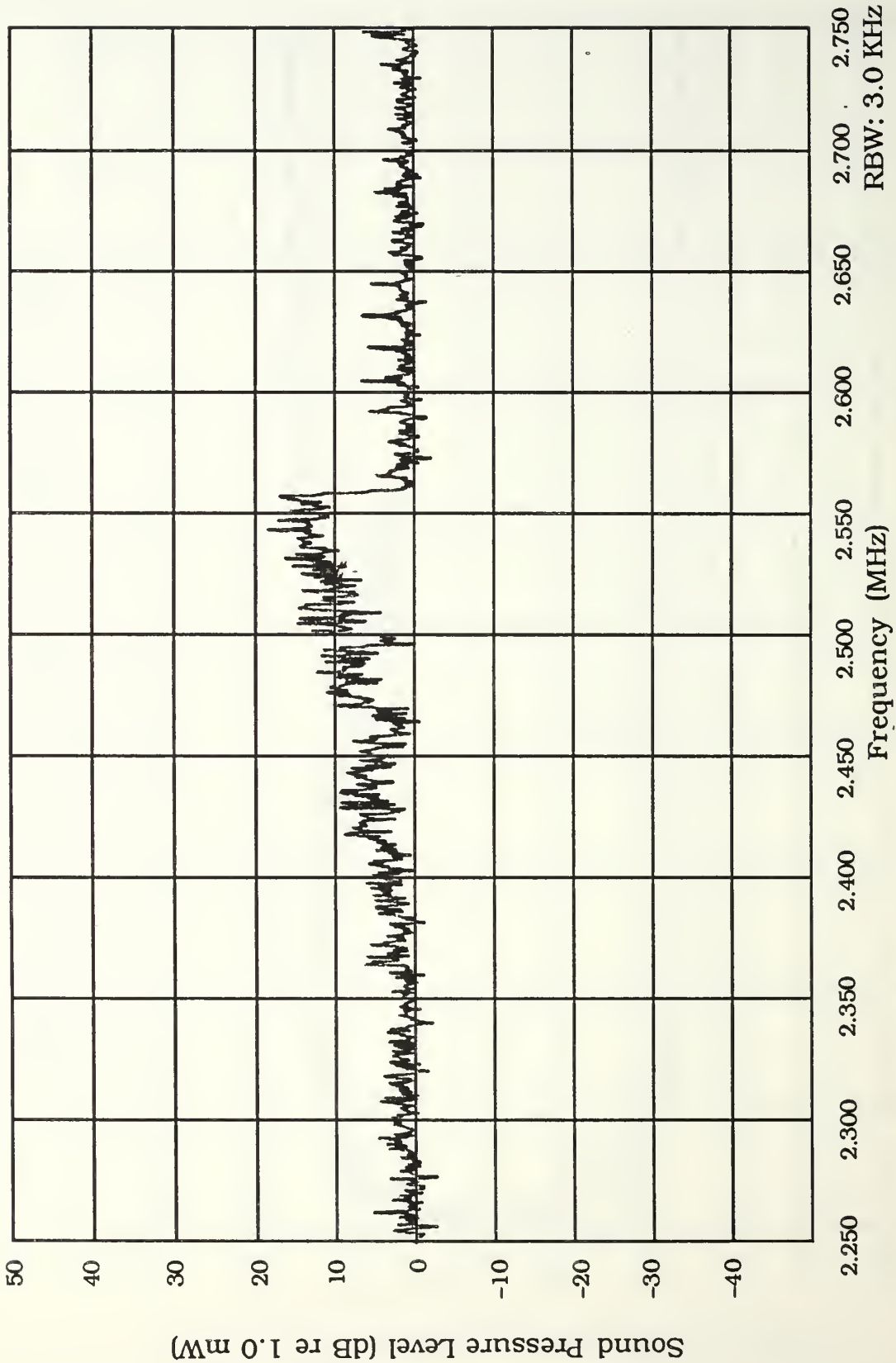
Figure 42c. Narrow Spectrum Analyzer Window—LTDPIFF₂—Upper Sideband—
Imaging and Pump/Imaging Only Difference

146

V. CONCLUSIONS AND RECOMMENDATIONS

The goal of this thesis is to provide a theoretical and experimental investigation into the feasibility of using the Dual Frequency Pump Technique to acoustically determine point–by–point bubble density distributions within surface ship wakes. The theoretical investigation reviewed bubble resonance, dual–frequency bubble excitation, and transducer beam patterns in Chapter II. The experimental considerations, such as transducer orientation, sample volume placement, bubble screening, and idealized transducer inputs were discussed in Chapter III. Data that was gathered during the experiment and some general observations concerning that data are presented in Chapter IV. Some general conclusions and recommendations are presented here in Chapter V.

A. CONCLUSIONS

The Dual Frequency Pump Method of acoustically detecting bubbles and determining point–by–point bubble cloud densities is very promising for surface ship wake measurements. The design of an actual measurement device requires a far more intensive and detailed research effort, but the dual frequency technique is practical for surface ship wake bubble density measurements. This thesis demonstrates that practicality through the discussion of the following topics.

1. Bubble Resonance

Bubbles undergoing resonance and volume pulsations are the keys to making the dual frequency pump technique work. Bubbles

147

resonate easily in both fresh and salt water as is evidenced by the presence of the harmonics of the resonance sound field plotted in Figures 28b and 37b. The harmonics verify that the bubbles are acting as a sound source. The data collected during the seawater experiments in the aquarium shows that dual frequency excitation works in seawater; but the data plotted in Figures 37 through 40 for seawater shows a slightly lower signal-to-noise ratios as discussed in the Chapter IV section on phase two data. The reason for a lower signal level in seawater is not clear.

Figures 27a, 27b, and 27c demonstrate the Dual Frequency Pump Method's ability to detect only bubbles, not solids, at the imaging frequency sidebands $(\omega_i \pm \omega_p)$. These figures are plots of the received spectrum when an aluminum dowel was used as a reflector instead of bubbles. Figure 27c is a plot of the sound pressure level of the reflected sound field for pump frequencies swept from 15 to 310 kHz. The lower frequency spectrum of the plot shows the reflected sound signal but the upper spectrum shows no sideband signals, indicating correctly that there are no bubbles present. Seawater, particularly in ship wakes, is rich in suspended solids and biological life. The Dual Frequency Pump Method can distinguish between a bubble and a suspended solid.

The solid reflector test was carried a step further by radiating the face of the receive transducer directly with the pump sound field. Figure 26 plots no significant frequency modulation, which could give a false bubble indication, caused by the maximum pump sound

pressure amplitude in the absence of bubbles. The receive transducer was radiated with the pump sound field in the presence of an imaging signal. However, it should be noted that the imaging sound field, which acts as the "carrier" of the pump sound field, was not aimed directly at the receiver. These two simple tests help demonstrate that the received signals plotted in all the figures are in fact a product of bubble resonance and dual–frequency excitation.

The results of Chapter II equations (7) and (8), which are presented in Tables Ia, Ib, and Ic, deserve comment. First, in direct regard to dual–frequency bubble excitation, these tables show the need for sweeping a wide range of pump frequencies. Shankar and Newhouse used only a limited pump sound field frequency range for their biomedical–based research [Refs. 3 and 12]. The arbitrary range of bubble radii selected for our demonstration of the surface ship wake measurement problem suggests a broad sweep range of approximately 20 kHz to 500 kHz in order to compensate for increased hydrostatic pressures. Second, the hydrostatic pressure term in equations (7) and (8) is significant to surface ship wakes in that it could help explain why surface ship wakes persist longer than expected at lower frequencies. Tables Ia, Ib, and Ic demonstrate that a bubble of given size has a much lower resonance frequency at the ocean surface where the hydrostatic pressure is low than at some depth where the pressure is greater. Remembering that the ship wake is defined by the presence of many different–sized bubbles of different resonance frequencies, the acoustic presence of the wake is determined by the large amounts of

absorption or scattering that occurs at those frequencies. Logic would dictate that the lower-frequency bubbles, which are larger in radius, would disappear faster, either by rising to the surface more quickly or by breaking up into smaller bubbles of higher resonance frequency. The small, high-resonance frequency bubbles with the slow rise times should be present for longer periods. Wake profile data, which is taken in vertical "slices" or columns, supports the logic by showing the presence of high-frequency wakes. However, the wake data also shows the presence of a lower-frequency wake which persists much longer than expected. A possible explanation could be that, if a bubble of particular radius started its rise toward the surface from deep in the wake, the bubble's resonance frequency becomes less as the bubble rises. A vertically oriented wake profiling device would not sense a change in the bubble's position within the water column, only the presence of the lower resonance frequencies. The bubble rise mechanism is coupled to many other variables such as turbulence, diffusion, and expansion of the bubbles, but it may offer a simplistic insight into a possible cause of low-frequency wake persistence. The Dual Frequency Pump Method of acoustic wake measurement could solve the lack of vertical position data by taking point measurements within the wake.

Bubble resonance can also have an adverse effect on the Dual frequency Pump Method if the resonance creates strong harmonics. Excessive pump pressure amplitudes at the sample volume location results in resonance harmonics far up the frequency spectrum. If the

harmonics extend to high enough frequencies, they raise the noise level about the imaging frequency, which creates difficulties in detecting the low-amplitude sideband pressures. These resonance harmonics are recorded in most of the plots and discussed again in a later section.

2.   <u>Bubble Screening and Sample Volume Size</u>

Early in the discussion of the experimental procedure, mention was made of the use of narrow bubble streams passing through the sample volume versus the generation of large bubble clouds. This was necessary due to the large amounts of bubble screening which take place in the presence of a large cloud.

The sample volume created by the intersection of the imaging and receive transducer beam patterns is small relative to a large bubble cloud. A large bubble cloud will contain the sample volume at some point on the cloud's interior. If this is the case, many bubbles are outside the sample volume. This has two degrading effects. First, the imaging and pump sound undergo large amounts of attenuation due to screening bubbles prior to radiating the target bubbles in the sample volume. Second, with the resonating target bubbles acting as a sound source, the receive transducer has difficulty detecting the radiated bubble sound field due to attenuation from screening bubbles. The effect of screening bubbles is, therefore, twofold when the sample volume is inside a large bubble cloud. This large cloud "mechanism" was supported by the results of initial data collection efforts. The receive transducer and spectrum analyzer were unable to detect any dual-

151

frequency sideband pressure levels while only barely detecting primary pump and imaging sound fields.

The use of narrow bubble streams passing through the sample volume yielded much greater success. Dual-frequency sideband pressure levels were detected during all three phases of the experiment when the small stream was used. The narrow bubble stream successfully eliminated the screening bubbles outside the sample volume. This provided all the sound fields clear paths to and from the transducer faces, thus keeping attenuation to a minimum. This evidence emphasizes the need to keep the bubble streams to be measured small and contained within the sample volume. If large bubble clouds, such as ship wakes, are to be measured, it will be necessary to isolate the sample volume from the bubble cloud so that sound paths will not be interrupted by screening bubbles..

3.   Dual Frequency Sideband Pressure Amplitudes

Data collected in phases one, two, and three of our experiments confirms the finding of Shankar and Newhouse concerning the dual-frequency sideband pressure levels. Shankar and Newhouse found that, in order to detect bubbles at the dual-frequency sidebands $(\omega_1 \pm \omega_p)$, it was necessary to maintain the ratio of the imaging signal level (equivalent to P_1) to sideband level (equivalent to P_+) ratio of approximately 63 dB. Figures 29a, 29b, and 29c provide a graphic illustration of this signal level ratio. The imaging (P_1) signal level in Figure 29b is approximately 80 dB above the background noise and the dual-frequency sideband levels (P_+ and P_-) are approximately 20 dB

152

above the noise at their peak level. The signal level difference between the two is approximately 60 dB. This ratio became important because, for every experiment that was conducted, the imaging sound level (P_1) needed to be at least 55 to 60 dB above the noise level before dual-frequency sideband levels could be detected. The sideband pressure amplitudes are very small compared to those of the reflected imaging and pump sound fields, therefore, a large signal-to-noise ratio is needed to make this technique successful.

Table III theoretical results of equations (28a) and (28b) also support the conclusion that the signal-to-noise ratios of the imaging, dual-frequency sideband, and background pressure amplitudes are key factors in the success of the Dual Frequency Pump Method. Table III results are calculated assuming that the pump and image sound fields are of constant pressure amplitudes for all frequencies. This means that p_i and p_p are constants in equations (28a) and (28b). The computed sideband pressure amplitudes compare favorably with those found by Shankar and Newhouse. Table III shows the sideband pressure amplitudes to be very small compared to the pump pressure amplitudes. The table also highlights the logical conclusions that both the sideband pressure amplitudes for a bubble at resonance and the noise pressure amplitude of the bubble not at resonance increase with bubble size.

The data plotted for all figures was collected using the "max hold" feature of the HP3585A spectrum analyzer. The "max hold" feature stores the peak pressure level at each frequency on the CRT of

153

the analyzer. Therefore, all the plots represent bubble size distribu-
tions rather than actual bubble counts. The pressure level peaks at the
sidebands indicate that at least one bubble of that size was present
during the 132-second statistical sample time.

The data plotted for all these phases of the dual-frequency
experiment shows an increase in pressure level as the sideband fre-
quencies increase and decrease about the center (carrier) imaging
frequency. Figures 42a, 42b, and 42c (plots of the upper sideband)
are good examples of the maximum sideband level being located at a
corresponding resonance frequency of approximately 300 kHz ($\omega_i +
\omega_p = 2.55$ MHz). This indicates the presence of a small bubble and
appears contrary to the results of equations (28), in that small bubbles
radiate small pressure amplitudes. The experimental results are not
contrary, however, due to the fact that the actual pump pressure
amplitude increases with frequency because of the pump transducer
response. The experiment provided the smaller bubble with a greater
p_p than the theoretical calculation. The theoretical calculation was
performed utilizing the pump pressure amplitude as a constant. Theo-
retical results similar to those plotted in the figures could be obtained
if the input (p_p) to equations (28a) and (28b) is varied with frequency.

The difficulties associated with obtaining actual bubble counts
and maintaining a constant acoustic pump pressure level (to make
theoretical calculation easier) can both be solved using software. A
computer could individually store the dual-frequency sideband pres-
sure levels on every sweep of the analyzer and add them over the

154

course of the statistical sample time. The computer could also compute theoretical pressure levels (P_+) for a variety of pressure level inputs (p_i and p_p) and compare those results to the signals received from the sample volume at discrete frequencies.

4.   Imaging and Pump Sound Fields

The importance of the pump sound field frequencies has already been discussed, however, the experimental results further show that the pump sound field amplitude, the imaging frequency, and the imaging sound field amplitudes are important. The imaging sound field amplitude has also already been mentioned in the previous section. The effect of two different imaging pressure levels can be observed in Figures 33 and 34, where the imaging input level was reduced for data in the Figure 34 plot. Reducing the imaging input voltage by half reduced the sideband levels by approximately 6 dBm and produced a less-favorable signal-to-noise level difference. This is as expected since equations (28) show that the upper sideband level (P_+) is directly related to both imaging and pump inputs.

The effects of the pump pressure amplitude on sideband pressure amplitude are plotted in Figures 31, 32a, and 32b. The phase one AQUPIFF$_f$ experimental data was recorded to demonstrate the effect reduced pump pressure amplitude had on harmonic and sideband pressure levels. High pump pressure amplitudes at the 42-volt peak-to-peak transducer input levels create harmonics which exist at high frequencies on the frequency spectrum. These harmonics create a noise level problem at the dual-frequency sideband ($\omega_i \pm$

155

ω_p) locations. The harmonics caused by an expanded pump frequency range (ω_p = 15 to 500 kHz) are also detected at both upper and lower dual-frequency sideband locations on the frequency spectrum (as plotted in Figure 31). The sideband pressure levels are barely above the noise of the harmonics. Therefore, reduced pump pressure amplitudes were tested and the results shown in Figures 32a and 32b. Figures 32a and 32b show a desirable reduction in harmonic noise. The dual-frequency sideband levels drop approximately 6 dBm, as expected (equation (28)), with each input level reduction.

The ideal imaging frequency was also investigated in both fresh water and seawater. Several transducer arrangements were used to compare results. The data of Figures 35, 36a, 36b, 36c, and 40 indicates that an imaging frequency higher than 2.25 MHz avoided the noise level that was created by harmonics. Increasing the imaging frequency was effective in avoiding harmonic noise from all transducer arrangements and both fluids. Surface ship wakes should have a low noise level at ultrasonic frequencies. Harmonics are one of few effects that can raise the ultrasonic noise level.

5. Sample Volume Location, Transducers, and Transducer Arrangements

The sample volume should be located in the far field of all transducer beam patterns. The increase in sound field pressure amplitudes is not significant to justify moving the sample volume to the near field. These plots of data collected with the sample volume in the near field (AQUPINF$_f$) of the imaging and receive transducers

156

(see Figures 33, 34, and 35) did not show an improvement over the experiments with the sample volume in the far field. The pump transducer was placed whenever possible so that the sample volume would be in the far field at the pump transducer. The LTDPIFF$_f$ and the AQDPIFF$_f$ arrangements required the pump transducer to be closer than the calculated far field point to the sample volume due to physical transducer arrangement limitations. Near field points were chosen carefully to provide equitable sound pressure levels to those of the far field.

The transducers used for these experiments were low cost and did not have ideal center frequencies or frequency responses. This was particularly true of the pump transducer. A lower center frequency would have allowed a better frequency response about resonance frequencies of interest. The receive transducer (center frequency 2.25 MHz) was not calibrated and therefore the pressure amplitudes of the dual-frequency sidebands could not be calculated from the HP3585A sound pressure level data. Calibrated receive transducers must be used to obtain sound pressure amplitudes.

Several transducer arrangements were studied in phases one, two, and three. The largest physical difference between any one arrangement was the upward-looking and downward-looking pump transducers. No appreciable system performance difference was detected between the upward and downward pump arrangements, except that the upward-looking arrangement was easiest to align with

the bubble stream. The upward-looking pump was used during most data collection because of its easily adjusted components.

The pump transducer orientation did have a slight effect on very slowly rising bubbles. If the bubbles were moving slowly enough, the bubble path could be altered very slightly by the pump sound field. The altered path was more pronounced for the downward-looking pump transducer arrangements.

The last experimental phase was conducted in the large acoustically insulated tank, and resulted in a lower (several dB) background noise level across the spectrum. This was significant in that the lower resonance frequency (larger radii) sideband pressure levels were slightly higher above the noise level than they had been in the aquarium. The large tank further demonstrated the need for a reflection-free environment to reduce background noise, just as the absorptive material had reduced reflections and noise in the aquarium. The ocean environment and surface ship wakes are quiet in the imaging frequency (ultrasonic) region. Use of absorptive material to eliminate reflections is also critical to the Dual Frequency Pump Method.

6. Bubble Counting, Photography, and HP3585 Resolution Band Width

Actual bubble counts were not obtained here using the Dual Frequency Pump Method of bubble density measurements for three reasons. The first and main reason was that the "max hold" feature on the spectrum analyzer, as previously mentioned, was not a method sophisticated enough to count bubbles. The second was that the

receive transducer was not calibrated and therefore the sideband sound pressure amplitudes could not be calculated from the recorded sound pressure levels. The third reason was that efforts at photography failed to provide a clear photo enlargement so that a bubble count in the bubble stream with a magnifying comparator could be accomplished. Photographs were taken with a Minolta XD-5 35 mm camera and a standard 50 mm lens. More sophisticated photographic equipment, specifically a short focal length lens, is needed to obtain close-up photographs.

Even though actual bubble counts at each sideband frequency were not obtained, the plots show the presence of different bubble sizes at the discrete $\omega_l \pm \omega_p$ locations on the frequency spectrum. The resolution bandwidth of the HP3585A spectrum analyzer is critical when determining the bubble sizes present using the "max hold" feature. Figure set 42 plots the upper dual-frequency sidebands using a 1.0 kHz resolution and an extra-wide spectrum window for accuracy. The plot shows that small resolution bandwidth provides narrow sound level "spikes" that are key to increased precision in bubble size determination.

Figure 42c shows the presence of discrete bubble sizes ranging in resonance frequency from 100 kHz to 310 kHz. The pump frequency cut-off was 310 kHz. Bubble size discrimination is possible, but not the actual number of bubbles present. More sophistication in photography, sound field amplitude control, transducer types, and computer software will provide the means to obtain actual bubble counts for each bubble size.

B. RECOMMENDATIONS

The recommendations for further investigation and conduct of dual-frequency pump bubble cloud density measurements are listed briefly here. The concept is most feasible. With further study and development, the design of an acoustical measurement device would not be overly difficult.

1. Only small, narrow bubble streams are practical for measurement due to bubble screening. The bubble stream dimensions must be smaller than that of the sample volume to avoid sound field attenuation through bubble screening. Measurement of large, dense bubble clouds must be done in a manner which isolates the sample volume to avoid screening.

2. The success of dual-frequency bubble cloud measurements rests on obtaining the proper signal-to-noise ratio. For this reason, noise levels in the sideband frequency range must be kept to a minimum so that low-amplitude sideband levels can be detected.

3. The sample volume should be placed in the far field of all transducer beam patterns to prevent the sample volume from being in a "null."

4. Use statistics as shown in this thesis to determine the duration of the sample time. Also, if a large bubble cloud is the target of a device, design the device to have several sample volumes and statistically average the results.

5. The problem is complicated enough to warrant the use of a computer to run the spectrum analyzer and plot its data. Integrate an HP300 series computer into the equipment rack to compare and control data. This is a most important step which is critical to conducting accurate bubble counts.

6. More sophistication is needed at the pump transducer and pump transducer input level. Investigate using broadband noise, transducers in series, high-quality flat-frequency response transducers, or computer-controlled transducer input power to solve the inability to provide *constant* pump pressure amplitudes at the sample volume.

7. Investigation of higher imaging frequency and higher imaging input power is needed to provide better signal-to-noise ratios.

Receive transducers with higher center frequencies should be used to increase transducer response.

8. Investigation of the optimum minimum pump pressure amplitude in the presence of the widest possible pump frequency range (ω_p) is needed. The pump frequency (ω_p) range must be as wide as possible to include all bubble sizes at different hydrostatic pressures. At the same time, the pump sound pressure amplitude (p_p) must be kept low enough to reduce harmonics (which raise the noise level). A balance between pump frequency ω_p and amplitude (p_p) must be found and at the same time provide the bubbles present with enough sound pressure amplitude to produce resonance.

9. Use of a calibrated receive transducer is critical to determining the received pressure amplitudes of the signals from the bubbles. A calibrated receive transducer would allow immediate computation of sideband pressure amplitudes and estimates of the bubble sizes and numbers present. The computer could also perform this function with data from the HP3585A.

10. Some improved means of visual or photographic verification is necessary to confirm the dual–frequency pump method of measurement. Investigate more sophisticated photography and background lighting. Also, investigate other acoustical means (such as those developed by Medwin) of bubble density measurements to partially validate the Dual Frequency Pump Method.

In summary, the Dual Frequency Pump Method offers many advantages over other acoustic techniques and, when linked to a computer with the proper software, may be the best technique for measuring bubble densities in ship wakes. Many hardware improvements are needed in the Naval Postgraduate School Dual Frequency effort, but the problem lends itself easily to further Acoustics/Systems Engineering graduate–level study. Therefore, further investigation and study into the Dual Frequency Pump Method is highly recommended.

161

APPENDIX A

RESONANCE FREQUENCY COMPUTATION PROGRAM

```
C
C      ***********************************************************************************************
C      BUBRAD IS A FORTRAN PROGRAM THAT CALCULATES THE RESONANCE
C      FREQUENCY FOR BUBBLES OF A GIVEN RADIUS IN SEAWATER NEAR THE
C      SURFACE.
C      ***********************************************************************************************
C
C      BUBBLE RADIUS DATA CAN BE FOUND IN FILE: BUBRAD1 DATA A1
C
C      ******************************* LIST OF VARIABLES *******************************
C
C      PI = PIE
C      GAMMA = RATIO OF SPECIFIC HEATS
C      SIGNA = SURFACE TENSION (DYNES/CM)
C      ROW = SEAWATER DENSITY (GRAMS/CM3)
C      R = MEAN BUBBLE RADIUS
C      P = PRESSURE (ATMOSPHERES)
C      W1 = NATURAL ANGULAR FREQUENCY
C      W2 = NATURAL ANGULAR FREQUENCY (SURFACE TENSION)
C      FREQ1 = FREQUENCY IN KHZ (WITHOUT SURFACE TENSION)
C      FREQ2 = FREQUENCY IN KHZ (INCLUDES SURFACE TENSION)
C
C      ***********************************************************************************************
C
       GAMMA=1.4
       SIGMA=70.0
       I=0
       ROW=1.026
       PI=3.141593
       DYNES=1.0133E+6
       WRITE(6,10)
  10   FORMAT(/,1X,'INPUT TOTAL HYDROSTATIC PRESSURE, P')
       READ(5,*) P
       P1=P*DYNES
       WRITE(6,1000) P
 100   READ(1,200,END=9999) R
 200   FORMAT(F7.4)
       I=I+1
       W1=(1.0/R)*SQRT((3.0*GAMMA*P1)/ROW)
       FREQ1=(W1/2.0*PI))*0.001
       W2=(1.0/R)*SQRT((3.0*GAMMA*(P1+(2.0*SIGMA/R))-(2.0*)/R))ROW)
```

162

```
      FREQ2=(W2/2.0*PI))*0.001
      WRITE(6,2000) R,FREQ1,FREQ2
      IF (I .LT. 10) GO TO 100
1000  FORMAT(/,1X,'FOR SEAWATER NEAR THE SURFACE AT PRESSURE P=',1X,F3.1
     *,///,1X,'RADIUS  (CM)',5X,'NATURAL  FREQ  (KHZ)',5X,'FREQ  W/SURF  TENS
     *ION',/)
2000  FORMAT(/,4X,F7.4,10X,F9.4,13X,F9.4)
9999  STOP
      END
```

APPENDIX B

SPEED AMPLITUDE (U_0) FOR A PULSATING SPHERE

Recall from Chapter II that the bubble radius R is defined by equation (10), which is written

$$R = R_0 (1 + x).$$

Differentiation of equation (10) with respect to time yields

$$U = \dot{R} = R_0 \frac{dx}{dt},$$

where U is the speed of the pulsation. The assumed solution for x is written in the form of

$$x = A_j \cos (\omega_j t + \varnothing).$$

Equation (12) expanded on this form in Chapter II to include the necessary frequencies of the pump and image sound fields. Now, from above, the equation for x is substituted into the equation for U and yields

$$U = R_0 \frac{dx}{dt}$$

$$U = R_0 A_j \frac{d}{dt} \cos (\omega_j t + \varnothing)$$

$$U = - R_0 A_j \omega_j \sin (\omega_j t + \varnothing).$$

164

Pulsation speed U can also be written as a function of the speed amplitude U_0. Ignoring the negative sign (we are concerned only with amplitude), pulsation speed is written

$$U = U_0 \sin(\omega_j t + \varnothing).$$

Therefore, the speed amplitude is

$$\underline{U_0 = R_0 \, A_j \, \omega_j.}$$

APPENDIX C

UPPER SIDEBAND PRESURE AMPLITUDE
COMPUTATION PROGRAM

```
C
C    ....................................................................................................
C    SIDEBND IS A FORTRAN PROGRAM FOR COMPUTING THE UPPER DUAL FREQUENCY
C    SIDEBAND PRESSURE AMPLITUDES (DYNES/CM2) FOR BUBBLES RADIATED BY
C    THE DUAL FREQUENCIES USING EQUATIONS (28A) AND (28B) AT 1.0 ATMOSPHERES.
C    ....................................................................................................
C
C    BUBBLE RADIUS DATA CAN BE FOUND IN FILE: BUBRAD1 DATA A1
C
C    ................................ LIST OF VARIABLES ................................
C
C        RO      = MEAN BUBBLE RADIUS
C        U       = VISCOSITY
C        ROW     = SEAWATER DENSITY
C        W1      = NATURAL ANGULAR BUBBLE FREQUENCY
C        W1      = IMAGING FREQUENCY
C        WP      = PUMP FREQUENCY
C        PI      = IMAGE PRESSURE (DYNES/CM2)
C        PP      = PUMP PRESSURE (DYNES/CM2)
C        R1      = DISTANCE TO THE BUBBLE (CM)
C        DELTA   = DAMPING COEFFICIENT
C        X2      = DIMENSIONLESS FREQUENCY AND DAMPING TERM
C        PPL1    = SUM SIDEBAND PRESSURE AT RESONANCE (DYNES/CM2)
C        PPL2    = SUM SIDEBAND PRESSURE NOISE (DYNES/CM2)
C
C    ....................................................................................................
C
        U=0.01
        R1=6.7
        I=0
        GAMMA=1.4
        ROW=1.026
        DYNES=1.0133E+6
        PP=830.8
        PI=659.9
        WRITE(6,1000)
100     READ(1,200,END=9999) RO
200     FORMAT(F7.4)
        I=I+1
        W1=(1.0/R0)*SQRT((3.0*GAMMA*DYNES)/ROW)
```

166

```
      F1=(W1/(2.0*3.141593))*0.001
      DELTA=(4.0*U)/(ROW*W1*(R0**2))
      WP=W1+W1/50.0
      OHM2=WP/W1
      Z1=(ROW*W1*R0)**2
      X2=1.0/SQRT((1.0-OHM2**2)**2+(DELTA**2)*(OHM2**2))
      PPL1=(ROW*PI*PP*RO)/(Z1*DELTA*R1)
      PPL2=(ROW*PI*PP*RO*X2)/(Z1*R1)
      WRITE(6,2000) R0,F1,PPL1,PPL2
      IF (I .LT. 10) GO TO 100
 1000 FORMAT(/,1X,'RADIUS (CM)',5X,'SUM PRESSURE * PEAK',5X,'SUM
      PRESSURE NOISE',/)
 2000 FORMAT(/,2X,F7.4,12X,F9.4,10X,F9.4,14X,F11.8)
 9999 STOP
      END
```

APPENDIX D

PUMP TRANSDUCER PRESSURE AMPLITUDE CALCULATION

In order to calculate the sound pressure amplitudes supplied by the pump transducer and measured at the sample volume by the LC-10 probe transducer, it is necessary to formulate two conversion formulas. The first conversion is for the plots from the HP3585A, shown in Chapter IV. The HP3585A spectrum analyzer plotted transducer response in units of dBm (dB re 1 mW), therefore, the first conversion changes the plotted output signal of the LC–10 from dBm to volts. Because dBm is referenced to milliwatts,

$$ dBm = 10 \, log_{10} \frac{P}{P_{ref}} $$

where P_{ref} = 1.0 mW. Substituting $P = V^2/R$ yields

$$ dBm = 10 \, log_{10} \left(\frac{V^2/R}{P_{ref}} \right) = 10 \, log_{10} \left[\frac{V^2}{(P_{ref})(R)} \right]. $$

Rearranging the terms gives the equation which converts dBm to volts:

$$ dBm = 20 \, log_{10} \left[\frac{V}{\sqrt{(P_{ref})(R)}} \right], $$

where

168

Two examples of these useful calculations would be to calculate the sound pressure from the pump transducer at the location of sample volume approximately 10 cm from the transducer face. From Figure D-2 at 100 KHz, the LC-10 sensed approximately -51 dB$_m$ at 10 cm distance away from the pump transducer using the HP3585A with the reference resistance (R) of 50 Ω. The pump sound field sweep time used to plot Figure D-3 was 0.01 seconds. Now,

$$-43.0 \text{ dB}_m = 20 \log_{10}\left[\frac{V}{\sqrt{(1.0 \times 10^{-3}w)(50\Omega)}}\right]$$

yields V = 1.583×10^{-3} volts. Therefore, pump sound pressure p_p measured at the sample volume is

$$p_p = V\mathcal{M} = (1.583 \times 10^{-3} \text{ volts})\left(1.4125 \times 10^5 \frac{\text{dynes/cm}^2}{\text{volts}}\right)$$

$$\underline{p_p = 223.6 \text{ dynes/cm}^2.}$$

If the pump sound field is swept every 0.10 seconds, the sound pressure level increases, in this case by 11.4 dBm. From Figure D-4, at 100 KHz the equation

$$-31.6 \text{ dBm} = 20 \log_{10}\left[\frac{v}{\sqrt{(1.0 \times 10^{-3})}(50 \ \Omega)}\right]$$

yields v = 5.88×10^{-3} volts. Therefore,

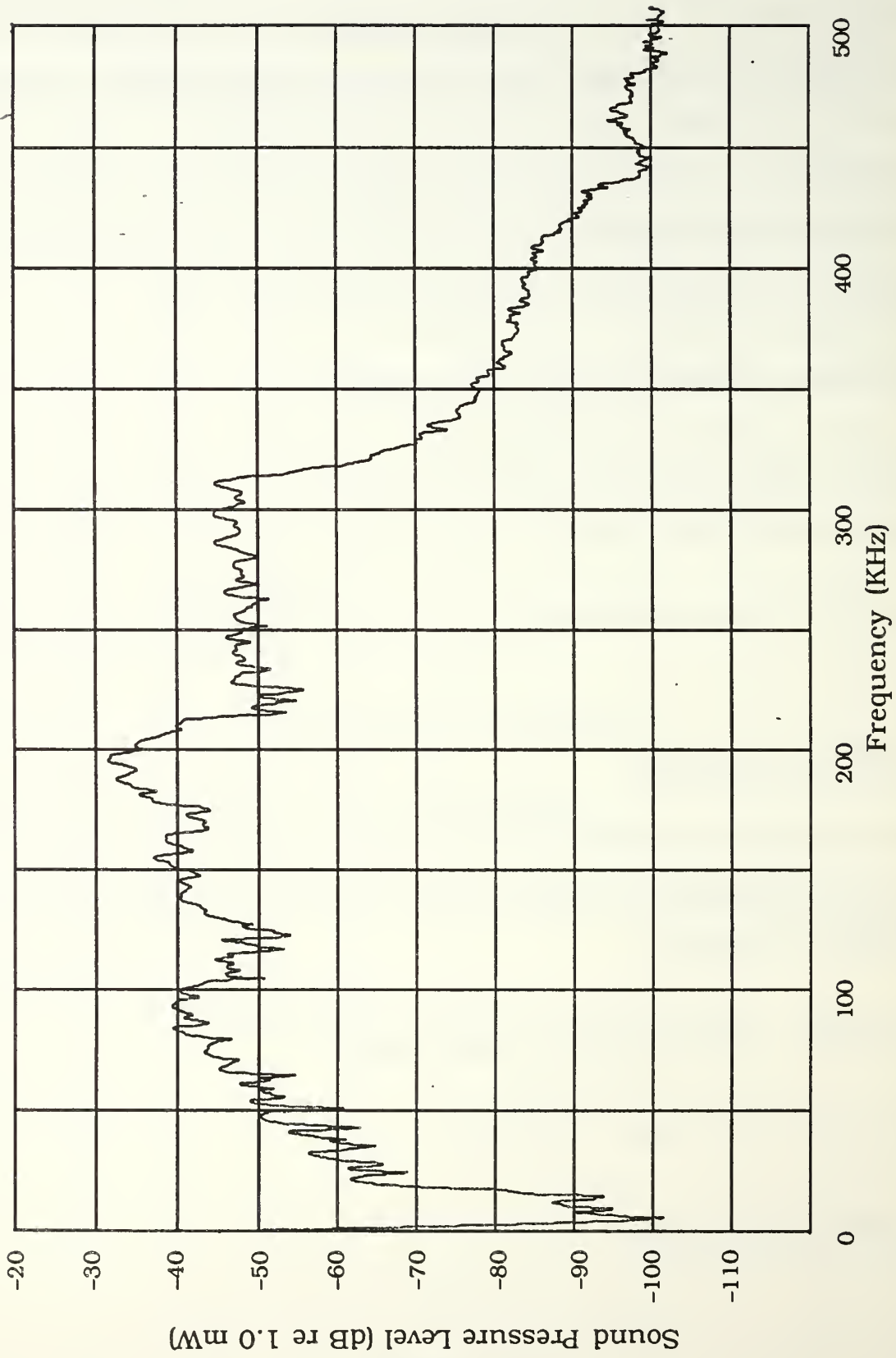$$\underline{p_p = 830.8 \text{ dynes/cm}^2.}$$

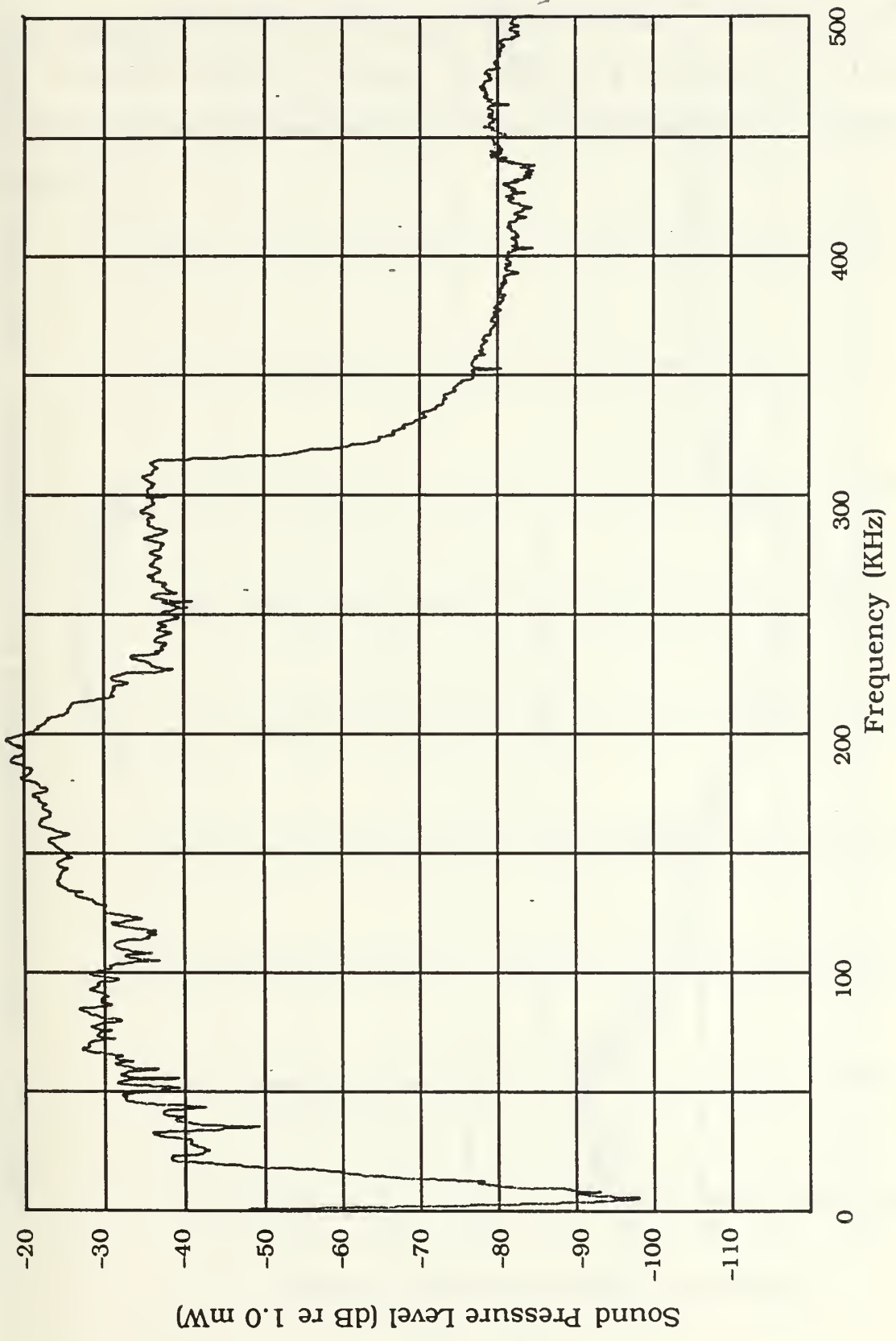Figure D-2. Pump Transducer Response at 10.0 Centimeters—Pump Sweep 0.01 Seconds

172

Figure D-3. Pump Transducer Response at 10.0 Centimeters—Pump Sweep 0.10 Seconds
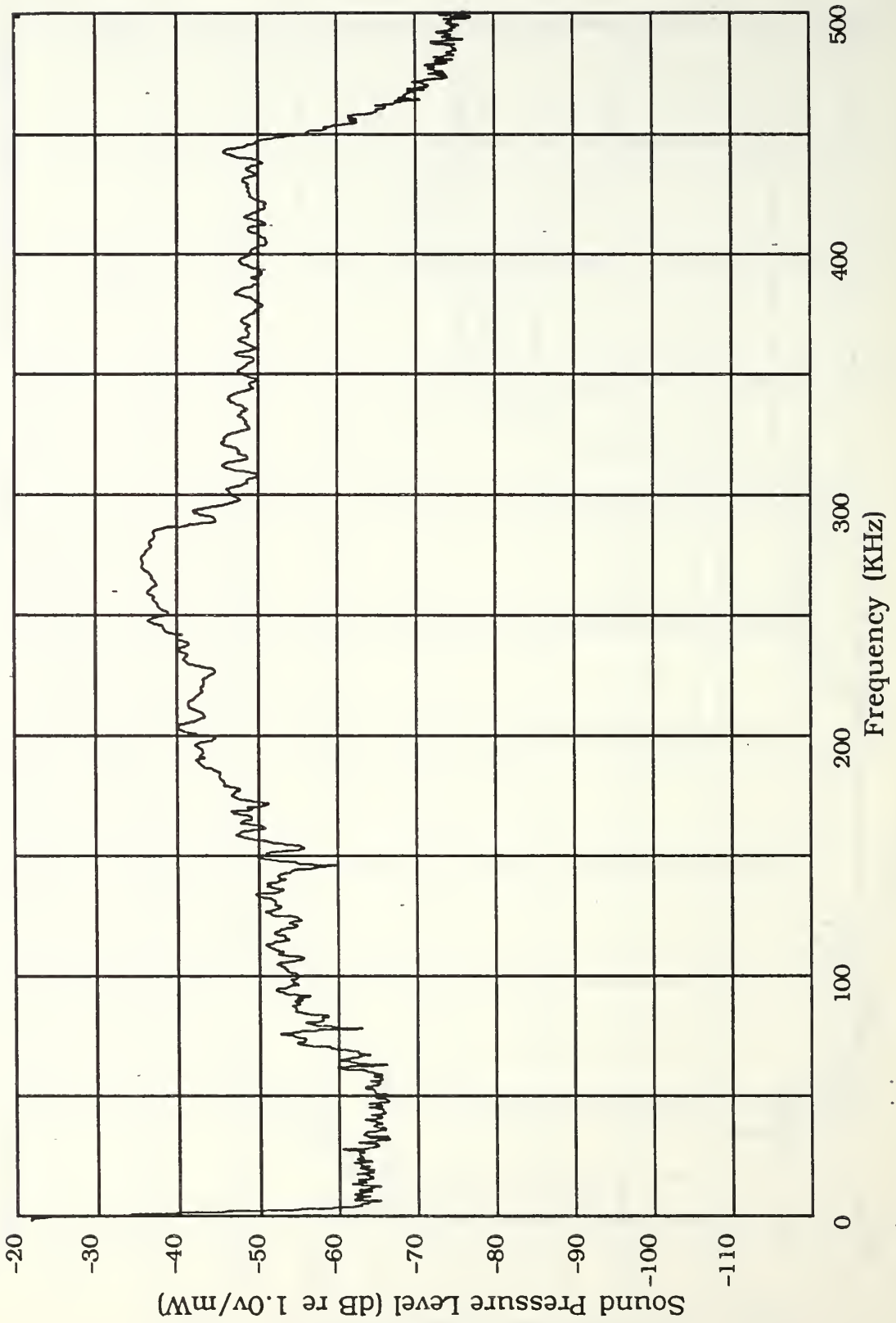
173

Figure D-4. Pump Transducer Response at 7.0 Centimeters—Pump Sweep 0.10 Seconds

174

The same set of equations is used to calculate the pump pressure amplitude at 7.0 cm from the pump transducer face. From Figure D-4, with a pump frequency sweep time of 0.10 seconds, the sound pressure level at 100 KHz is -39.2 dBm. Therefore, $p_p = 346.3$ dynes/cm^2.

IMAGE TRANSDUCER PRESSURE AMPLITUDE CALCULATION

Appendix D calculated the pump transducer's pressure amplitude (p_p) at the sample volume using the sound pressure level recorded on the HP3585A and knowing the calibrated frequency response of the LC–10 hydrophone. The image transducer's pressure amplitude (p_i) at the sample volume is calculated in the same fashion, only here the sound pressure level is measured with an ultrasonic hydrophone, the MA–1, designed by Bob Bruce and Bob Middleton of the Naval Postgraduate School, Monterey, California. The ultrasonic hydrophone calibrated frequency response is shown in Figure E–1. The sensitivity levels of 2.25 MHz and 2.50 MHz are -97.0 dB and -97.5 dB, respectively. Using the equation from Appendix D,

$$\mathcal{ML} = 20 \log_{10} \frac{\mathcal{M}}{\mathcal{M}_{\text{ref}}} \, ,$$

and that the reference level $\mathcal{M}_{\text{ref}}$ is 1.0 volts/Pa, the conversion factor $\mathcal{M}$ is calculated as

$$\mathcal{M} \ (2.25 \ \text{MHz}) = 7.0795 \times 10^4 \ \frac{\text{Pa}}{\text{v}} = 7.0795 \times 10^5 \ \frac{\text{dynes/cm}^2}{\text{v}}$$

and

$$\mathcal{M} \ (2.50 \ \text{MHz}) = 7.4989 \times 10^4 \ \frac{\text{Pa}}{\text{v}} = 7.4989 \times 10^5 \ \frac{\text{dynes/cm}^2}{\text{v}}$$
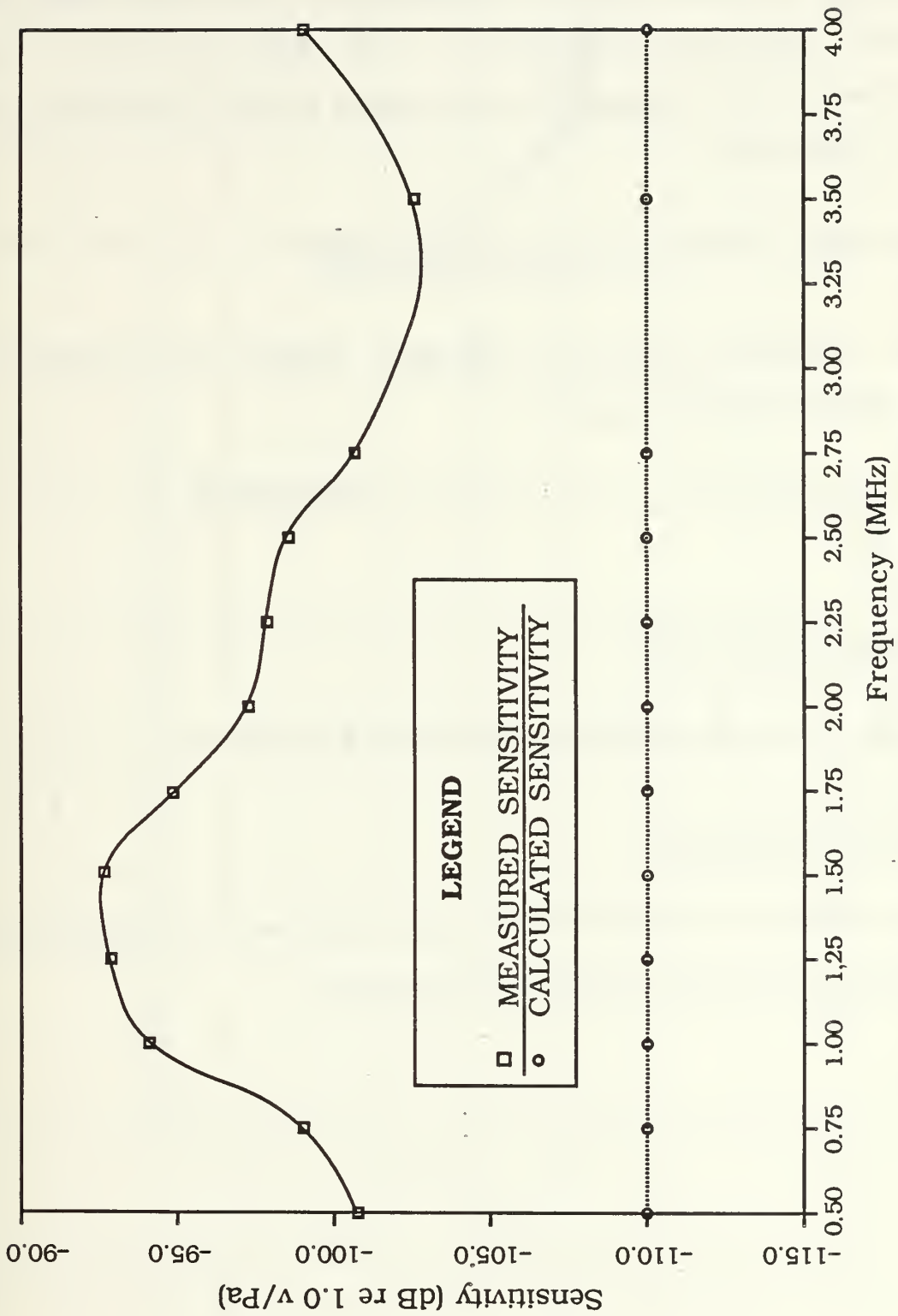
Figure E-1. MA-1 Hydrophone Pressure Sensitivity

177

When the imaging transducer was driven at 6.0 volts, the ultrasonic hydrophone sensed a level of – 47.6 dBm and – 48.1 dBm (using the HP3585A Spectrum Analyzer) at 2.25 MHz and 2.50 MHz, respectively, in the imaging far field sample volume (see Figure E–2). Now, at 2.25 MHz,

$$-47.6 \text{ dBm} = 20 \log_{10}\left[\frac{V}{\sqrt{(1.0 \times 10^{-3}\text{w})(50\Omega)}}\right]$$

yields $V = 9.3215 \times 10^{-4}$ volts. Therefore, imaging sound pressure p_i at the far field sample volume is
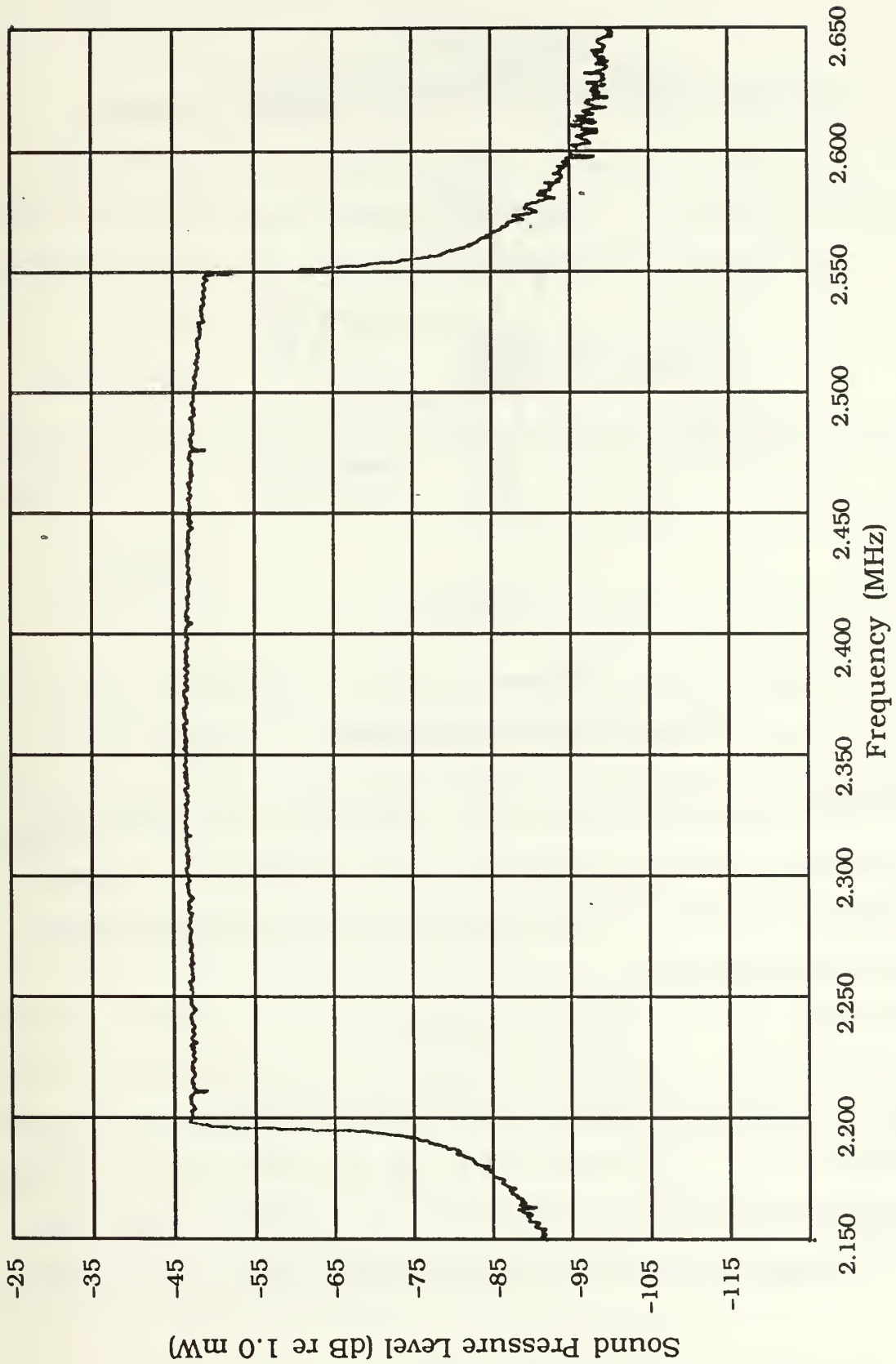
$$p_i = V\mathcal{M} = (9.3215 \times 10^{-4})\left(7.0795 \times 10^5 \frac{\text{dynes/cm}^2}{\text{v}}\right)$$

$\underline{p_i = 659.9 \text{ dynes/cm}^2.}$

Likewise, the imaging sound pressure p_i at 2.50 MHz is

$\underline{p_i = 659.9 \text{ dynes/cm}^2.}$

Slightly different transducer frequency responses and hydrophone sensitivities produced the same sound pressure.

Figure E-2. Imaging Transducer Response at 6.7 Centimeters

179

APPENDIX F

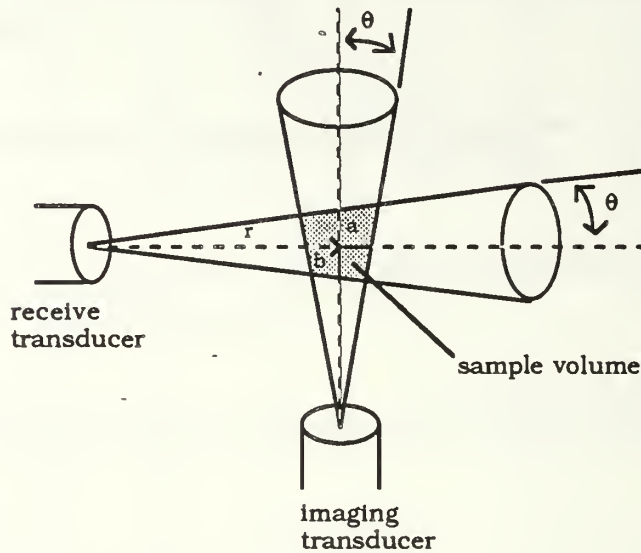## CALCULATION OF INSONIFIED SAMPLE VOLUME

Figure F–1

Sample Volume Definition

The sample volume formed by the intersection of the main lobes of the transducer beams (3 dB down) can be considered an approximate cylinder of radius a or b and length 2a or 2b. Table II shows for the 2.25 MHz transducers

$\theta = 3.10°$ $\qquad\qquad$ r = 4.74 cm

where r is the distance to the center of the sample volume.

Therefore, $a \approx b \approx 4.74 \tan(3.10°) = .257$ cm. Now, volume = area times length = $(\pi a^2)(2b)$. If $a \approx b$, then Volume = $2\pi a^3 = 2\pi (.257 \text{ cm})^3$ = .107 cm³. <u>Sample volume</u> is approximately .107 cm³.

APPENDIX G

STATISTICAL SAMPLE TIME

Calculation of the sample time or duration of the "look" begins with knowing how many samples are needed. To obtain a 95-percent confidence factor with a maximum error (E) of 5 percent, use

$$E \quad = \quad .05$$

$$Z_{\alpha/2} \quad = \quad 1.96$$

from the normal distribution tables. Equation (41) is now used and yields

$$n = \frac{1}{4} \left[\frac{1.96}{.05} \right]^2 .$$

The number of samples, n = 384.2, is rounded up to n = 385.

From Appendix 5, the length of the sample volume is 2b = .514 cm. A length must be sampled 385 times for a total sample length of

sample length = (n) (2b) = 197.9 cm.

Bubbles between 50 and 100 micrometers (μm) rise at a rate of .75 and 2.1 centimeters/second, respectively [Ref. 23]. If the bubbles are rising, for example, at a rate of 1.5 cm/s through the sample volume, then

Total Sample time = 131.9 seconds.

Smaller bubbles rise even more slowly, so an even greater sample time would then be required to get the statistically correct number of samples.

LIST OF REFERENCES

1. Surface Ship Torpedo Defense (SSTD) Project Review, Naval Coastal Systems Center, Panama City, Florida, December 1986.

2. Pacific Fleet ASW Improvement Program Review, Commander Training Pacific Fleet, San Diego, California, May 1987.

3. Newhouse V. L., and P. M. Shankar, "Bubble Size Measurements Using Non–Linear Mixing of Two Frequencies," Journal of the Acoustical Society of America (JASA), Vol. 75(5), pp. 1473–1477, May 1985.

4. Thorpe, S. A., "On the Clouds of Bubbles Formed by Breaking Wind–Waves in Deep Water, and Their Role in Air–Sea Gas Transfer," Phi. Trans. R. Soc. Lond., Vol. 304, pp. 155–210, February 1982.

5. Naval Research Laboratory Report No. 2117, Ship Wake Research, by A. J. Hiller, J. H. Caldwell, and C. W. Klee, June 1970.

6. Medwin, H., "Acoustical Determination of Bubble Size Spectra," JASA, Vol. 62, No. 4, pp. 1041–1044, October 1977.

7. Medwin, H., "In–Situ Acoustic Measurements of Microbubbles at Sea," Journal of Geophysical Research, Vol. 82, pp. 971–976, February 1977.

8. Medwin, H., "Counting Bubbles Acoustically: A Review," Ultrasonics, 15, pp. 7–13, January 1977.

9. Huang, T. T., and S. Gowing, Characteristics of Air Bubbles in Ship Wakes (Preliminary Proposal), David Taylor Research Development Center, Code 1542, September 1986.

10. Naval Coastal Systems Center Letter Report 412–01–86, Acoustic Measurements in a Ships Wake, by D. G. Toderoff and D. Trivett, November 1986.

11. Naval Coastal Systems Center Report QQ12, Bubble Swarm Acoustics, by K. W. Commander and Elan Moritz, paper presented at JASA Meeting, Panama City, Florida, December 1986.

12. Chapelon, J. Y., P. M. Shankar, and V. L. Newhouse, "Ultrasonic Measurements of Bubble Cloud Size Profiles," JASA, Vol. 78(1), pp. 196–201, July 1985.

13. Urick, Robert J., Principles of Underwater Sound, 3rd ed., Chapter 8, McGraw–Hill Book Co., 1983.

14. Kinsler, L. E., A. R. Frey, A. B. Coppens, and J. V. Sanders, Fundamentals of Acoustics, 3rd. ed., Wiley, 1982.

15. Strasberg, M., "Gas Bubbles as a Source of Sound in Liquids," JASA, Vol. 28, No. 1, p. 20, January 1953.

16. Strasberg, M., "The Pulsation Frequency of Nonspherical Gas Bubbles in Liquids," JASA, Vol. 23, No. 3, p. 536, May 1953.

17. Littlejohn, W. C., Analysis of Wake Profiling Data, Unclassified Preliminary Report, Naval Coastal Systems Center, November 1986.

18. Lauterborn, Werner, "Numerical Investigation of Nonlinear Oscillations of Gas Bubbles in Liquids," JASA, Vol. 59, No. 2, p. 283, February 1976.

19. Miller, D. L., "Ultrasonic Detection of Resonant Cavitation Bubbles in a Flow Tube by Their Second Harmonic Emissions," Ultrasonics, 19, p. 217, 1981.

20. Ziomek, L. J., Underwater Acoustics: A Linear Systems Theory Approach, Academic Press, Inc., 1985.

21. Private communication with Dr. P. M. Shankar of Drexel University, 21 August 1987.

22. Freund, John E., and Irwin Miller, Probability and Statistics for Engineers, Prentice–Hall Inc., 1985.

23. Carstensen, E. L., and L. L. Foldy, "Propagation of Sound Through a Liquid Containing Bubbles," JASA, Vol. 19, No. 3, p. 481, May 1947.

INITIAL DISTRIBUTION LIST

1. Department of the Navy   4
    Naval Sea Systems Command
    PMS-415
    Washington, D.C. 20362-5101

2. Captain J. M. Schantz   2
    Navy Department OP951D
    Pentagon Room 5D-577
    Washington, D.C. 20350-2000

3. Commander, Naval Coastal Systems Center   3
    Leon Walters— Code 204
    Panama City, Florida 32407-5000

4. Commander, Naval Coastal Systems Center   4
    Dr. Elan Moritz— Code 4120
    Panama City, Florida 32407-5000

5. Commander, Naval Coastal Systems Center   1
    Dr. Ronald Peterson— Code 4210
    Panama City, Florida 32407-5000

6. Commander, Naval Coastal Systems Center   1
    Bill Littlejohn— Code 2340
    Panama City, Florida 32407-5000

7. Commander, Naval Coastal Systems Center   1
    Clifton Bonney— Code 3210
    Panama City, Florida 32407-5000

8. Library, Code 0142   2
    Naval Postgraduate School
    Monterey, California 93943-5002

9. Professor Anthony Atchley, Code 61AY   4
    Physics Department
    Naval Postgraduate School
    Monterey, California 93943-5002

10. LCDR Gregory Netzorg, Code 61NZ   1
    Physics Department
    Naval Postgraduate School
    Monterey, California 93943-5002

11. Professor Steven Garrett, Code 61GX   1
    Physics Department
    Naval Postgraduate School
    Monterey, California 93943-5002

12. William L. Hampton   2
    3825 Bradee Road
    Brookfield, Wisconsin 53005

13. LT Stephen W. Hampton   1
    3825 Bradee Road
    Brookfield, Wisconsin 53005